SALP/Lot 7, 5 BC3001-5-47
CLS.DOS/NT/03.907
Issue : 1rev1 **Ramonville, 18 December 2003**
Nomenclature : SALP-RP-P2-EA-15162-CLS

Envisat RA2/MWR ocean data validation and cross-calibration activities
Yearly report
Contract N° 731/CNES/00/8435/00

		COMPANY	DATE	INITIALS
PREPARED BY	Y. FAUGERE F. MERTZ J. DORANDEU	CLS		
QUALITY VISA	M. DESTOUESSE	CLS		
ACCEPTED BY	J. DORANDEU	CLS		
APPROVED BY	N. PICOT	CNES		

CLS 8-10 Rue Hermès - Parc Technologique du Canal - 31526 Ramonville St-Agne - FRANCE
Telephone 33 5 61 39 47 00 Fax 33 5 61 75 10 14

DOCUMENT STATUS SHEET

Project Control Initials	ISSUE	DATE	REASON FOR CHANGE

D :page deleted I :Page Inserted M :Page modified

List of tables and figures

List of tables :

Liste of figures :

CONTENTS

1. INTRODUCTION

This report is an overview of Envisat validation and cross calibration studies carried out at CLS during the year 2003. This work was performed under SALP contract (N° 731/CNES/00/8435/00) supported by CNES at the CLS Space Oceanography Division. It is divided into to parts:

- CAL/VAL Envisat activities – Lot 7
- Envisat/ERS-2 and Envisat/Jason-1 cross calibration activities – Lot 5 (N° 4500007045/DSO310)

Some of the results described here were presented at the CCVT meeting (Frascati, March 2003), joint EGS/AGU meeting (Nice, April 2003), QWG meetings (Toulouse, October 2003).

Since the beginning of the mission, Envisat data have been analysed and monitored in order to assess the quality of Envisat GDR products for ocean applications.

A statistical evaluation of Envisat altimeter data has been carried out to produce a global calibration of this mission. All relevant parameters from altimeter measurements (Ocean 1 retracking) and geophysical corrections are evaluated and tested. Moreover, Sea Surface Height (SSH) crossovers and along-track analyses have also been performed.

Cross-calibration methods have been developed and applied to assess the consistency of Envisat data with the ERS-2 and Jason-1 missions.

2. DATA

2.1. AVAILABLE CYCLES

7 GDR cycles have been produced with two different IPF processing chain and CMA Reference Software

- 04/10/2002 to 13/01/2003: Cycles **10**, **11**, **12** (IPF 4.53, CMA V5)
- 09/04/2003 to 11/08/2003: Cycles **15** (from pass 453), **16**, **17**, **18** (IPF 4.54, CMA V6)

Cycles 10, 11 and 12 have been extensively analysed during the validation phase. This report will mainly focus on cycle 15 to 18.

GDR products of cycle 15 to 17 have been produced by the CMA software using Level 1B directly supplied by the two Payload Data Handling Station (PDHS) in Kiruna and Frascati. From cycle 18 there is new step in the Level 1B generation loop: the Low Rate Reference Archive Center (LRAC) receives Level 1 B from PDHS and produces a consolidated Level 1B. The CMA uses now this consolidated Level 1B to produce GDRs.

A quality assessment report has been carried out for each cycle and is available on http://www.aviso.oceanobs.com/html/donnees/calval/validation_report/en/welcome_uk.html. The purpose of this document is to report the major features of the data quality from the Envisat mission.

2.2. INSTRUMENT AND PLATEFORM STATUS

The events for cycle 15 to 18 are presented in Table 1:

Cycle	Pass	Event
15	1 to 452	Wrong setting of Ra2 parameters (no CTI tables have been up-loaded on-board) from 18 Mar 2003 18:50:40 to 9 Apr 2003 17:12:24
	437 to 452	RA-2 unavailability (Format Header Error forcing ICU to RS/WT/INI) from 8 Apr 2003 15:08:57.000 to 9 Apr 2003 17:12:24.000
	613 to 624	RA-2 unavailability (Format Header Error forcing ICU to RS/WT/INI) from 8 Apr 2003 15:08:57.000 to 9 Apr 2003 17:12:24.000
	879 to 901	RA-2 unavailability: Multiple SEU caused ICU switchdown
16	191 to 215	RA2 unavailability (known SEU failure) from 5 May 2003 12:30:17.000 to 6 May 2003 10:01:10.000
	361 to 387	RA-2 unavailability (ICU in SUSPEND due to TM FMT Error when a Reduced FMT was requested) from 11 May 2003 11:06:33.000 to 12 May 2003 10:14:35.726.
	460 to 462	Orbit Maintenance Maneuver (from 2003/05/14 22:40:13 to 2003/05/15 00:40:19 TAI)
	548 to 602	RA-2 unavailability (Switch-down for PMC SW upgrade and OCM) from 18 May 2003 06:25:17.000 to 19 May 2003 15:59:28.000. MWR unavailability (Switch-down for PMC SW upgrade and OCM) from 18 May 2003 06:25:24.000 to 19 May 2003 14:45:40.000. DORIS unavailability (Switch-down for PMC SW upgrade and OCM) from 18 May 2003 06:25:25.000 to 19 May 2003 13:21:28.000.
	610 to 612	Orbit Maintenance Maneuver (from 2003/05/20 04:11:53 to 2003/05/20 06:23:31 TAI).
	967 to 987	RA-2 unavailability (ICU went to RS/WT/INI) from 1 Jun 2003 14:36:40.000 to 2 Jun 2003 09:20:35.000.
17	119 to 122	Orbit Maintenance Maneuver (from 2003/06/07 01:08:16 to 2003/06/07 03:08:23 TAI).
18	91 to 94	Orbit Maintenance Maneuver (from 2003/07/11 0:58:45 to 2003/07/11 03:49:08 TAI)
	538	RA2 unavailability (RA-2 in STBY/REF due to MCMD timeout) from 26 Jul 2003 15:28:11 to 26 Jul 2003 17:25:35
	682	RA2 unavailability (RA-2 picked up Mission Planning schedule) from 31 Jul 2003 16:11:02 to 31 Jul 2003 18:06:30

Table 1 Instrument and platform event

2.3. ALGORITHMS

2.3.1. IPF and CMA version

The following modifications have been implemented in CMA V6:

- MWR correction: neural algorithm (the algorithm is described in Labrou et al., 2003)
- Mean Sea Surface: CLS01.1
- Oceanic tides: GOT2000 and FES2002
- Sea State Bias: non parametric SSB
- DORIS ionospheric correction: several changes in the computation
- Rain flag: implementation of new algorithm

2.3.2. Updates

In order to assess the product quality some updates were necessary:

- Ice flag: The same method as in the ERS-2 OPR quality assessment (e.g. Mertz et al., 2003) has been used for ENVISAT (see 3.2.1.2)
- S-Band anomaly flag: see 3.2.1.3
- Model ionosphere correction: There is no model available in the product. Thus the JPL GIM ionosphere correction is computed to assess the dual frequency and Doris corrections. The GIM model has been computed thanks to the procedures kindly provided by Remko Scharroo to the CCVT (Scharroo, 2002).
- Filtered dual frequency ionosphere correction: A 300-km low pass filter is applied along track on the dual frequency ionosphere correction to reduce the noise of the correction.

3. MISSING AND EDITED MEASUREMENTS

3.1. MISSING MEASUREMENTS

The daily percentage of missing measurements over ocean has been plotted on Figure 1. Table 2 summarizes the number of missing passes for each cycle. The missing measurements are all caused by:

- Ra2 or Payload module unavailability
- Processing or disseminating troubles on PDHS side

Pass 1 to 452 of cycle 15 have not been delivered because of a wrong setting of Ra2. That explains the large ratio of missing measurements. For cycle 16 to 18, the data availability seems to improve continually.

	Cycle 15	Cycle 16	Cycle 17	Cycle 18
Missing passes (not delivered)	523	171	79	25
% of missing measurement over ocean	54%	20%	12%	4%

Table 2 : Data unavailability

3.2. EDITED MEASUREMENTS

Data editing is necessary to remove altimeter measurements having lower accuracy. There are 4 steps in the editing procedure. The first step is based on flags. Then, measurements are edited using thresholds on several parameters. The third step uses cubic splines adjustments to the ENVISAT Sea Surface Height (SSH) to detect remaining spurious measurements. The last step consists in removing entire pass where SSH-MSS mean and standard deviation have unexpected value.

The two first steps are detailed below.

3.2.1. Editing by flags

Three flags are used on Envisat data: the land/sea radiometer flag, the ice flag and the S-Band anomaly flag. The first flag is given in the products whereas the two others are not.

3.2.1.1. Land/sea radiometer flag

When this flag is set over ocean, it means that the radiometer data is missing. The percentage of missing measurements over ocean has been plotted on Figure 2. The mean value is around 12% but the radiometer unavailability is not constant. For example, in early July, more than 50% of radiometer data were missing during a 7 day-period.

3.2.1.2. Computed ice flag

No ice flag is available in Envisat product. However, as Envisat operates between ±82° of latitude, sea ice is major issue for Envisat altimetric data. A study has been performed during the validation phase (see Part 5) and an empirical algorithm has been chosen for quality assessment. A measurement is set to ice if:

|latitude| >50 deg	And	**N_{20Hz} criterion**: the number of 20Hz valid data < 17 Or **MWR criterion**: |MWR–ECMWF| > 10cm Or **Peakiness criterion**: Peakiness>2

Figure 3 shows the cycle by cycle percentage of edited points by the sea ice flag over ocean. The Blue and green curve respectively represent the ratio of sea ice over the Northern and Southern Hemisphere. The red curve is the sum of these two ones. The observed trend is due to the annual cycle: melting of sea ice in the North (Spring-Summer) and increasing of the sea ice pack in the South (Automn-Winter).

3.2.1.3. Computed S-Band anomaly flag

An anomaly occasionally occurs on the S-Band. This anomaly concerns the "summation of the S-Band power echoes". Consequently the Dual Frequency ionosphere correction is not reliable during these periods. A measurement is set if:

$$\boxed{|Sigma0(Ku) - Sigma0(S)| > 5dB}$$

Figure 4 and Figure 5 illustrate the starting of an S-Band anomaly. An interesting fact is that the anomalous measurements start exactly when the satellite flies over a small Indonesian island. This seems to be the general behaviour: the other S-Band anomaly event always start over land. The daily percentage of flagged measurements over ocean is plotted on Figure 6.

The mean value is around 4%. There were in average 3 S-Band anomaly events by month during this period.

Table 3 summarizes the number of pass entirely edited by land/sea radiometer flag and the computed S-Band anomaly flag.

	Cycle 15	Cycle 16	Cycle 17	Cycle 18
Passes with no radiometer correction	43	57	128	34
Passes impacted by the S-Band anomaly	27	35	14	61

Table 3 Number of pass edited by land/sea and S-Band anomaly flag

3.2.2. Editing by thresholds

The thresholds are expected to remain constant throughout the ENVISAT mission, so that monitoring the number of edited measurements allows a survey of data quality. Table 4 gives for each tested parameter, the minimum and maximum thresholds used in the routine quality assessment. These thresholds have been derived from the Topex experience. However, the variability relative to MSS and the standard deviation of 18Hz range have been refined specifically for Envisat data.

Parameter	Min threshold	Max threshold
Sea surface height (m)	-130	100
Variability relative to MSS (m)	-2	2
Number of 18Hz valid points	10	-
Std. deviation of 18Hz range (m)	0	0.25
Off nadir angle from waveform (deg2)	-0.200	0.160
Dry tropospheric correction (m)	-2.500	-1.900
Invert barometer correction (m)	-2.000	2.000
MWR wet tropospheric correction (m)	-0.500	0.001
Dual Ionospheric correction (m)	-0.200	-0.001
Significant wave height (m)	0.0	11.0
Sea state Bias (m)	-0.5	0
Backscatter coefficient (dB)	7	30
Ocean tide height (m)	-5	5
Long period tide height (m)	-0.500	0.500
Earth tide (m)	-1.000	1.000
Pole tide (m)	-5.000	5.000
RA2 wind speed (m/s)	0.000	30.000

Table 4 : Editing thresholds

Figure 7 shows the cycle by cycle percentage of points edited on each criterion. The main editing criteria are the Rms of Ku range, the off nadir angle and SSH-MSS. The other ratios are lower than 0.2%. No anomalies have been detected on these editing ratios.

Compared to other altimeters like Jason or Topex these ratios are strongly lower. Figure 8 shows a comparison of the editing ratio between Envisat and Jason. Figure 9 and Figure 10 show the measurements edited respectively on Envisat and Jason. The edited measurement density on Envisat is strongly lower than on Jason, especially in wet areas.

4. STATISTICAL MONITORING

Both mean and standard deviation of Envisat data main parameters have been monitored since the beginning of the mission. In particular, it is important to analyze the differences between corrections of the same type as a function of time. Only valid points (according to editing criteria) are used to analyze the behavior of these parameters over a long time series.

4.1. ALTIMETER PARAMETER

4.1.1.1. Number and RMS of Ku and S elementary measurements

The daily mean RMS of Ku and S 18Hz elementary data are plotted on Figure 11. The mean values are about 19.98 and 19.90 respectively for Ku and S band. These values are very high compared to other altimeters.

Histograms of RMS of Ku and S-band Range are plotted on Figure 12. The daily mean RMS of Ku and S 20Hz elementary data are plotted on Figure 13. These parameters are quite stable. The mean values are respectively 9.0 and 31.1 cm. In Ku Band, it corresponds to about 2 cm at 1Hz, assuming uncorrelated 20Hz measurements. It is consistent with the expected value.

4.1.1.2. Ku and S SWH

Histograms of Ku and S-band SWH are plotted on Figure 14. The Ku SWH histogram has a good shape. The new retracking has improved the low waves (0-1m) but a zero class has appeared. The daily mean Ku and S SWH are plotted on Figure 15. The curve reflects sea state variations. The mean values are respectively 2.7 and 2.6 cm. No anomalies have been detected.

4.1.1.3. Ku and S Sigma0

Histograms of Ku and S-band Sigma0 are plotted on Figure 16. The daily mean Ku and S Sigma0 are plotted on Figure 17. The mean values are respectively 11.1 and 10.6 dB. Notice that the Ku Sigma0 has been adjusted on ERS-2 mean to be compliant with the wind speed model (Witter and Chelton, 1991).

4.1.1.4. Squared mispointing

The histogram of the squared mispointing is plotted on Figure 18. It has a good shape but it has a strong bias of 0.027 deg^2 which corresponds to 0.16 degrees. Investigations are on-going at algorithm level to deal with the bias issue. The daily mean squared mispointing is plotted on Figure 19. The curve has several particular features:

- First the shape of the curve is not flat: there is an increasing trend between cycle 10 to 12, which seems to flatten out between cycle 12 and 15. From cycle 15 to 18, the squared mispointing is about 0.028 deg^2.
- The second particular feature is the drop of the squared mispointing between the 15th of May (Cycle 16 pass 466) and the 3rd (Cycle 17 pass 19) of June where the mean value is between 0.026 and 0.027 deg^2. There is no explanation for this particular behaviour. On the 14th and 20th of May, two maneuvres were performed but there is no obvious link between these two facts.
- The last particular features are the numerous strong drops of this parameter. Each drop corresponds to a Ra2 or payload module unavailability. Figure 20 illustrates this behaviour. After the 11th-12th May instrumental event, the first data delivered have very low values (less than 0.015 deg2). Then the off-nadir angle gradually increases to reach the usual value after about 13 hours.

4.1.1.5. Ionosphere correction

Comparisons have been made between the Dual Frequency (DF) ionosphere correction, the Doris one, and JPL GIM model. The daily mean and standard deviation are plotted on Figure 21 and Figure 22. There is a -0.7 cm bias between DF and GIM corrections. This difference was +4 cm using the data set produced with the previous IPF/CMA version (cycle 10, 11, 12). This change is probably due to the use of a wrong value in the characterisation file which impacted the range values in the two bands, and consequently the ionosphere correction. The standard deviation difference is about 1cm. The changes on the Doris correction have been positive. This correction is now much more consistent with the two others.

4.2. PSEUDO TIME TAG BIAS

Mean of pseudo time tag bias is plotted on Figure 23. If we only consider cycle 16 to 18, the mean of this parameter is about 0.28 ms, which is a good performance.

4.3. WET TROPOSPHERE CORRECTION

Mean and standard deviation daily of MWR-ECMWF model difference are plotted on Figure 24 and Figure 25. On cycle 10 to 12, a parametric algorithm is used for the MWR correction.

The use of the neural algorithm for cycle 15 to 18 has a strong impact on the consistency with the ECMWF model: the mean difference is reduced by 0.7cm and the standard deviation by 0.5cm. For cycle 15 to 18, the mean and standard deviation are respectively 0.4 and 1.8 cm. As an example, the scatter plot of MWR correction according to ECMWF model for cycle 18 is given on Figure 26.

A particular feature is visible from July the 2nd and 5th of July. The daily mean is around 0.1 cm during 4 consecutive days. This is due to a specific sampling of the ocean, caused by a strong MWR unavailability. Indeed a particular feature is visible on Figure 2 for the same period.

A complete monitoring of all the radiometer parameters is available in the cyclic Envisat Microwave Radiometer Assessment Report (http://earth.esa.int/pcs/envisat/mwr/reports/).

4.4. CROSSOVER ANALYSIS

Crossover differences are systematically analysed to estimate data quality and SSH performances. The standard SSH calculation for Envisat is defined below.

SSH=Orbit –Range

+ Inverse dry troposphere correction

+ Inverse barometer correction

+Radiometer Wet troposphere correction

+Dual Frequency correction (filter 300km)

+Non parametric SSB

+GOT00V2

+Earth tide correction

+Pole tide correction

4.4.1.1. Impact of selection

The number, mean and the standard deviation crossover differences using 3 selections are respectively plotted on Figure 27, Figure 28 and Figure 29. On the Red curve, no selection is applied. On the blue curve, areas with shallow waters have been removed (bathy<-1000m). On the green curve, areas with shallow waters (1000 m), of high ocean variability (> 20 cm) and high latitudes (> |50| degrees) have been removed. Standard deviation for Cycle 15 is strongly different because of the low number of crossover points. There are 10000 crossovers only whereas on cycles 16 to 18 there are more than 20000.

The mean difference is positive which mean that SSH on descending tracks > SSH on ascending tracks. The mean difference is 0.6 cm but on the last available cycle, the mean reaches 1cm. This behaviour is under study to determine the reason of this bias (orbit error, instrumental problem, …).. That might be connected with the orbit error.

The standard deviation is between 9 and 10 cm when no selection is applied. The last selection allows monitoring the Envisat performance. In that case the standard deviation is between 7.5 and 8 cm.

4.4.1.2. Impact of correction

Figure 30 and Figure 31 show the impact of using another SSH formula on the mean and the standard deviation crossover differences (Bathy<-1000). For this analysis an orbit error has been computed. The orbit error estimation is performed by a global minimization of crossover differences using a (1 and 2 cycles/revolution) sinusoidal model. The orbit error correction strongly improves the performances. The mean difference drops to zero using this orbit error. The gain is 4 cm rms. The use of FES02 model instead of GOT00V2 slightly improves the performances for cycle 16 to 18. However, note that when the full data set is used better results are obtained with Got00V2 for cycle 16 and 17. Got00V2 uses local model for coastal area which improve the SSH performance in this regions. The use of GIM ionosphere correction instead of the dual increases the mean by 2-3 and slightly degrades the performances.

4.4.1.3. Geographic patterns

The map of mean crossover from cycle 15 to 18 is on Figure 32. It shows systematic differences between ascending and descending passes in some areas. The mean locally overtakes 4 cm (in South Pacific and South Atlantic), which is probably due to geographically-correlated orbit errors. This behaviour is currently under study.

The map of standard deviation crossover differences on Figure 33 shows usual results with high variability areas linked to ocean variability.

4.5. SEA LEVEL ANOMALY

Figure 34 and Figure 35 show the cycle by cycle mean and standard deviation of SSH–MSS CLS01V1. The mean is around 43.5 cm. The increasing trend is due to seasonal effect. The standard deviation is around 10.7 cm. The decreasing trend on the standard deviation may be connected with the data availability.

Figure 36 and Figure 37 show the daily mean and standard deviation of SSH –MSS CLS01V1. There is a slight jump (~1 cm) between the 17th of May and the 20th of May on the mean. This jump disappears when using the adjusted orbit error. There is not any particular feature on the standard deviation.

This jump may have 2 explanations:

- It can be connected to the PMC SW upgrade. 18th and 19th of May are missing because of this event.
- It can be a consequence of a manoeuvre. As described in the cycle 16 ECAR report the western side of the ground track dead-band has been violated starting from 17 April 2003. An out-of-plane orbit inclination maintenance was executed on the 20th of May

5. SEA ICE DETECTION

The purpose of this study is to define a simple, straightforward, empirical method to detect sea ice. First the method used on ERS-2 is applied on ENVISAT data. Then the peakiness parameter, available in the GDR product is tested. Finally an algorithm combining these two methods is proposed.

5.1. ERS-2 ALGORITHM

This algorithm has been developed by J. Stum for ERS-2 OPR quality assessment. The ice flag is set if at high latitude one of the 2 conditions is true:

- |Latitude| >50
- **N_{20Hz} criterion**: the number of 20Hz valid data < 17

  Or

  MWR criterion: |MWR–ECMWF| > 10cm

  Where MWR is the radiometer wet troposphere correction and ECMWF the model one.

Figure 44 and Figure 45 illustrate the "efficiency" of these two criteria. The N_{20Hz} criterion only flags a few points whereas the MWR criterion flags a large amount of data in the north and in the south. Thus all the work is done by the MWR criterion. That seems specific to ENVISAT. So it can be a problem when the MWR correction is not available.

The sea ice measurements retrieved by the ERS-2 full method are plotted on Figure 46. This method seems to work well on ENVISAT data. However it is not perfect: there are measurements which have been missed in the middle of the pack ice.

Figure 47 points out another drawback of this method. It shows the ocean data where RMS of Ku range is greater than 20cm. There is a band of data along the ice/ocean transition. The waveforms have apparently been corrupted by sea ice. These data should have been ice-flagged.

Figure 48 illustrates this problem on a particular pass. South of 61.7S, the altimeter measurements are corrupted by sea ice. There is no impact on N_{20Hz}. On the ocean/ice transition, the MWR/ECMWF difference increases gradually to exceed 10 cm at 62S. 5-10 of points have been missed by the ERS-2 method between 61.7S and 62S

5.2. PEAKINESS INFORMATION

On Envisat there is a parameter which does not exist on ERS-2, the peakiness parameter. This parameter is derived from the waveforms. It is proportional to the maximum/mean ratio of the waveform. Figure 49 shows the histogram of peakiness valueson ocean data. The peakiness ranges between 1.6 and 1.8 and the mean is about 1.7.

Figure 50 shows the map of this peakiness parameter. Red points correspond to peakiness >1.9. The sea-ice signature is clearly evidenced. However the zoom over Antarctic shows values around 1.7 in the middle of the pack ice. Depending on the season, 0 to 5 % of the sea ice shows an “ocean-like peakiness” (Seimour Laxon, March 2003, Internet communication).

We tried to apply a threshold on peakiness to see how ice is retrieved. Figure 51, Figure 52 and Figure 53, show respectively the ice and the ocean data for a threshold of 1.8, 1.9 and 2.0. It is globally efficient but for thresholds of 1.8 and 1.9, many points in open ocean are ice-flagged. On the other hand, even with a 1.8 threshold, not all the sea-ice is retrieved, as said previously.

But on the particular pass (Figure 57), we can see that the ice/ocean is better described with the peakiness than with the MWR-ECMWF differences. As soon as the waveform is corrupted, the peakiness value is immediately higher than 2.

5.3. COMBINATION OF ALTIMETER AND RADIOMETER CRITERIA

The 2 methods seem to be complementary. The MWR criterion is quite reliable except on ice/ocean transitions. Adding a peakiness criterion, with a 2.0 threshold, improves the sea ice detection in these areas. Figure 55 shows this improvement for cycle 10 to 12. 5000 to 10000 (1 to 2%) points have been detected thanks to the addition of the peakiness criterion.

Finally, the proposed algorithm for Envisat is defined as follows. The ice flag is set if:

- |Latitude| >50
-
  N_{20Hz} criterion: the number of 20Hz valid data < 17

  Or

  MWR criterion: |MWR–ECMWF| > 10cm

  Or

  Peakiness criterion: Peakiness>2

6. NOISE AND HIGH FREQUENCY ANALYSIS

6.1. INTRODUCTION

The present study is based on user products and aims at analysing the high frequency signals. Two types of methods are used: spectral analysis and high pass filtering. The two methods are presented in the diagram below. They are applied to the $SLA_{nc/MSS}$ signal of Envisat where:

$SLA_{nc/MSS}$= Raw SSH – MSS CLS 01V1

Raw SSH means not corrected for any geophysical correction. We have selected 10 days of cycle 11 (November 9, 2002 to November 19, 2002) and compared the results with the same period of Jason-1 (Cycle 11) and ERS-2 (cycle 79). A selection on latitude (<60°) and on bathymetry (<-500m) has been performed to get 3 consistent datasets.

The two methods have been applied on elementary 20Hz data and 1Hz data.

Analysis of High Frequency Signals

We use a high-pass filtering technique (Tran et al., 2001) to estimate a HF signal on the Sea Level Anomaly.

SLA relative to a MSS or from repeat-track analysis

Lanczos low-pass filter

Low frequency signal S_{LF}

High frequency signal $S_{HF} = SLA - S_{LF}$

STD of HF signal integrates:
- instrumental noise
- residual geoid signal
- and possibly HF ocean signals

Spectral Analysis

The power spectrum of ε(t), a pure white noise (i.e a random variable with Gaussian distribution) with standard deviation equal to σ is :

$S_p(k) = \alpha = 2.\Delta t.\sigma^2$ where Δt is the resolution of the signal sample

Therefore, if the signal to analyze is X(t) = s(t) + ε(t) , the power spectrum will be composed of :

- the spectrum of the oceanic signal s

+

- the spectrum of the noise ε (i.e α)

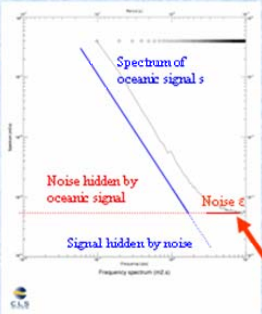

A plateau on a power spectrum can be the signature of a white noise. The STD of its distribution can be obtained by :

$$\sigma = \sqrt{\frac{\alpha}{2.\Delta t}} \quad \text{(I)}$$

Plateau α

Two methods for a single result

Computing the variance of high frequency filtered signals is equivalent to integrating the power spectrum of the original signal from the cut-off frequency fc to the Shannon frequency fs (highest frequency available on a signal).
If the original signal contains white noise, the high frequency part of the power spectrum is constant (plateau) and equal to α, hence :

$$V(fc) = \int_{fc}^{1/2\Delta x} Sp(f).\delta f \rightarrow V(fc) = \alpha\left(\frac{1}{2\Delta x} - fc\right) \quad \text{(II)}$$

The HF method gives the value of V(fc), i.e the energy of HF signal. But, the slope of V(fc) is a direct measurement of the spectral plateau α.

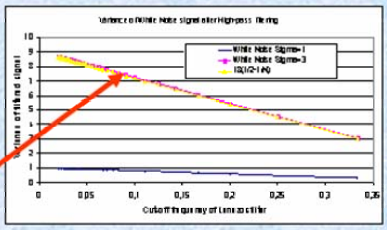

Slope α

6.2. ANALYSIS ON 20HZ DATA

6.2.1. Global results

Figure 56 shows the power spectrum of ENVISAT. It decreases until 3Hz with a swelling around 0.4Hz. At frequencies greater than 3Hz the signal is hidden by a plateau at 10^{-3} m²/cps which corresponds to a white noise of

$$\sigma_{20Hz} = \sqrt{\frac{\alpha}{2 * \Delta t}} = \sqrt{\frac{10^{-3}}{2 * 0.0557}} = 9.5cm$$

Assuming uncorrelated 20Hz measurements, it is equivalent at 1Hz to

$$\sigma_{equiv.1Hz} = \frac{\sigma_{20Hz}}{\sqrt{20}} = 2.1cm$$

<u>Warning:</u> This is only computed to give an order of magnitude at 1 Hz. As explained below this formula is not relevant.

Figure 57 shows the power spectrum of Jason. It has a similar shape as ENVISAT with a plateau at 6.10^{-4} m²/cps which corresponds to a white noise of 7.3cm (1.6cm at 1Hz). The swelling is still more pronounced. Using residuals (SLA relative to a mean profile), to remove short wave length of Geoid, does not change the shape of the spectrum. This feature has no explanation so far.

The plateau we observe on 20Hz data will not be visible on 1Hz data because it begins at frequencies higher than 1Hz. So, even if there is a plateau on 1Hz-spectrum, the equation $\sigma_{1Hz} = \sigma_{20Hz}/\sqrt{20}$ should not be used.

Now, using the high pass filtering method, we plot the energy of the high frequency according to the cut-off wavelength (Figure 58) and the cut-off frequency (Figure 59). On this last plot, we can see that the curves become linear at 0.4 km^{-1} (2Hz). The noise is estimated from the slope of each straight line. The last two points of each curve are used for the computation of the slope. Results are summarized in Table 5.

	Envisat 20Hz	**Jason 20Hz**
Mean of SWH (m)	2.77	2.71
Noise estimated by high pass filtering method, deduce from the slope (cm)	9.2 (2.1)	7.3 (1.6)
Noise estimated by spectral analysis, deduced from the slope (cm)	9.5 (2.1)	7.3 (1.6)

Table 5 : Noise estimation of $SLA_{nc/mss}$ using 20 Hz elementary data

6.2.2. Geographic distribution

The geographic distribution of this high frequency signal is mapped on Figure 60 for ENVISAT and Figure 61 for Jason. Each box contains the standard deviation of the high frequency signal in a 4°x4° bin. As expected, there is a strong correlation with the SWH (Figure 62). Figure 63 shows the difference between the two standard deviation maps. The ENVISAT standard deviation is larger than the Jason one almost every where.

6.3. ANALYSIS ON 1HZ DATA

6.3.1. Global results

Figure 65 shows the 1Hz ENVISAT spectrum. With 1Hz data fewer samples are available than with 20Hz data. The accuracy is then reduced and it makes the spectrum noisier. There is a sort of small plateau at 0.3Hz. But it is not enough pronounced to assert that it is a white noise signature. From the 20Hz study, it can be stated that it is not white noise. But assuming it was the case, the standard deviation corresponding to the plateau would be 3.2 cm. The ERS-2 (Figure 66) spectrum gives higher results: the standard deviation corresponding to the plateau would be 5 cm which is much higher than the ENVISAT value. On the Jason spectrum (Figure 66) the plateau is still less visible. The standard deviation corresponding to the plateau would be 3.9 cm.

As previously, the energy of the high frequency is plotted according to the cut-off wavelength (Figure 67) and the cut-off frequency (Figure 68). With 1Hz data, no linear trend is visible. It confirms that we cannot estimate a white noise on 1Hz data. Calculating a slope is not meaningful with 1 Hz data. We can only calculate the standard deviation of the high pass filtered signal.

	Envisat **Cycle 11**	**ERS-2** **Cycle 79**	**Jason** **Cycle 31**
Number of points $\sigma(HF[SLA_{nc/mss}])$ (cm) (using a 3 points cut-off wave length)	294416 1.61	-	429749 2.11
Noise of $SLA_{nc/mss}$ estimated by spectral analysis (cm)	3.2	5.0	3.9

Table 6 : HF energy and noise estimation of $SLA_{nc/mss}$ using 1Hz data

Table 6 summarizes the results. As expected, the results obtained with the high pass filtering method are lower than those obtained by spectral analysis. But the two methods show the same tendency: 1Hz ENVISAT high frequency content is lower than Jason, while opposite results are obtained with 10 Hz data. It is not consistent.

Figure 69 and Figure 70 illustrate this problem. These plots show the HF[$SLA_{nc/mss}$] at 20Hz (red) and 1Hz (blue) according to latitude on Jason and ENVISAT particular passes in the Pacific ocean. Unlike at 20Hz, the 1Hz Jason signal is visually and statistically more energetic than the ENVISAT one: it has larger peaks all along the pass, and seems strongly noisy at several times like for example at -16° of latitude.

In order to explain these differences, one should consider the ENVISAT and Jason compression algorithms, that is to say the computation of 1Hz averaged measurements from 20Hz elementary data. These algorithms are not the same due to different regression methods. Moreover, an anomaly has been detected in the Jason algorithm. It has been recently corrected and improved by adding the MQE criteria (P Thibaut, Jason SWT, New Orleans, October 2002). Reprocessed Jason data will be soon available and this analysis will have to be performed again. It would also be interesting to compare the ENVISAT and Jason 1Hz signals, computed with the same compression algorithm.

6.3.2. Distribution

6.3.2.1. Geographic distribution

The geographic distribution of this high frequency σ(HF[$SLA_{nc/mss}$]) is mapped on Figure 71 for ENVISAT and Figure 72 for Jason. Each box contains the standard deviation of the high frequency signal in a 4°x4° bin. Figure 73 shows the difference between the two standard deviation maps. The ENVISAT standard deviation is lower almost every where, especially in the wet areas.

6.3.2.2. As a function of SWH

Figure 74 and Figure 75 show the scatter plot of σ(HF[$SLA_{nc/mss}$]) according to waves. On the ENVISAT plot, we see clearly the wave dependency whereas on Jason there are strong HF values even for low waves.

7. OTHER INVESTIGATIONS

7.1. ANOMALOUS MEASUREMENTS AFTER AN INSTRUMENTAL EVENT

High SSH-MSS (>1m) have been found on data delivered just after an instrumental event. Two examples illustrate this problem:

➢ May the 5th 2003

Passes 191 to 215 are missing due to a known SEU failure (RA-2 to reset wait). SSH-MSS on pass 216 is plotted on Figure 38 and Figure 39. The first data delivered are in red on the map and gradually decreases to reach usual values. At 43° latitude, the difference between Envisat and ERS-2 is greater than 1m. After 1 minute and 40s, this difference is much lower. The altimetric parameter SWH and Sigma0 seem to be ok on this pass (see Figure 40 and Figure 41).

➢ May the 11th 2003

Passes 361 to 387 are missing due a TM format error (RA-2 to suspend) After the RA-2 recovery (see Figure 42 and Figure 43), about 20 anomalous measurements are delivered (over Med. sea). Then the satellite flies over Africa and no ocean data is available. Finally, standard measurements are again available (over South Atlantic). So the anomaly disappears after a few minutes (~2) somewhere over Africa.

Conclusion:

- This is not a thunderstorm or physical effect (it would be visible on ERS-2)
- It doesn't come from corrections (They are not applied here)
- The drop observed doesn't look like an orbit error
- It is connected to Ra-2 events
- Only the range seems to be suspicious.

Investigations have been carried out at ESA. The result of this analysis is that the instrument needs a certain time to stabilise, in particular because of the USO (ultra stable oscillator). This has of course a direct impact on the range measurement. The range is compensated for the USO correction in the Level 1b, but only on average value (over ~100 minutes). Therefore the correction is smooth and can not account for peak values just after anomalies.

7.2. RAIN FLAG ASSESSMENT

A new rain flag algorithm has been implemented in the last IPF/CMA version. This preliminary analysis aims at assessing the rain flag quality.

As it can be seen in Table 7, the rain flag impacts a large amount of points. Most of these points are not edited by the classic altimeter and radiometer editing criteria. So this flag bring some new information on the data quality. Using the rain flag in the editing procedure would reduce by about 1% the number of valid points.

	Cycle 16	Cycle 17
Number of rain-flagged points on the full data set	14141	13087
Number of rain-flagged points on the valid data set	11389	10656
Number of rain-flagged points on the valid data set / valid points	1.14%	1.02%

Table 7 : Number of rain-flagged points

Figure 76 and Figure 77 allow us to compare the rain-flagged points over ocean with the map of edited measurements. Note that measurements impacted by S-band anomaly have been removed. Wet areas signature is visible on both maps but the density is higher on the first one. Moreover some regions, like mid latitude in Atlantic Ocean, are almost exclusively edited by the rain flag. At mid and high latitude more than fifty consecutive points can be rain flagged. Figure 78 and Figure 79 show 2 examples of SSH-MSS on Envisat and ERS-2 on pass segments where the rain flag is set on. In the first case, the rain flag seems to be efficient: between -23 and -29 deg of latitude, the altimetric signal is disturbed on both satellites. In the second case, Envisat is rain flagged between 49 and 55 deg of latitude whereas the 2 SLA seem consistent.

Table 8 shows the impact of using the rain flag on the performances. It slightly improves the performances:

	Cycle 16		Cycle 17	
	Without rain flag	With rain flag	Without rain flag	With rain flag
Crossover standard deviation	9.49	9.45	9.31	9.28
SSH-MSS standard deviation	10.87	10.83	10.60	10.56

Table 8 : Impact of the rain flag on performances

<u>Conclusion:</u>

Using the rain flag in the editing procedure would have a significant impact: 1% of our actual valid data-set would be removed. Using this flag slightly improve the performances at crossover and along-track. More cycles are needed to assess it more precisely.

8. CROSS CALIBRATION

Comparisons with ERS-2 and Jason-1 have been performed by computing, on one hand, along track residuals between ERS-2 and ENVISAT and, on the other hand, crossovers between Jason and ENVISAT. Indeed, ENVISAT and ERS-2 have the same ground track and the time difference between both satellites is about 28 minutes.

8.1. CROSS CALIBRATION WITH JASON-1

Jason-1 GDR cycles 46 to 58 have been used for this analysis. Three types of cross-calibration method have been performed. First, Envisat and Jason-1 are compared using dual crossover. Then an orbit error computation allows us to qualify the big wave length differences. Finally performances of Envisat and Jason-1 are compared on the same space/time sampling.

8.1.1. [Envisat - Jason-1] dual-crossovers

Dual crossovers are computed with a 1 and 3 hour time lag for altimeter and radiometer parameters, and a 10-day time lag for SSH differences in order to reduce geophysical variability. Figure 80 shows the number of crossover points for cycle 15 to 18. There are more available crossover points at the end of the period which is due to the better availability of the Envisat data. Moreover the number and the location of dual crossovers vary with a 120 day period. Indeed Envisat is heliosynchronous contrary to Jason-1.

8.1.1.1. SWH and SIGMA0 comparisons

Figure 81 show the [Envisat – Jason-1] Ku SWH differences at 1H/3H crossovers. There is a good consistency between the 2 satellites. The global SWH mean value is around 14.5/15.5 cm, Envisat being higher than Jason. The standard deviation is 22.2/28.3 cm.

Figure 82 shows the [Envisat – Jason-1] Ku Sima0 differences at 1H/3H crossovers. There is a good consistency between the 2 satellites. The global mean value is -2.9/-2.9 dB and the standard deviation is 0.2/0.4 dB. Jason-1 Ku-band sigma0 is strongly higher than Envisat. Envisat Ku-band sigma0 has been aligned on ERS-2 to satisfy the MWC wind model. Notice that Jason-1 Ku-band sigma0 is 2.3 dB higher than TOPEX. This difference is described in (Vincent et al., 2003).

8.1.1.2. Ionosphere and troposphere comparisons

Figure 83 and Figure 84 shows the [Envisat – Jason-1] dual and DORIS ionosphere correction differences at 1H/3H crossovers. In average, the absolute value of the Jason-1 dual ionospheric correction is 1 cm higher than Envisat. Jason-1 is flying 530 km above Envisat. The electron content between 800 and 1330 km is low but explains a large part of this difference.

Figure 85 shows the [Envisat – Jason-1] radiometer correction differences at 1H/3H crossovers. There is a good consistency between the 2 satellites. The global mean value is 0.6/0.6 cm and the standard deviation is 0.8/1.1 cm.

8.1.1.3. SSH comparisons

SSH comparisons have been computed on dual-crossover differences with a 10-day time lag. The following table summarises the corrections used on the two satellites for SSH computation in the initial configuration:

initial configuration	**ENVISAT**	**JASON**
Orbit	CNES (product)	CNES (product)
Range	product	product
Inverse barometer	time varying pressure (product)	time varying pressure (product)
Dry troposphere	product	Product
Wet troposphere	ECMWF (product)	ECMWF (product)
Ionosphere	Dual Frequency (product)	Dual Frequency (product)
SSB	Non parametric (product)	Non parametric (product)
Ocean tide	GOT99 (updated)	GOT99 (product)
Earth tide	product	product
Pole tide	product	product

Table 9 : Parameters used to compute SSH for ENVISAT and Jason.

Figure 86 shows the [Envisat – Jason-1] mean and standard deviation SSH differences. Envisat measures 26 to 27 cm higher than Jason-1 depending on the selection. The standard deviation is stable when the latitude, the bathymetry and the variability are selected. Using the model troposphere correction does not change the results.

The maps of mean and standard deviation [Envisat-Jason-1] SSH differences at crossover from cycle 15 to 18 are on Figure 87. There are systematic differences which locally overtakes 4 cm. They are probably due to geographically-correlated orbit errors (South-East pacific, South Atlantic) and a different behaviour in wet areas (Indonesia). The map of standard deviation crossover differences on shows usual results with high variability areas linked to ocean variability.

8.1.2. Long wave length error reduction

The Envisat long wave length error has been computed by global minimization of 10-day (EN-J1) SSH differences. The method is described in (Le Traon et al., 1998).

The mean and standard deviation of the long wave length error have been computed for cycle 15 to 18. The maps are plotted on Figure 88. The geographical patterns of the mean are consistent with the [Envisat-Jason-1] SSH mean differences. The long wave length error variability ranges from 2 cm to 5 cm in South East Pacific.

Figure 89 shows the [Envisat – Jason-1] mean and standard deviation SSH differences using the adjusted long wave length error on Envisat. As expected the 26 cm bias (which is not due to orbit error) disappear and the standard deviation is reduced by 0.6 cm witch corresponds to 3.1 cm rms. This reduction is quite stable over the 4 cycle of data.

The maps of mean and standard deviation [Envisat-Jason-1] SSH differences at crossover from cycle 15 to 18 using the adjusted orbit error on Envisat are in Figure 90. Most of the systematic differences visible on the mean SSH differences before correction are not visible on this map. But some differences greater than 2 cm appear near the Mexico coast for example.

8.1.3. Performance comparisons on same time/space sampling

It is interesting to compute statistics from the same geographic area and from the same time period, since both satellites should give comparable general results. To compare the 2 satellites from the same geographical area, a selection on latitude (-66°S < latitude < 66°N) is applied on Envisat. The time periods are the periods corresponding to Envisat cycles. For each Envisat cycle, Envisat and Jason-1 performances are analysed between the date of the first and the last Envisat available measurement. Note that the number of Envisat measurements is lower than Jason-1 one due to product Envisat unavailability.

8.1.3.1. Crossover

The objective is to compare the long term monitoring of Envisat and Jason-1 crossover performances. In order to compare performances, SSH crossovers have been interpolated with a spline tension equal to 0. Therefore the SSH is not filtered along track. Areas with shallow waters have been removed (bathy<-1000m).

Performances at crossovers are compared, for the two satellites on Figure 91. The number of Jason crossover points is strongly greater than the Envisat one. Indeed a lot of Envisat pass are missing. Moreover, the density of Jason-1/Jason-1 crossovers is higher than the Envisat/Envisat one between 50° and 66° because of the orbit inclination .The mean of Envisat/Envisat and Jason-1/Jason-1 SSH difference at crossovers are respectively 0.9 cm and 0.3 cm. The standard deviation of Envisat/Envisat and Jason-1/Jason-1 SSH difference at crossovers are respectively 7.7 cm and 7.6 cm. Performances are slightly better on Jason-1 except for cycle 18.

A more accurate comparison can be made applying a selection on latitude (-50°S < latitude < 50°N) on both Envisat and Jason-1 data. Cycle by Cycle statistics are in Figure 92. The number of Envisat crossover points is closer to Jason-1 one especially for cycle 18. There is a very slight change on the mean. The standard deviation of Envisat/Envisat and Jason-1/Jason-1 SSH difference at crossovers are respectively 6.7 cm and 6.8 cm. With this additional selection, the standard deviation is now lower for Envisat.

To conclude, the Envisat performances at crossover are very close to Jason-1 ones. Systematic ascending/descending bias is greater on Envisat but standard deviation is comparable.

8.1.3.2. SLA

Figure 93 shows the [Envisat – Jason-1] number of points, mean and standard deviation of along track Sea Level Anomaly relative to MSS CLS01V1. The mean of Envisat and Jason-1 are respectively 43.5 cm and 16.8 cm. The difference of the means [Envisat-Jason-1] is quite stable, about 26.7 cm. This is consistent with the [Envisat-Jason-1] SSH difference bias estimated at crossover. The standard deviation of Envisat and Jason-1 are respectively 9.5 cm and 9.6 cm The Envisat SLA performances are slightly better than Jason-1 ones.

8.2. CROSS CALIBRATION WITH ERS-2

To perform the comparisons with ERS-2, OPR cycles (version 6.4) from CERSAT centre have been used. Each ERS-2 cycle (from 83 to 86) has been processed as described in the ERS-2 Quality assessment reports (Mertz et al., 2003). All the necessary updates were performed on ERS-2 data to be homogeneous with the Envisat data set. Envisat and ERS-2 data are collocated by repeat track analysis in order to compare the main relevant parameters. In this part, the day by day means and standard deviations are reported.

8.2.1. Particular events

During cycles 15 to 18 Envisat, some events occurred on the two satellites leading to missing measurements in the data sets, as shown on Figure 94, which is the number of collocated points for each day.

- 6 days of data are missing on ERS-2 (8 to 14th May 2003) due to a manoeuvre.
- Data from 17th to 20th May are missing because of RA-2 unavailability, MWR switch-off, S-band anomaly on Envisat and manoeuvre, edited measurements on ERS-2.
- Due to the failure of the ERS-2 Low Bit Rate register on June 22nd 2003 (end of cycle 85), ERS-2 data are only available in the visibility of ESA ground stations (over Europe, North Atlantic, the Arctic and western North America).

The outcome of the last point implies that from cycle 18 onwards, the cross calibration can be performed only on a reduced zone. Then, the differences between Envisat and ERS-2 will not be homogeneous before cycle 18 and after this cycle.

8.2.2. SWH and SIGMA0 comparison

The global mean difference of significant wave height is -21.7 cm and the standard deviation is 26.7 cm. ERS-2 measures lower SWH than Envisat. For each cycle, the scatter plot shows a good consistency between the two parameters, nevertheless, the differences are higher in strong SWH geographical areas (Figure 94 and in Figure 95).

Figure 97 shows the mean and standard deviation of (ERS-2 - Envisat) SWH differences for each day. Except the particular situation of cycle 18, there is no specific behaviour in the differences.

The mean difference of backscatter coefficient is 0.05 dB and the standard deviation is 0.3 dB. Note that the ERS-2 SIGMA0 has been corrected for a +0.25 dB bias as described in Dorandeu, 2000. Figure 96 is the histogram of ERS-2 Sigma0 for cycle 79: two main peaks and many secondary peaks are present in the distribution of the Sigma0 values for ERS-2. Although the Envisat Sigma0 histogram is better than ERS-2 one (Figure 16), two secondary peaks appear on each side of the mean, no explanation can be given at this time. From the daily mean and standard deviation differences (Figure 98), no special behaviour can be detected.

8.2.3. Radiometer parameters comparison

As described in Labroue 2003, the neural algorithm used to compute the radiometer wet troposphere correction better retrieves the dry troposphere areas than the parametrical algorithm. The algorithm present in the Envisat GDR products is the neural one. ERS-2 data set has then been updated with the neural algorithm proposed by Labroue. Previously, the drift correction of the 23.8 GHz brightness temperature was applied on ERS-2 (Eymard et al., 2003).

The global mean and standard deviation of the (ERS-2 – Envisat) radiometer wet troposphere difference are respectively 0.12 cm and 0.95 cm on cycles 15 to 17 and they are 0.37 cm and 0.81 cm for cycle 18. Figure 99 shows the daily mean and standard deviation values. The values in blue are computed on a reduced geographical zone (Atlantic) contrary to the red ones, the change between the two periods is thus not significant. The global values are stable before 8th May around 0 cm. They increase after 14th May and recover after 23rd May, and another change occurs on 11th June. The 1.8 cm drop observed is linked to the switch-off of the MWR (18 and 19th May) as said in section 8.2.1 since a lapse of time is necessary for the instrument to reach its internal temperature.

Brightness temperatures have also been monitored (Figure 100 and Figure 101). The 23.8 GHz differences are a bit more than 3K before 8th May and around 4K after that date, with a drop up to 6.4 K on 21st (for the same reason as described below). The same behaviour is also observed for the 36.5 GHz differences. The change in the two TBs is noticed in the radiometer parameters, as described in Dedieu et al.: on the residual temperature contribution for 36.5 GHz (figure 5) and on the hot load count for 23.8 GHz (figure 4). It is also confirmed by each daily mean in the TBs for ERS-2 and Envisat (Figure 102). The time series is not long enough yet to conclude about the recovery of the values.

8.2.4. SSH comparison

In order to compare the SSH estimations from the two missions, Envisat and ERS-2 data sets have been updated with similar algorithms and corrections, as described in Table 10.

initial configuration	**ENVISAT**	**ERS-2**
Orbit	CNES (product)	Cycles 15 to 17: DGME-04 Cycle 18 : DPAF
Range	product	SPTR+USO+time tag bias applied
Inverse barometer	time varying pressure (product)	time varying pressure
Dry troposphere	ECMWF (product)	ECMWF rectangular grid
Wet troposphere	ECMWF rectangular grid	ECMWF rectangular grid
Ionosphere	GIM model	GIM model
SSB	Non parametric (product)	BM3 (Gaspar and Ogor, 1996)
Ocean tide	GOT00 (product)	GOT00
Earth tide	product	product
Pole tide	product	Computed

Table 10 : List of parameters used to perform SSH comparisons between Envisat and ERS-2 along track residuals. In yellow, the parameters are in the product.

DGME-04 orbits (Scharoo and Visser 1998) have been updated on ERS-2 products until cycle 85 (corresponding to cycle 17 Envisat). The mean and standard deviation of (ERS-2 – Envisat) SSH difference are -34.6 cm and 5 cm for cycles 15 to 17. Figure 103 shows the mean and standard deviation for each day from cycle 15 to 17 of SSH differences. Except for the dates of the special events, the values are stable. Figure 104 is a map of the differences for one cycle and orbit error signal appears, mainly due to ERS-2.

The variability relative to the CLS01V1 MSS has been mapped for each cycle (see the cross calibration cyclic reports) for ERS-2 and Envisat for the three cycles. Removing shallow waters (1000 m) and areas of high ocean variability (20 cm), the statistics are the following: the mean values are 43.9 cm (Envisat) and 9.27 cm (ERS-2) and the standard deviation values are 9.6 cm (Envisat) and 10.6 cm (ERS-2). In terms of variability, Envisat thus shows good performance.

9. CONCLUSION

7 GDR cycles have been produced since the beginning of the Envisat mission. Cycles 10 to 12 have been extensively analysed during the verification phase. Cycles 15 to 18 have been produced in a new version of IPF/CMA.

For cycle 15 to 18 the data availability is not optimum. 13% of the data are missing in average over ocean. Among the available data, 11% have no MWR correction and 4% are impacted by the S-Band anomaly.

The ENVISAT Ra-2 and MWR data show good general results. Statistics and performances of altimeter and radiometer parameters are consistent with expected values:

- Editing ratios are stable
- Mean of RMS of 20Hz: ~9cm
- The MWR neural algorithm strongly improve the consistency with the ECMWF model
- Standard deviation of SSH difference at crossovers is about 9 cm in open ocean
- The SSH-MSS standard deviation is about 10 cm and the mean is around 43-44 cm in open ocean.

However some anomalies have to be investigated:

- The S-band anomaly needs to be solved or at least flagged in the product
- The waveform-deduced mispointing bias has to be investigated
- The mean (1 cm) of Envisat/Envisat SSH difference at crossover has to be analysed

Cross calibration with Jason-1 confirms these good results. The Envisat and Jason-1 altimeter and radiometer parameters have a good consistency. Performances at crossover and along track on a same time/space sampling are very close. The SSH bias between the two missions is 26.7cm.

Cross calibration with ERS-2 has been performed on cycles 15 to 17 on the whole ocean, contrary to cycle 18 where smaller geographical data set is available for ERS-2. SWH and SIGMA0 show good consistency between the two satellites. The neural algorithm has been updated on ERS-2 to be homogeneous with Envisat and better results are obtained on dry areas. About the SSH, the results on cycle 18 are not comparable to those of previous cycles. A bias of -34.6 cm is obtained over cycles 15 to 17 and it will be useful to perform the long term monitoring on cycles 18 onwards because the geographical coverage will be similar.

GDR cycles 9 to 15 will be soon reprocessed in the last version of IPF/CMA. So, by mid 2004, more than one year of homogeneous Envisat data will be available. This will allow a better quality assessment and more accurate long-term monitoring.

REFERENCES

Dedieu M., Eymard L., Marimont C., Obligis E., Tran N., Envisat Microwave Radiometer assessment reports (cyclic). http://earth.esa.int/pcs/envisat/mwr/reports/

Dorandeu J., F. Mertz and J. Stum 2000: Note on ERS-2 Sigma0 variations since January 2000. August 2000. CLS/DOS/NT/00.286. http://www.ifremer.fr/cersat.

EOP-GOQ and ESRIN PCF team, Envisat Cyclic Altimetry Reports http://earth.esa.int/pcs/envisat/ra2/reports/pcs_cyclic/

Eymard L., E. Obligis and N. Tran, 2003: "ERS-2/MWR drift evaluation and correction", CLS/DOS/NT/03.688

Faugere Y., Mertz F., Dorandeu J., Envisat GDR quality assessement report (cyclic), http://www.aviso.oceanobs.com/html/donnees/calval/validation_report/

Faugere Y., Mertz F., Dorandeu J., Envisat validation and cross calibration activities during the verification phase. Synthesis report. ESTEC contract N°16243/02/NL/FF WP6, May 16 2003

Labroue S. and E. Obligis, January 2003, Neural network retrieval algorithms for the ENVISAT/MWR, Technical note CLS.DOS/NT/03.848

Le Traon P. Y., F. Ogor, 1998: "ERS-1/2 orbit improvement using TOPEX/POSEIDON: the 2 cm challenge." *J. G. Res*., VOL 103, p 8045-8057, April 15, 1998.

Martini A. and P. Féménias, 2000: The ERS SPTR2000 Altimetric Range Correction: Results and Validation. ERE-TN-ADQ-GSO-6001. 23 November 2000.

Mertz F., Faugere Y., Dorandeu J., Envisat GDR cross calibration report (cyclic).

Mertz, F., Y. Faugere and J. Dorandeu, Validation of ERS-2 OPR cycle 083-086. CLS.OC.NT/03.702 issue 083-086. April 17, 2003.

Pontonnier G., M. Ablain, B. Soussi, P. Thibeau, Jason-1 GDR quality assessement report (cyclic), http://www.aviso.oceanobs.com/html/donnees/calval/validation_report/

R. Scharroo and P. N. A. M. Visser : "Precise orbit determination and gravity field improvement for the ERS satellites", *J. Geophys. Res.*, 103, C4, 8113-8127, 1998

Scharroo R., Routines for iono corrections, internet communication to the CCVT community, December 12, 2002

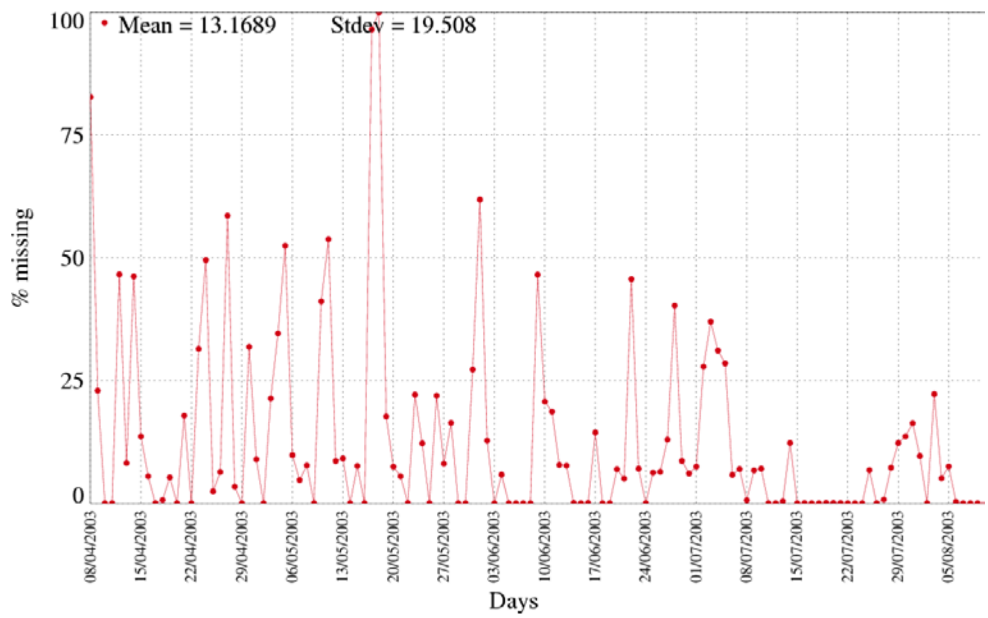

Figure 1 : % of missing measurements relative to a nominal track over ocean

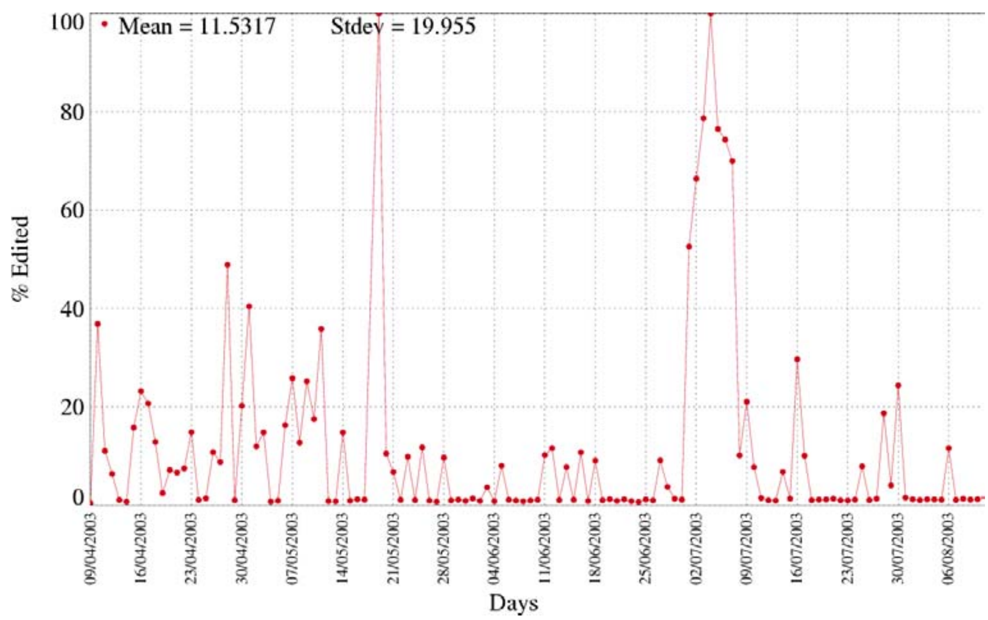

Figure 2 : % of measurements edited by the land/ocean radiometer flag over ocean

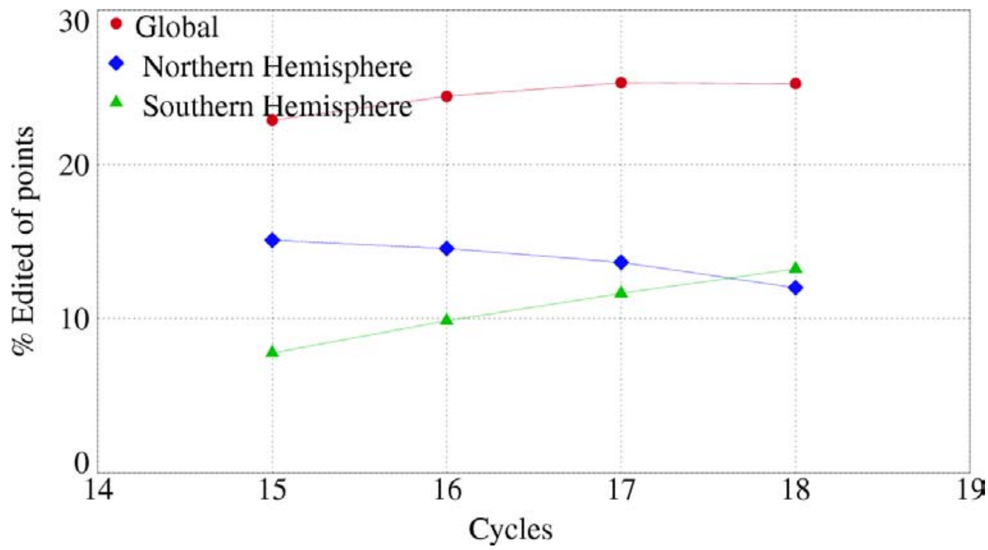

Figure 3 : % of edited points by sea ice flag over ocean

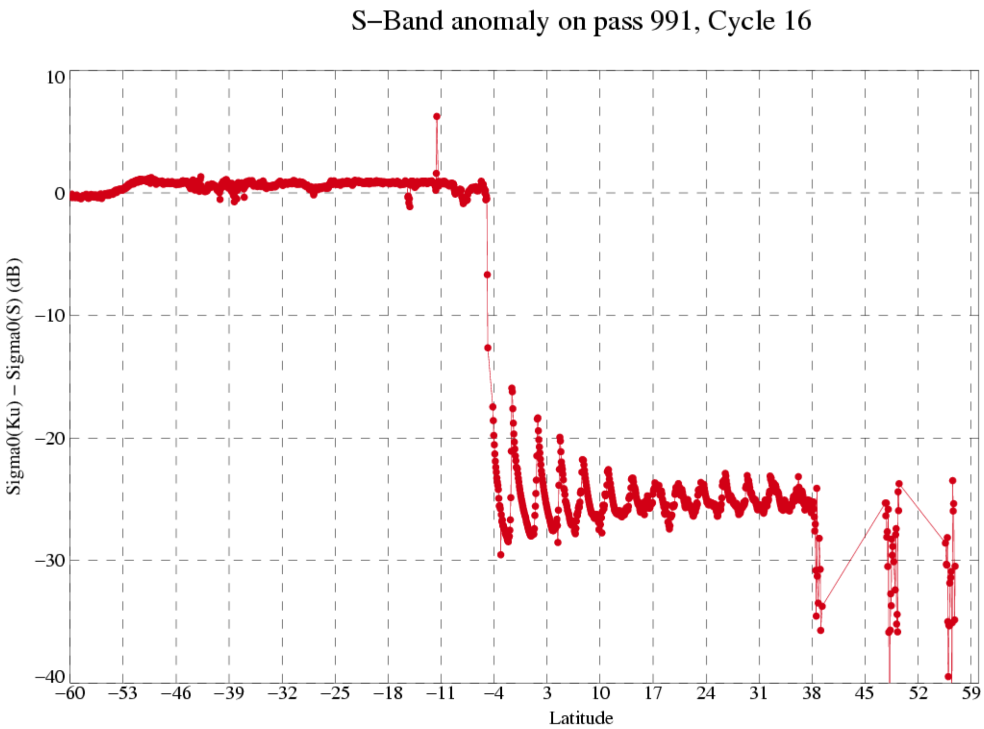

Figure 4 : Starting of an S-band anomaly on pass 991, cycle 16

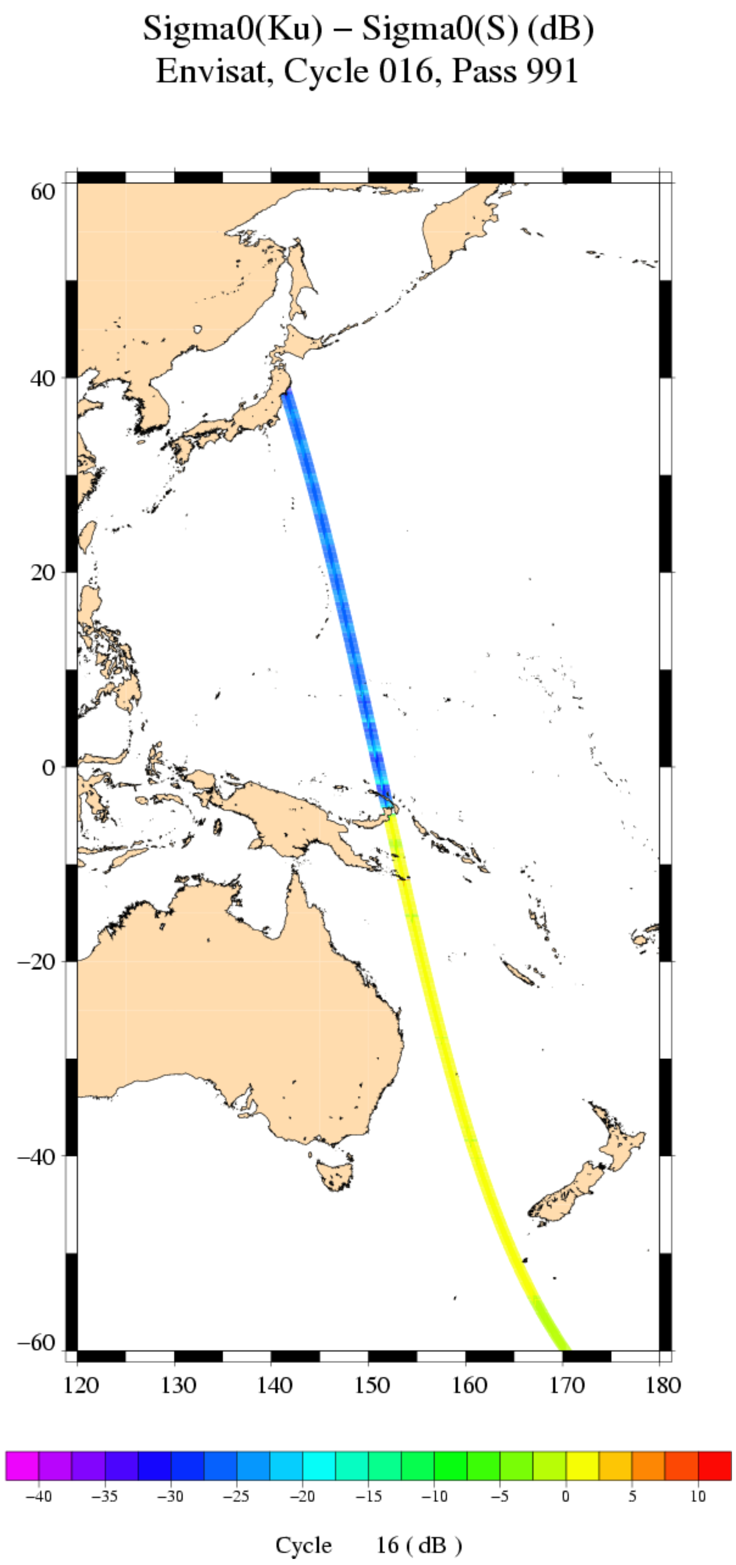

Figure 5 : Starting of an S-band anomaly on pass 991, cycle 16

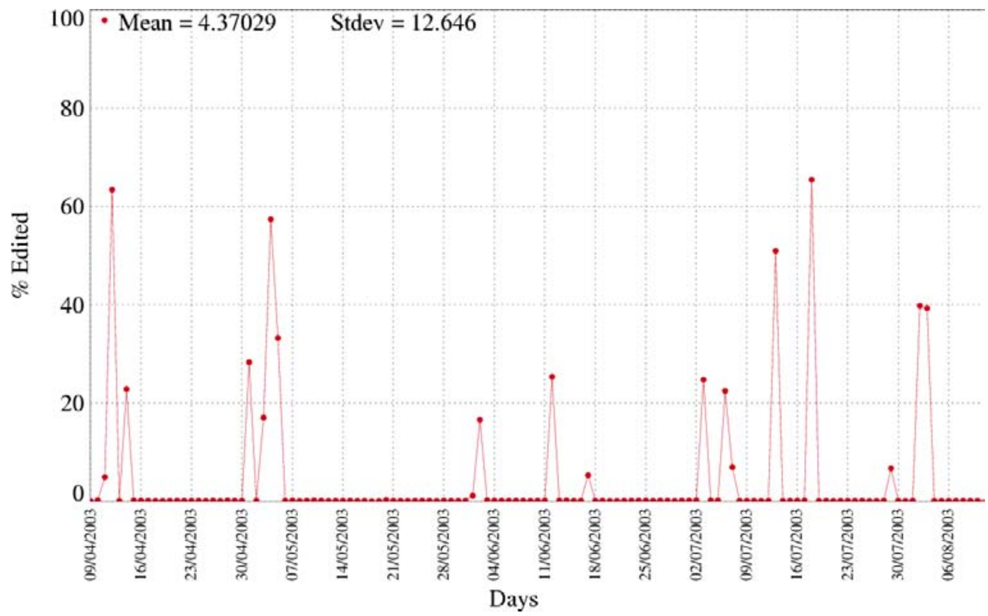

Figure 6 : % of measurements edited because of the S-Band anomaly over ocean

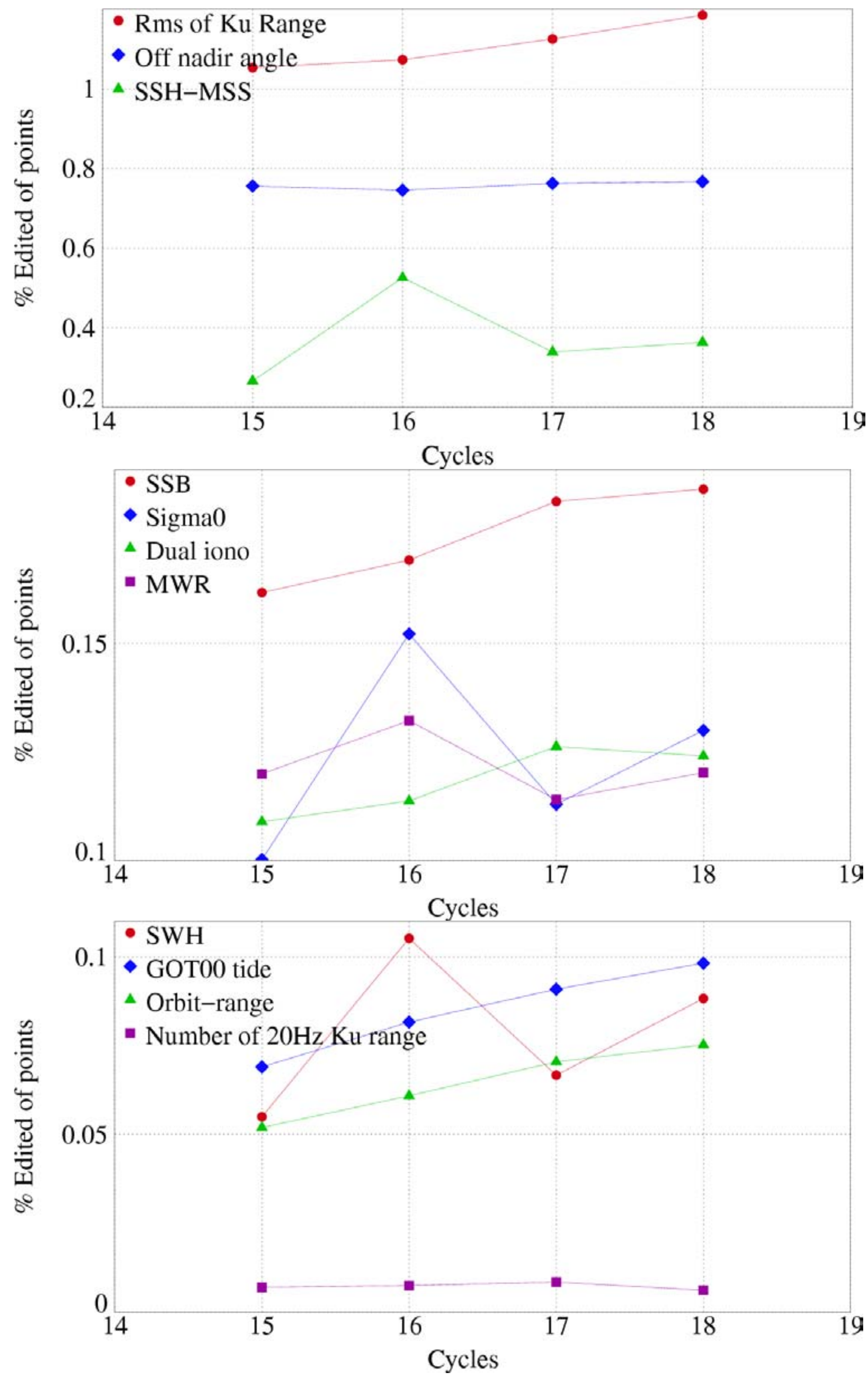

Figure 7 % of edited points by threshold

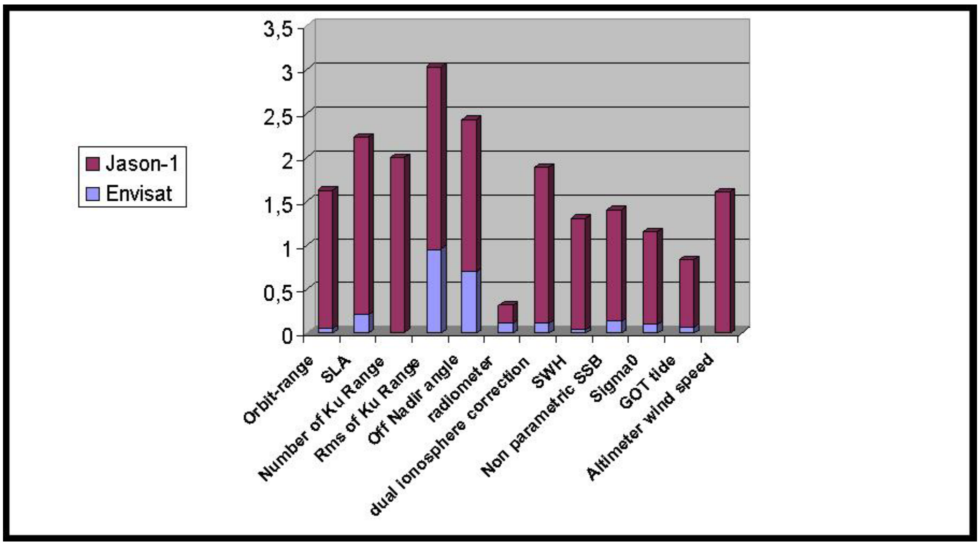

Figure 8 : % of edited measurements on a 10 day period

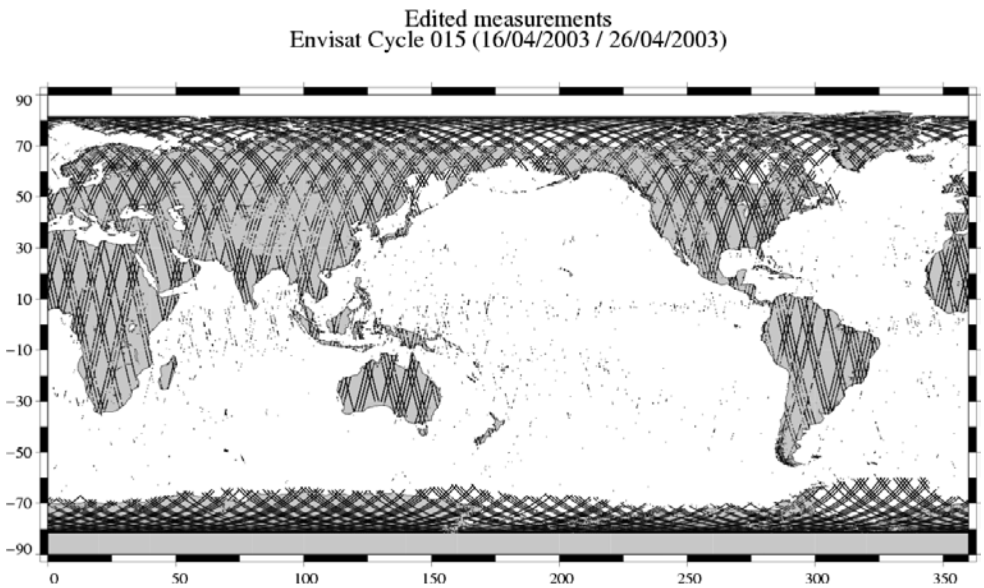

Figure 9 : Map of Envisat edited measurements on a 10 day period

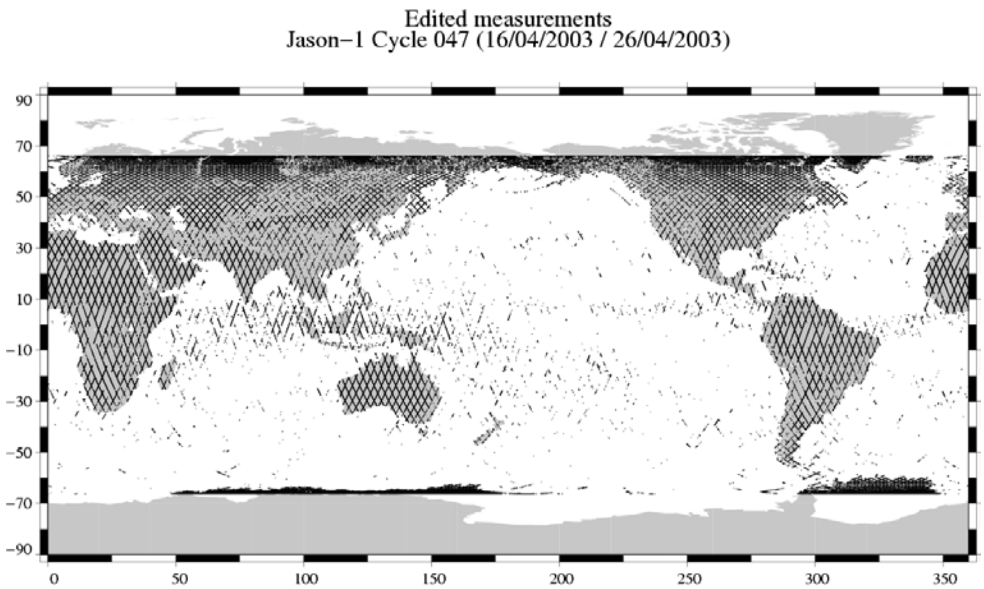

Figure 10 : Map of Jason-1 edited measurements on a 10 day period

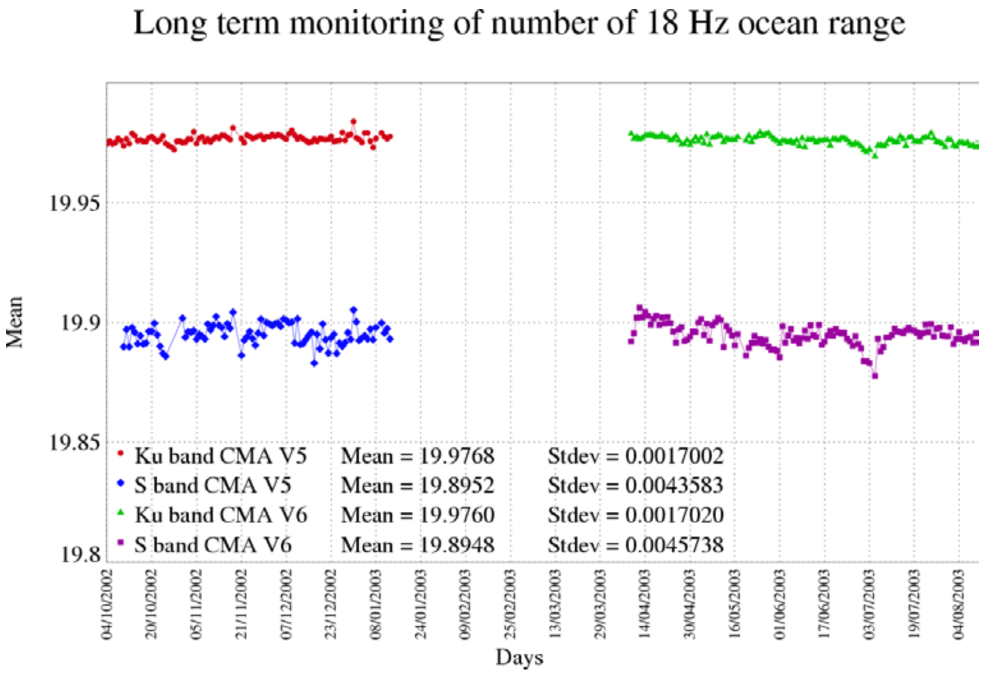

Figure 11 Mean of Number of Ku and S elementary range

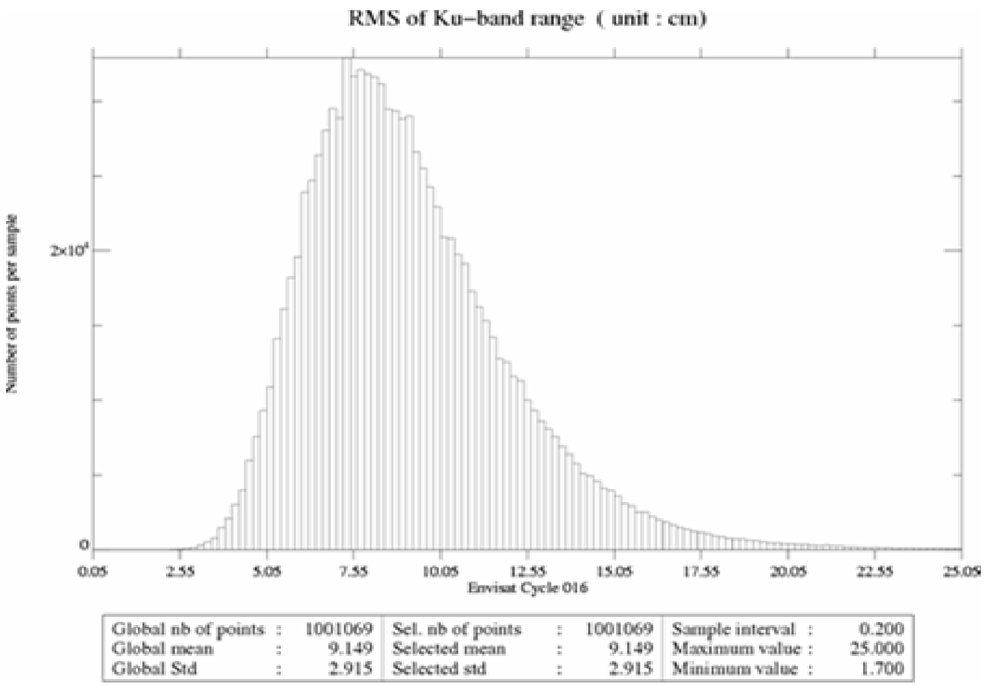

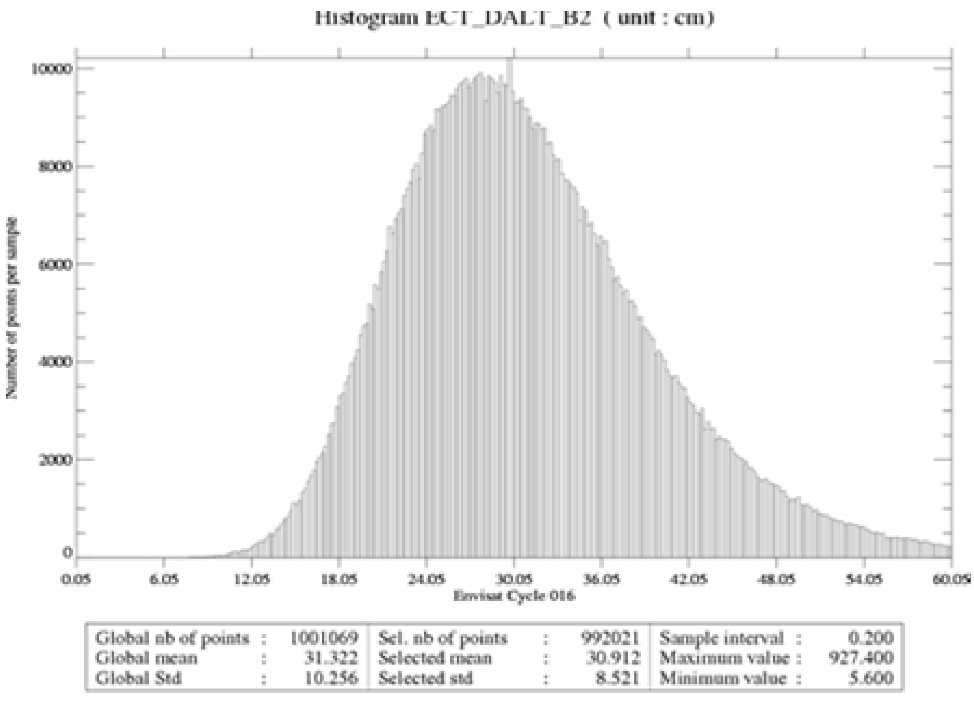

Figure 12 Histogram of RMS of Ku and S range (cm)

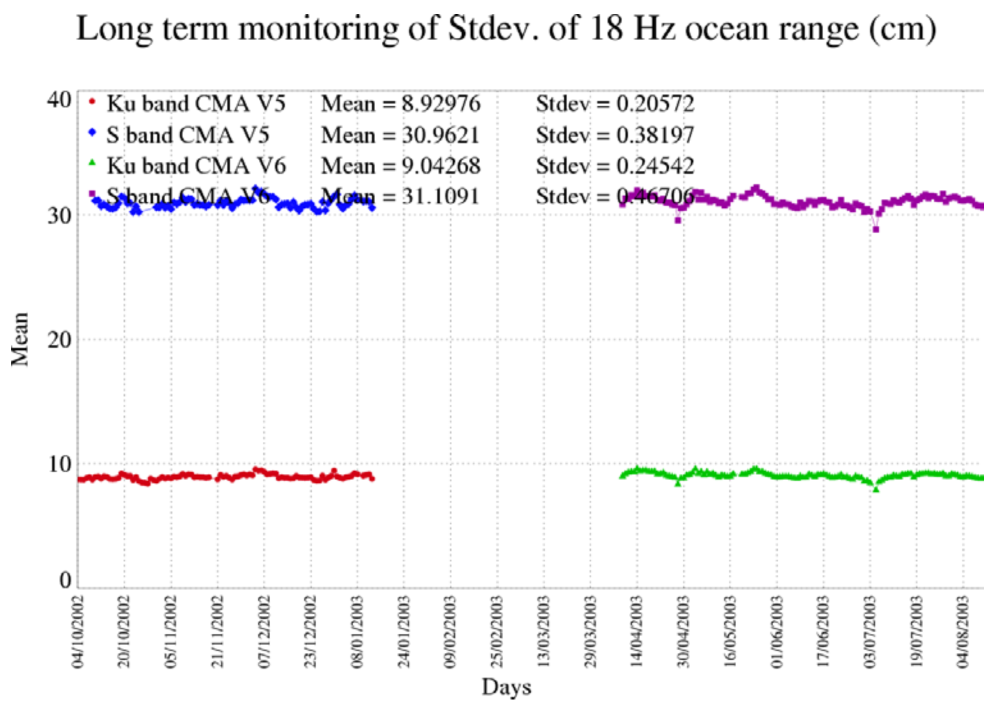

Figure 13 : Mean of RMS of Ku and S range (cm)

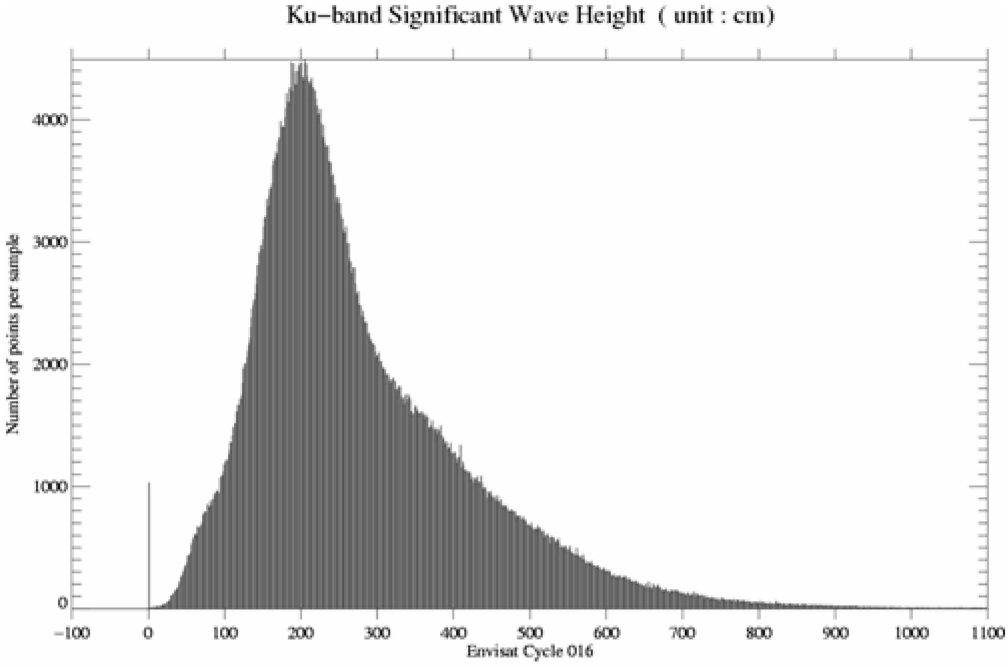

Global nb of points :	1001069	Sel. nb of points	:	1001069	Sample interval :	1.000
Global mean	:	276.312	Selected mean	:	276.312	Maximum value :	1100.000
Global Std	:	140.591	Selected std	:	140.591	Minimum value :	0.000

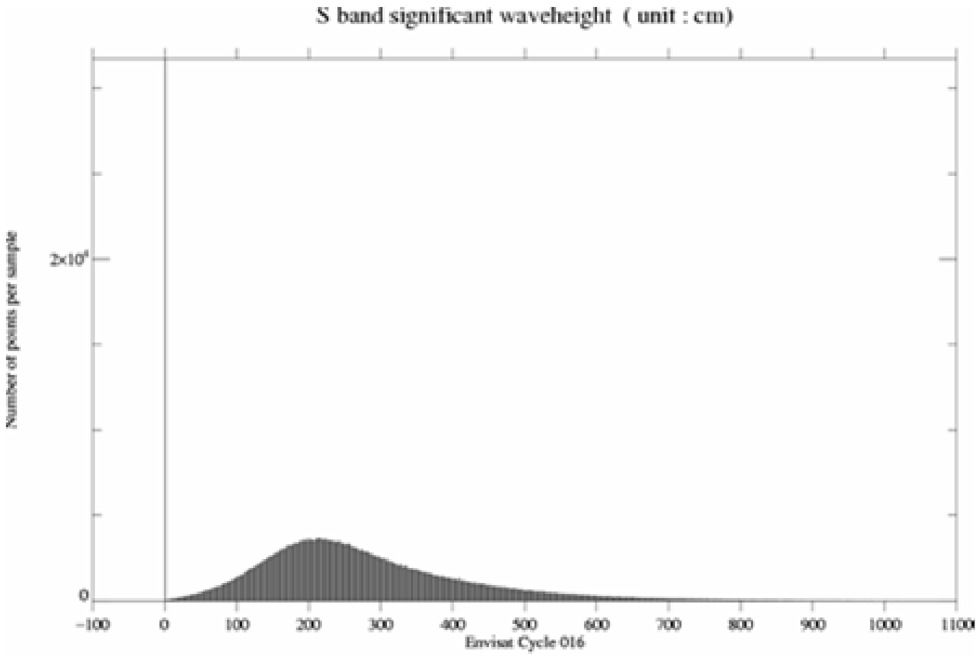

Global nb of points :	1001069	Sel. nb of points	:	1000928	Sample interval :	1.000
Global mean	:	267.097	Selected mean	:	266.951	Maximum value :	2449.200
Global Std	:	144.624	Selected std	:	144.078	Minimum value :	0.000

Figure 14 Histogram of Ku and S SWH (m)

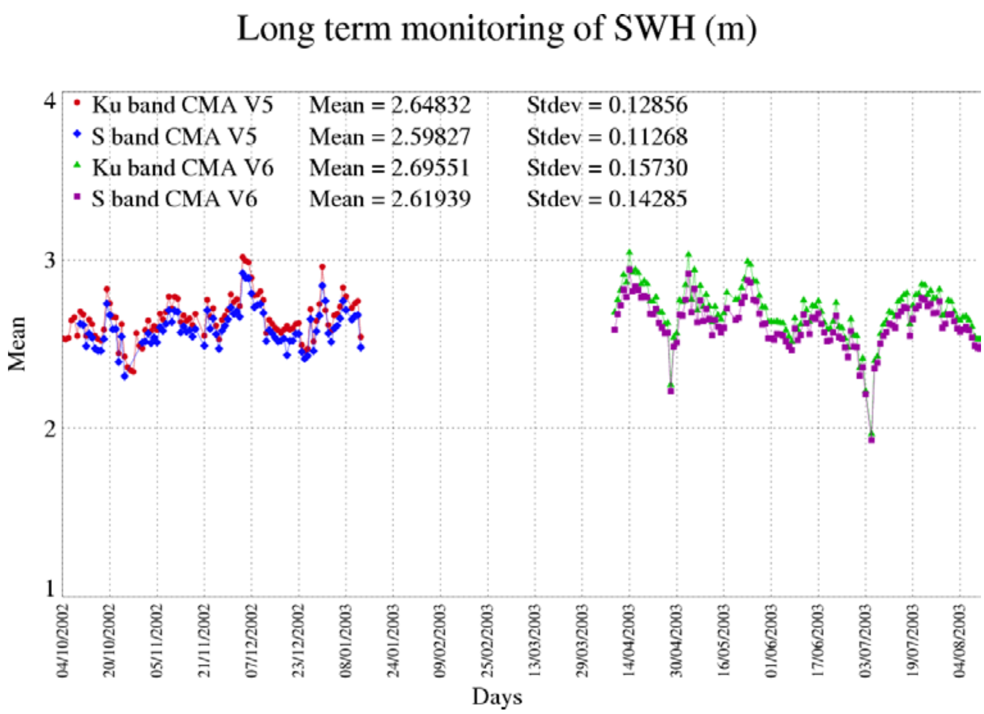

Figure 15 : Mean of Ku and S SWH (m)

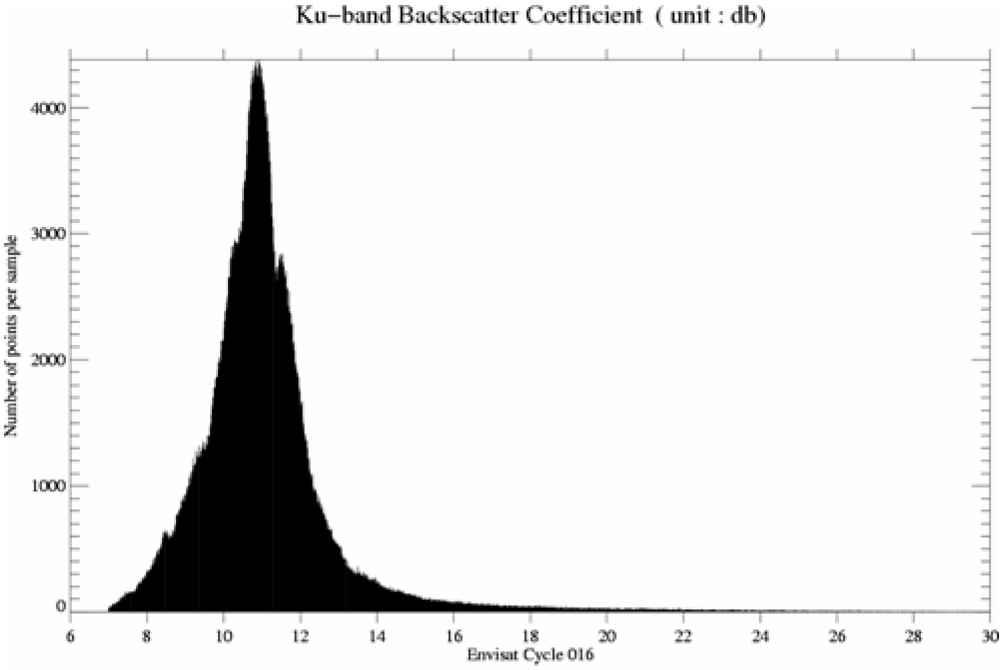

Global nb of points	:	1001069	Sel. nb of points	:	1001069	Sample interval	:	0.010
Global mean	:	11.069	Selected mean	:	11.069	Maximum value	:	30.000
Global Std	:	1.853	Selected std	:	1.853	Minimum value	:	7.000

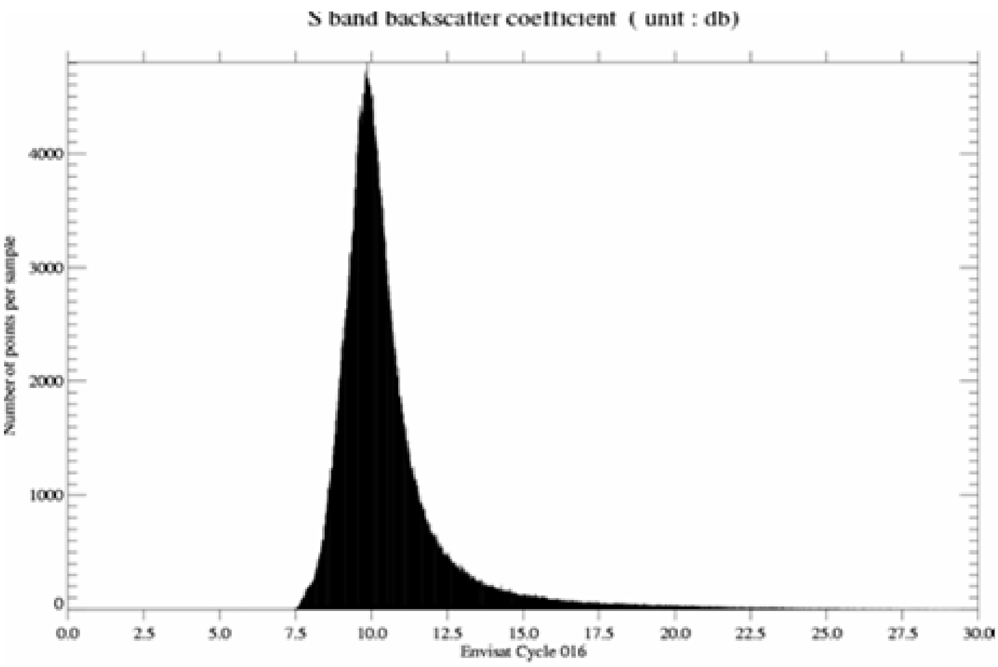

Global nb of points	:	1001069	Sel. nb of points	:	1001056	Sample interval	:	0.010
Global mean	:	10.550	Selected mean	:	10.550	Maximum value	:	31.890
Global Std	:	1.945	Selected std	:	1.944	Minimum value	:	7.270

Figure 16 Histogram of Ku and S Sigma0 (dB)

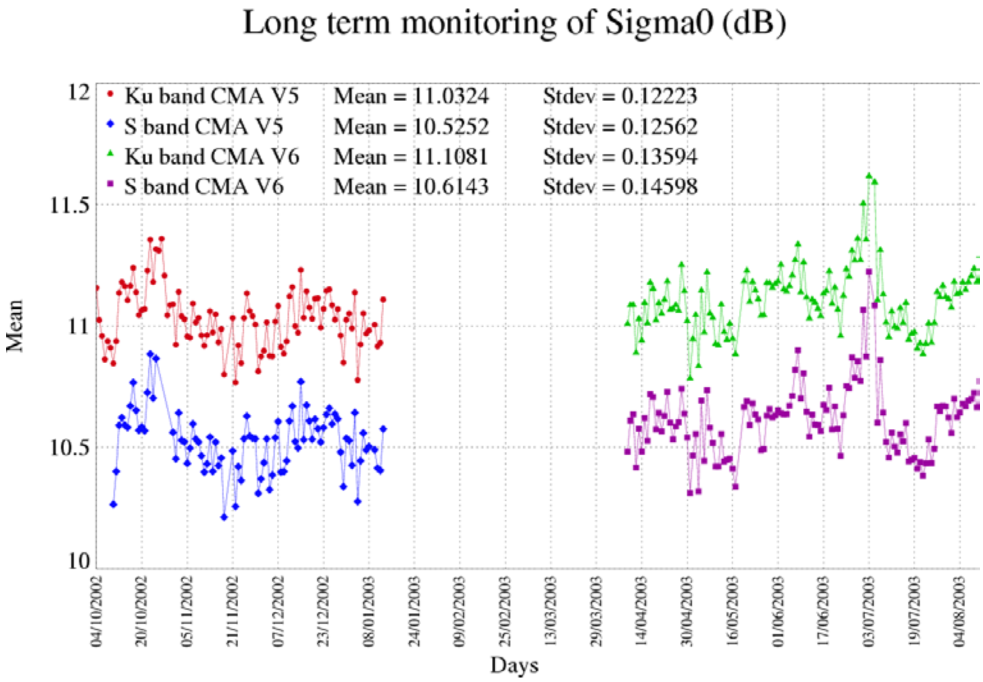

Figure 17 : Mean of Ku and S Sigma0 (dB)

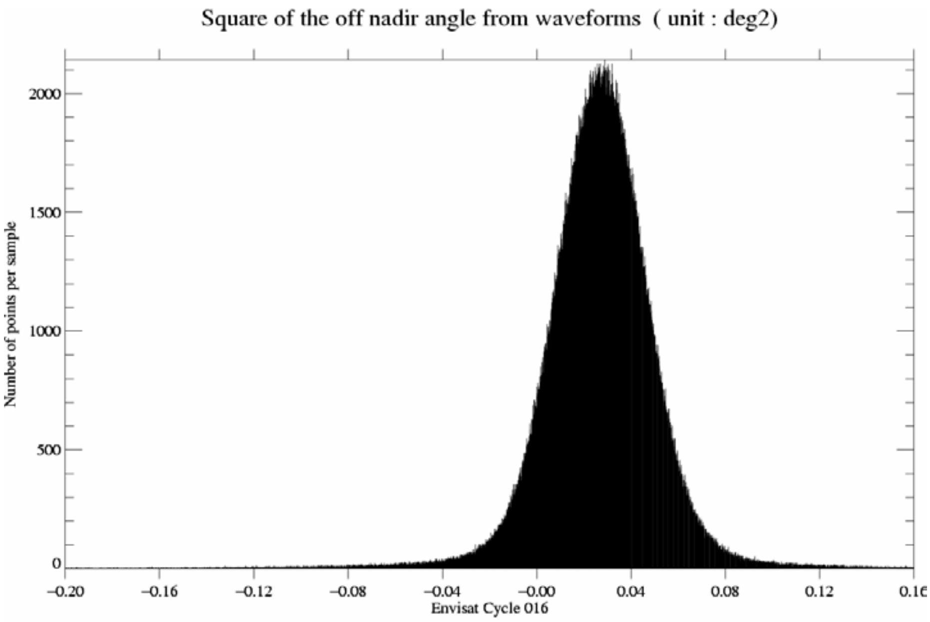

Global nb of points :	1001069	Sel. nb of points :	1001063	Sample interval :	0.000
Global mean :	0.027	Selected mean :	0.027	Maximum value :	0.160
Global Std :	0.025	Selected std :	0.025	Minimum value :	−0.200

Figure 18 Histogram of off-nadir angle from waveforms (deg2)

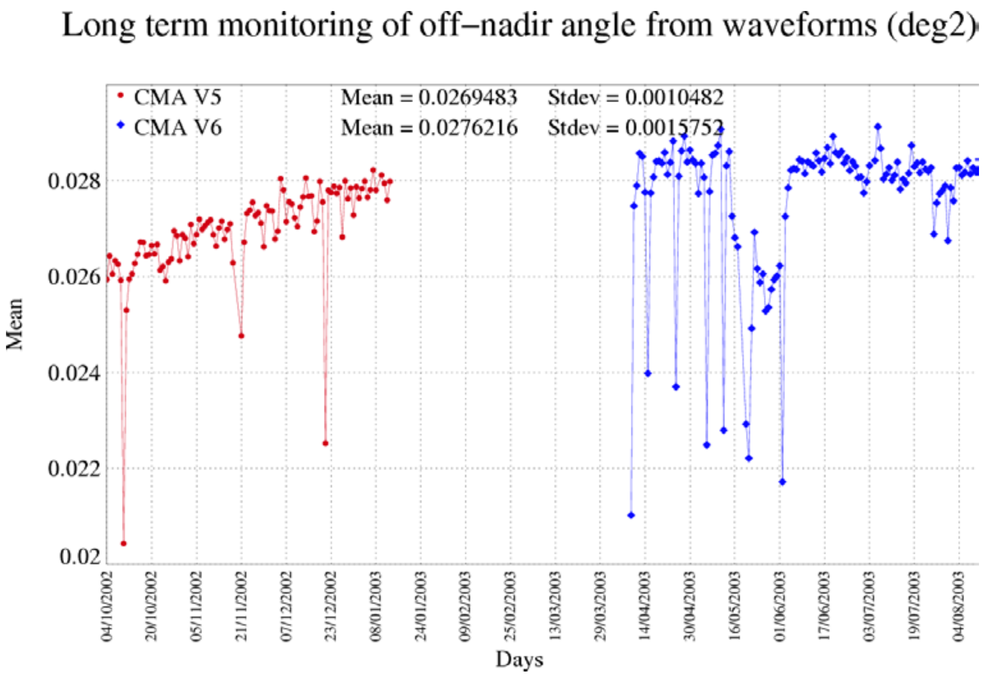

Figure 19 : Mean of off-nadir angle from waveforms (deg2)

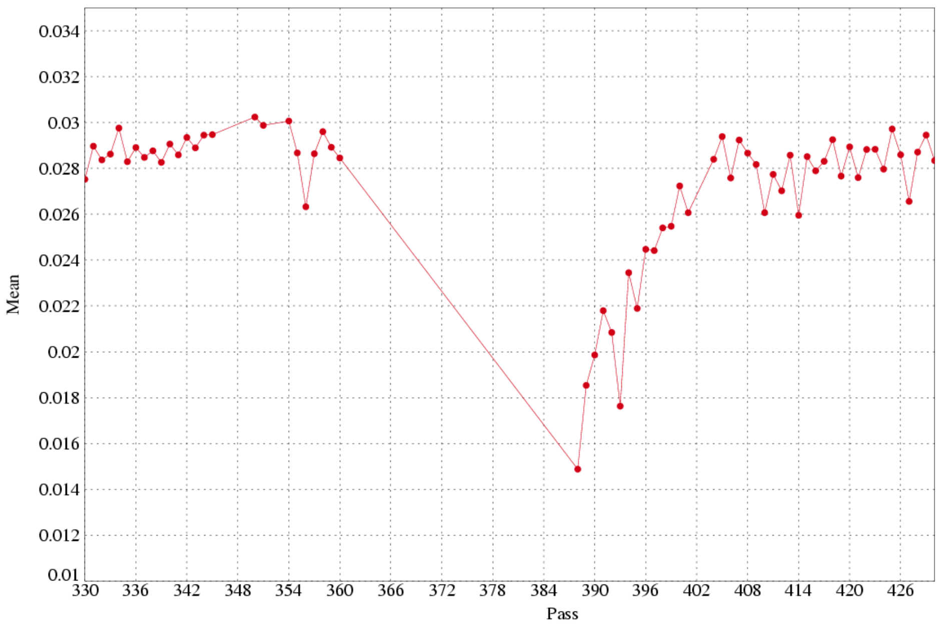

Figure 20 Mean of off-nadir angle from waveforms during the 11th -12th May event (deg2)

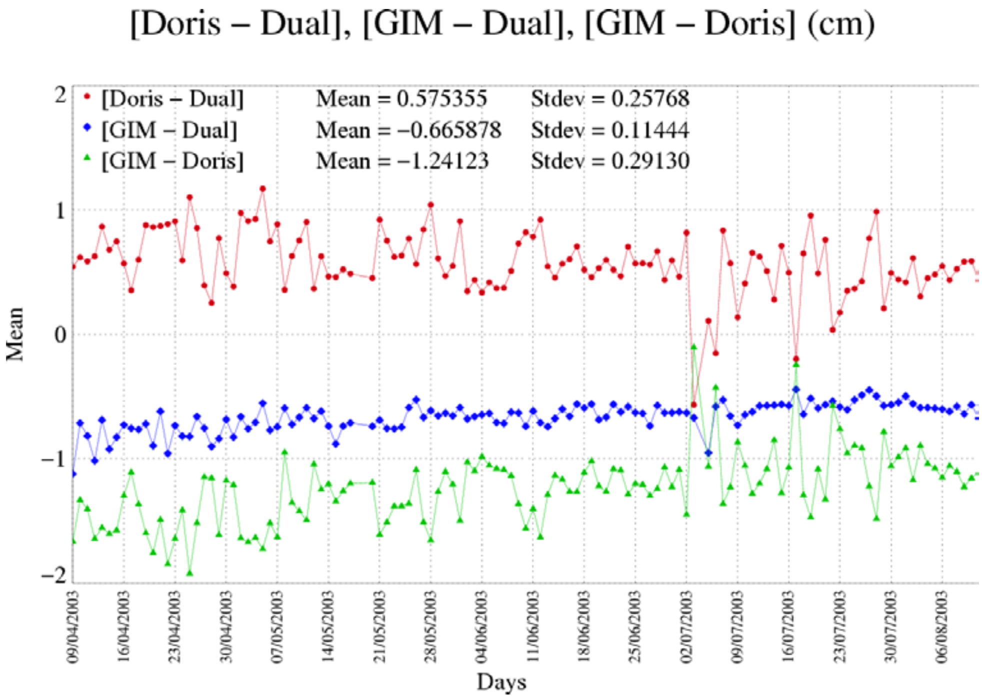

Figure 21 : Mean of [Doris-Dual], [GIM – Dual] and [GIM-Doris] ionospheric correction (cm)

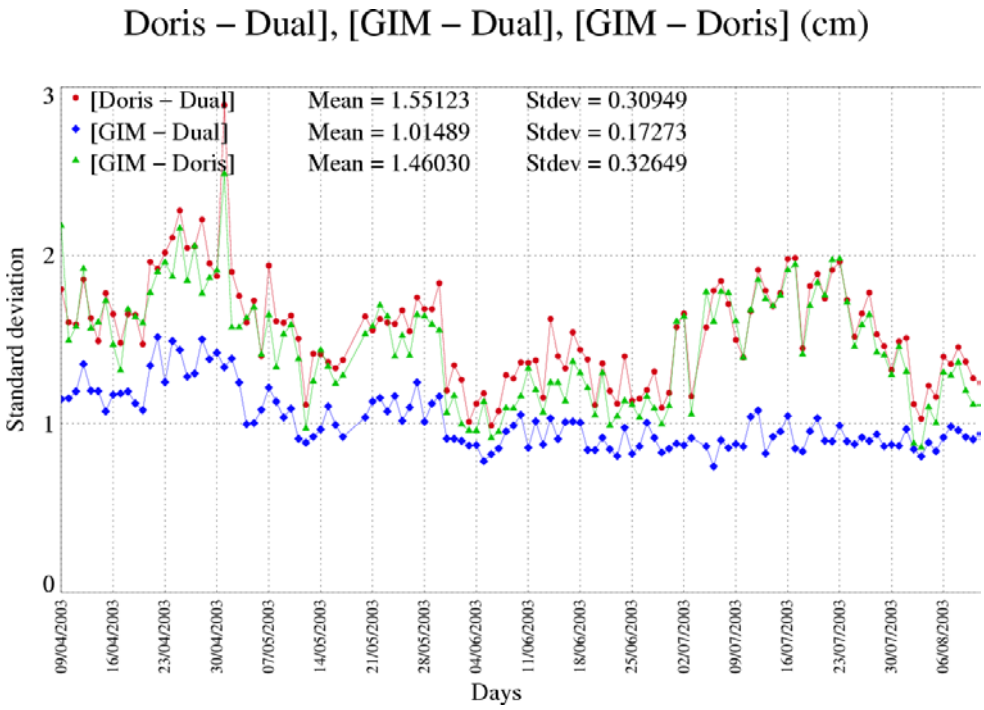

Figure 22 : Standard deviation of [Doris-Dual], [GIM – Dual] and [GIM-Doris] ionospheric correction (cm)

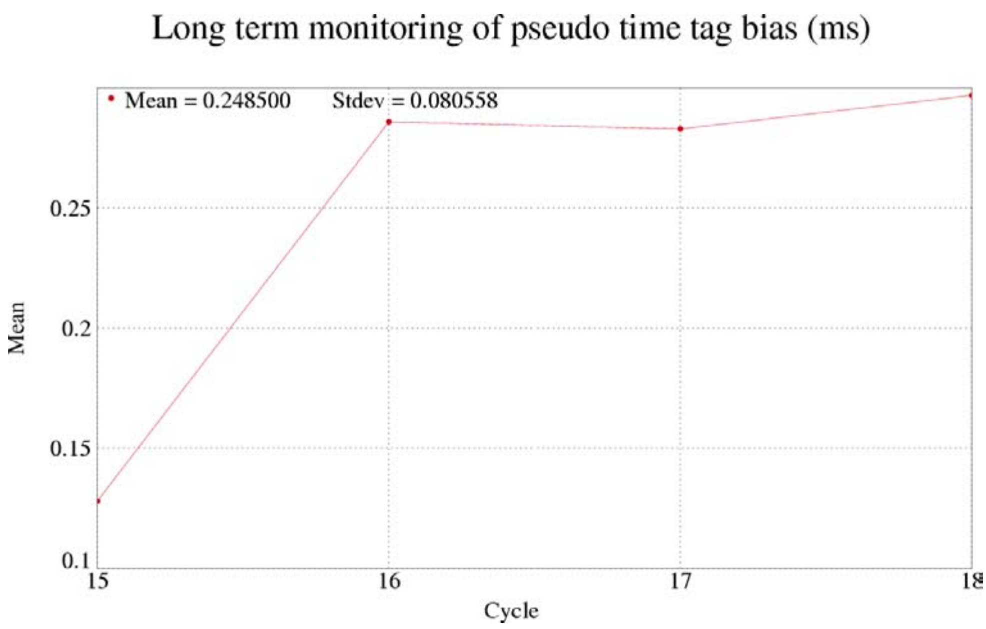

Figure 23 Mean of pseudo time tag bias (ms)

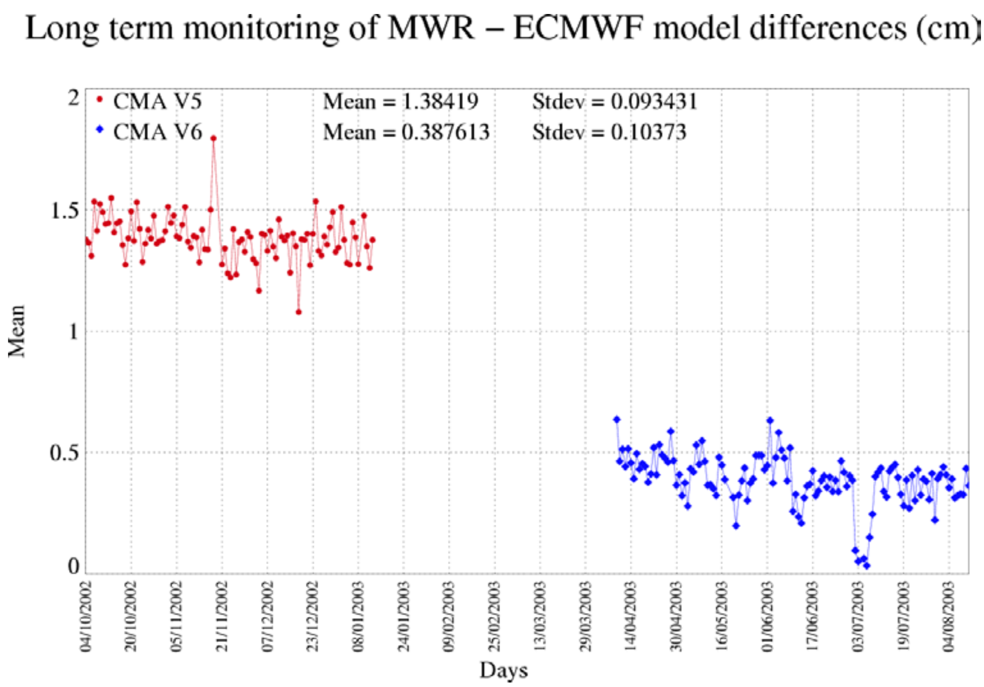

Figure 24 Mean of MWR-ECMWF model differences (cm)

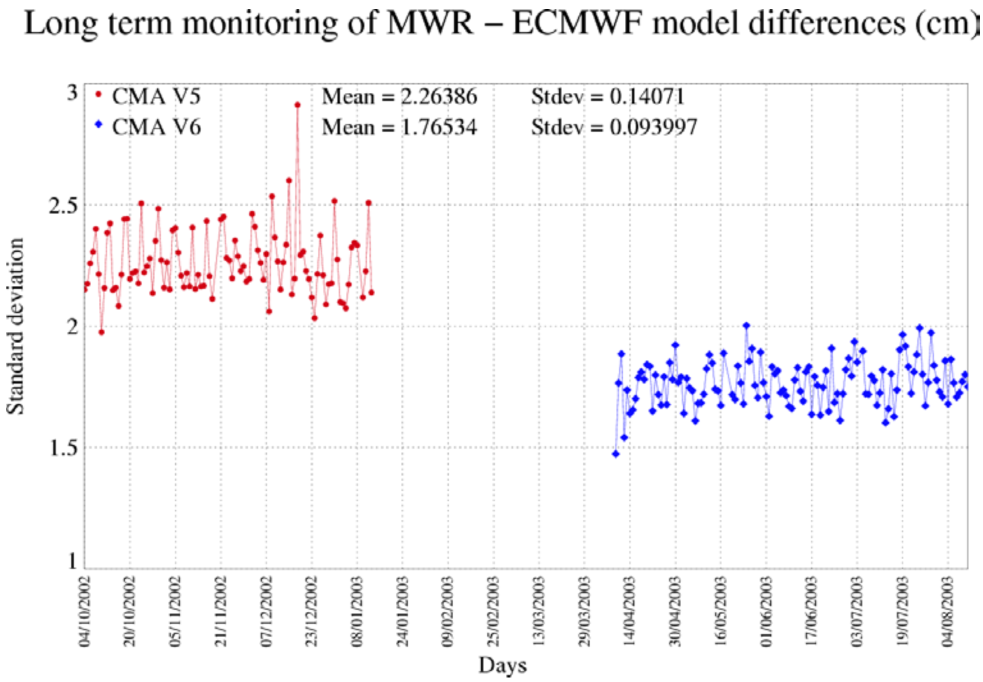

Figure 25 : Standard deviation of MWR-ECMWF model differences (cm)

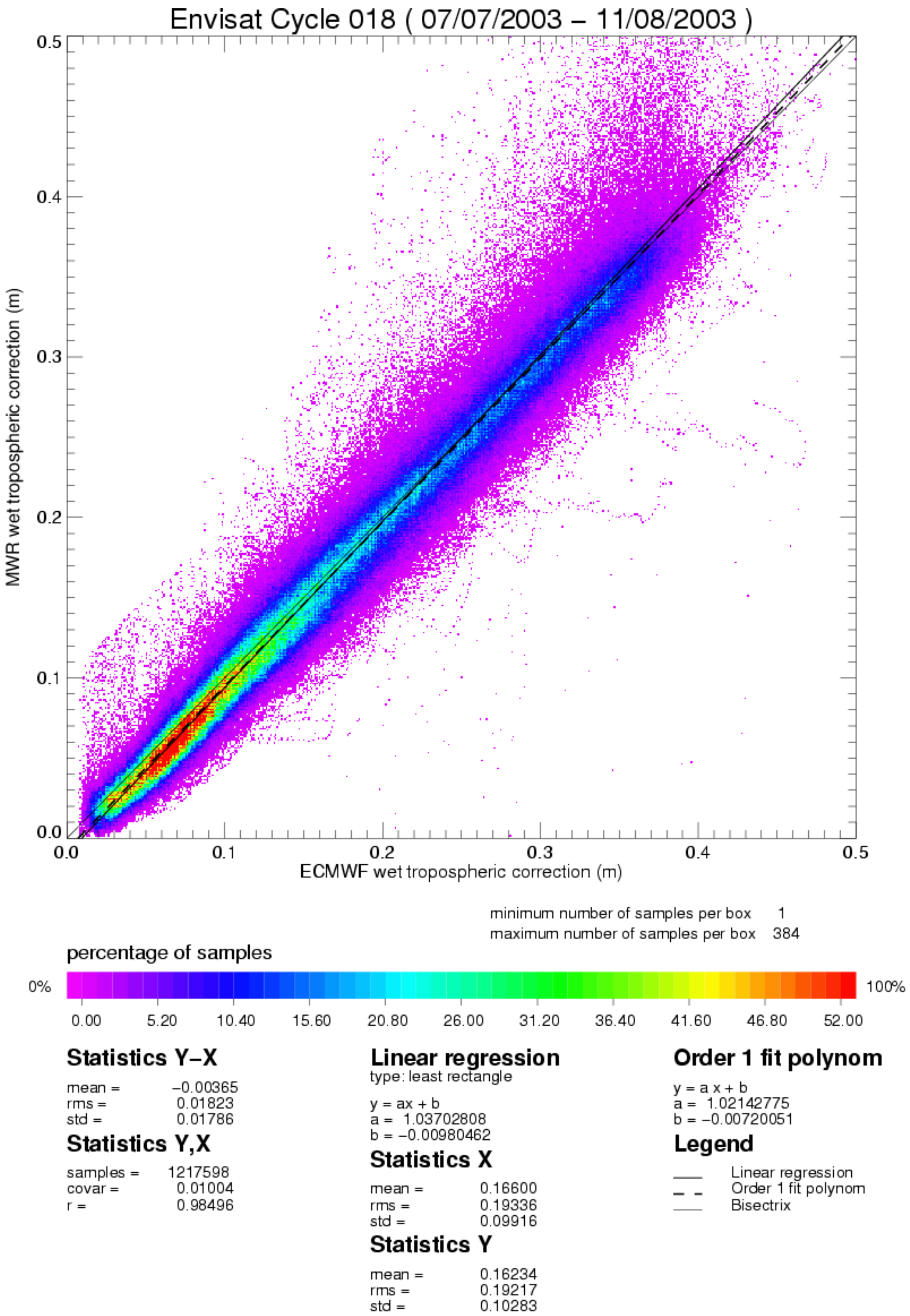

Figure 26 : Scatter plot of MWR correction according to ECMWF model (m)

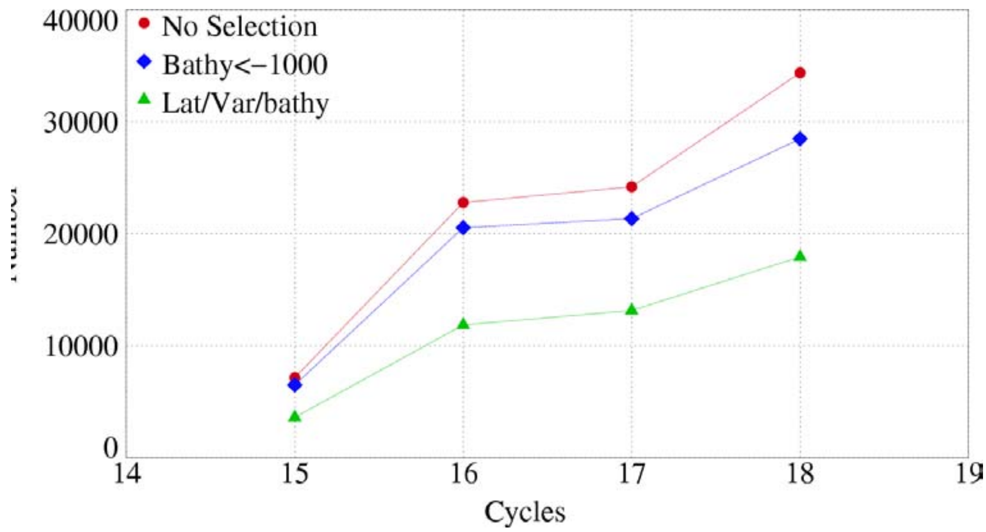

Figure 27 : Cycle by cycle number of crossovers, impact of selection

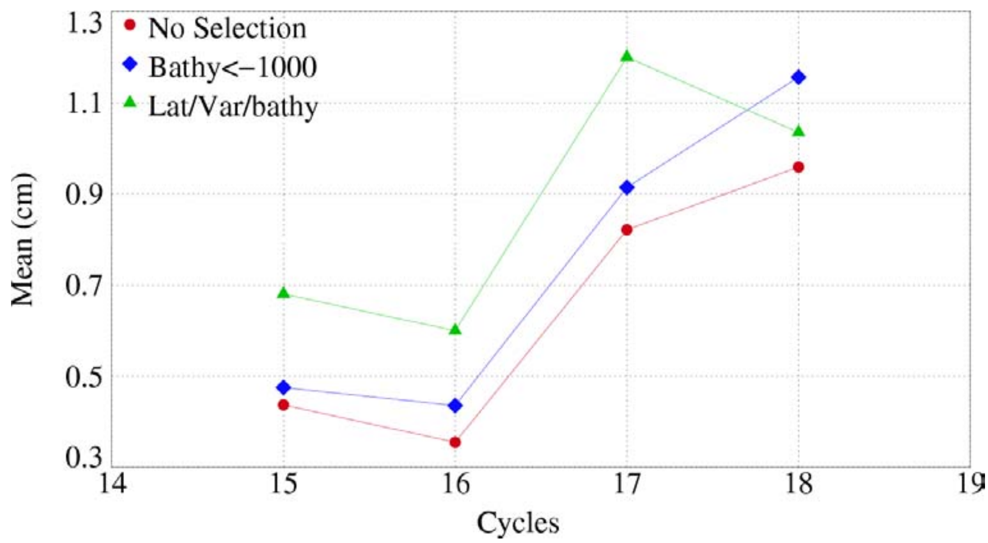

Figure 28 : Cycle by cycle mean at crossovers, impact of selection

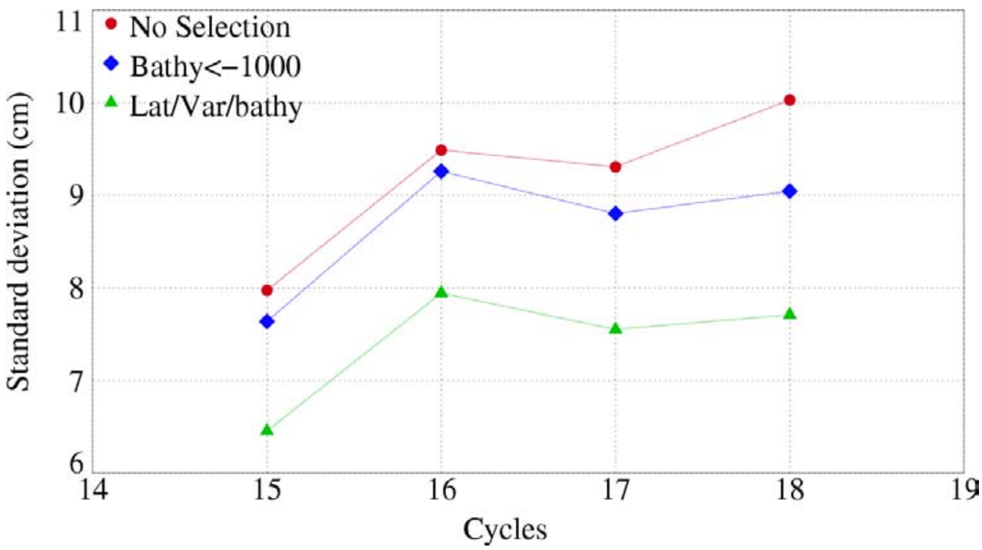

Figure 29 : Cycle by cycle standard deviation at crossovers, impact of selection

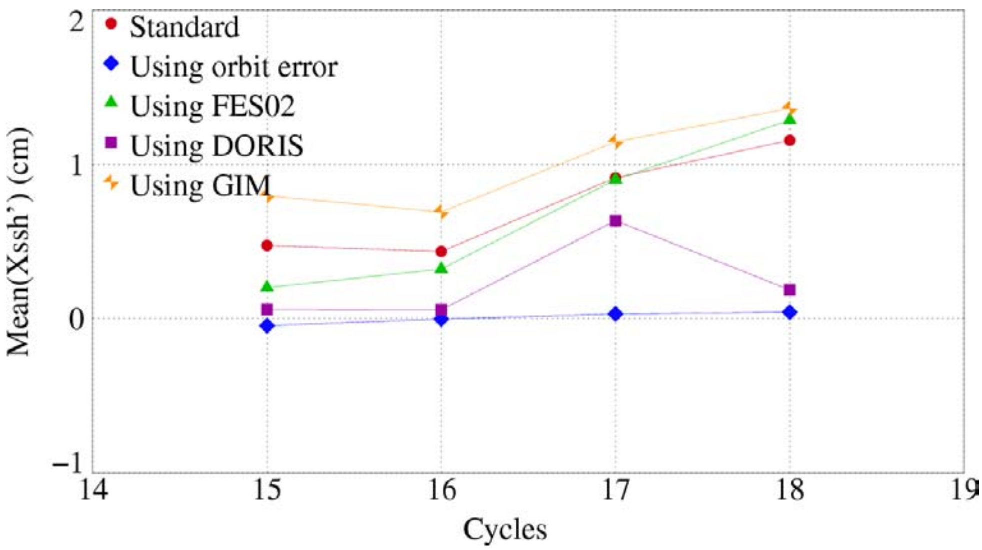

Figure 30 : Cycle by cycle mean at crossovers, impact of correction, Bathy<-1000

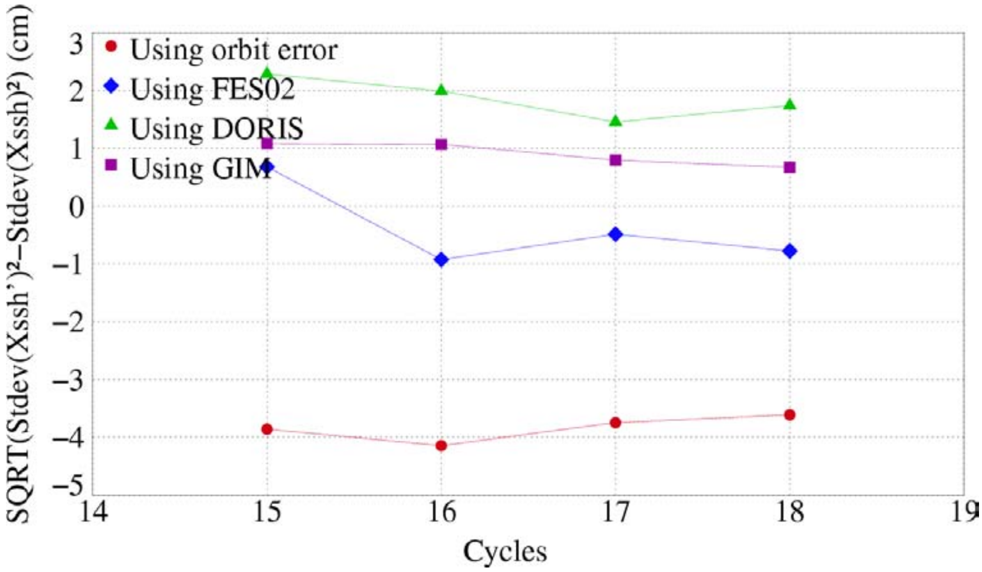

Figure 31 : Cycle by cycle gain at crossovers, impact of correction, Bathy<-1000

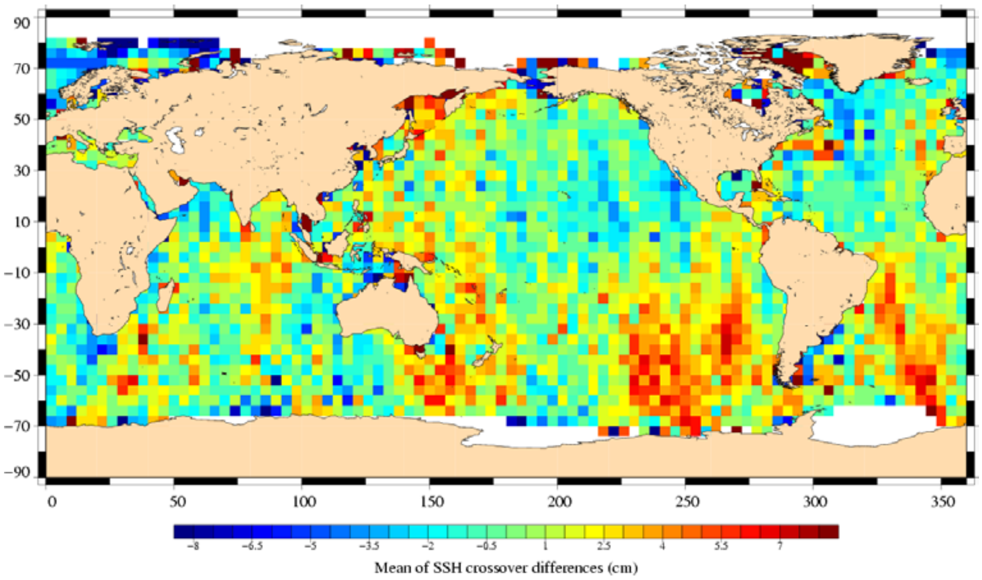

Figure 32 : Geographical pattern (4x4 degree bins) of crossover standard deviation (cm), from cycle 16 to cycle 18

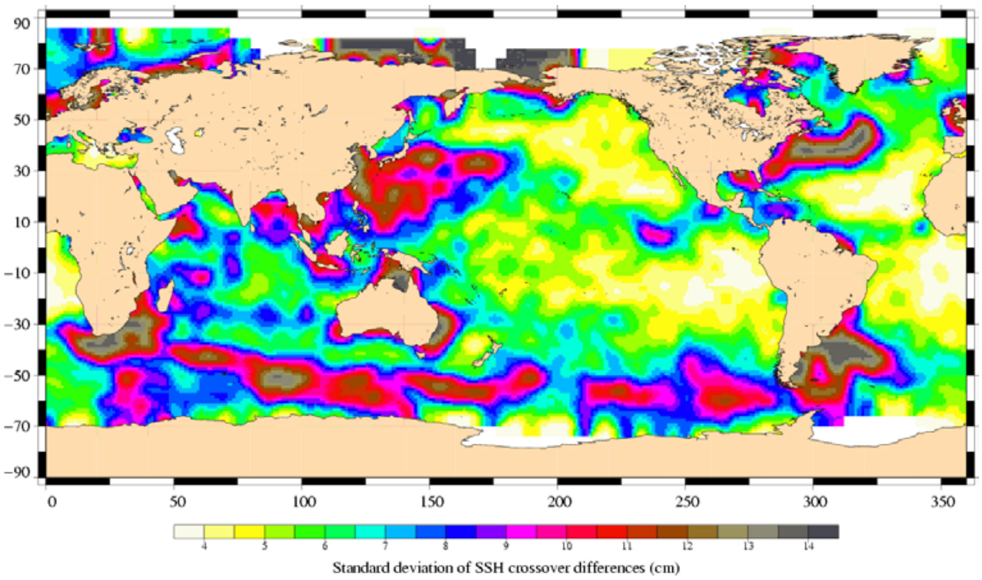

Figure 33 : Geographical pattern (4x4 degree bins) of the mean of crossover differences, from cycle 16 to cycle18

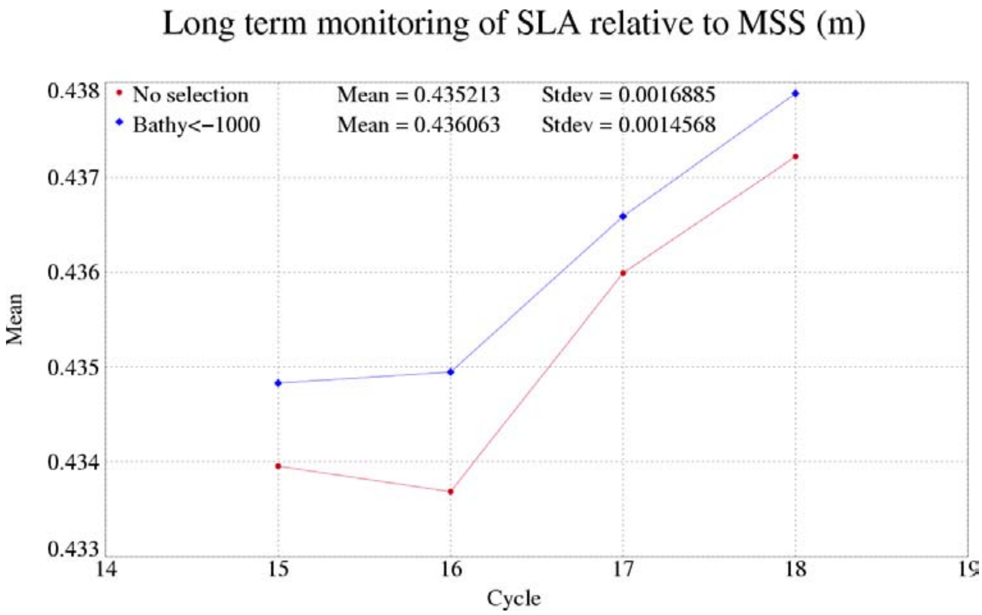

Figure 34 : Cycle by cycle mean of SSH-MSS

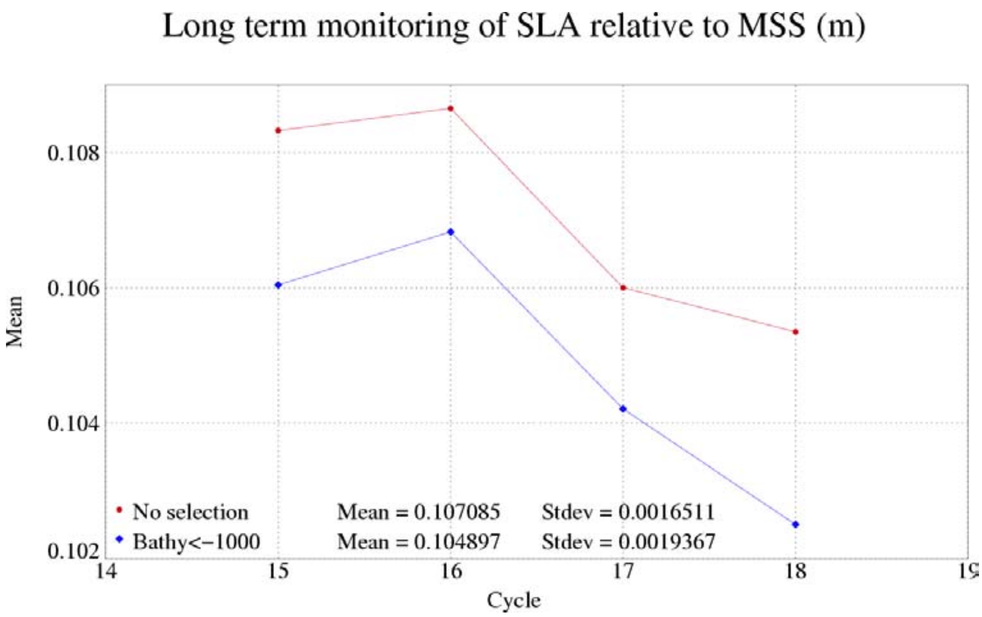

Figure 35 Cycle by cycle standard deviation of SSH-MSS

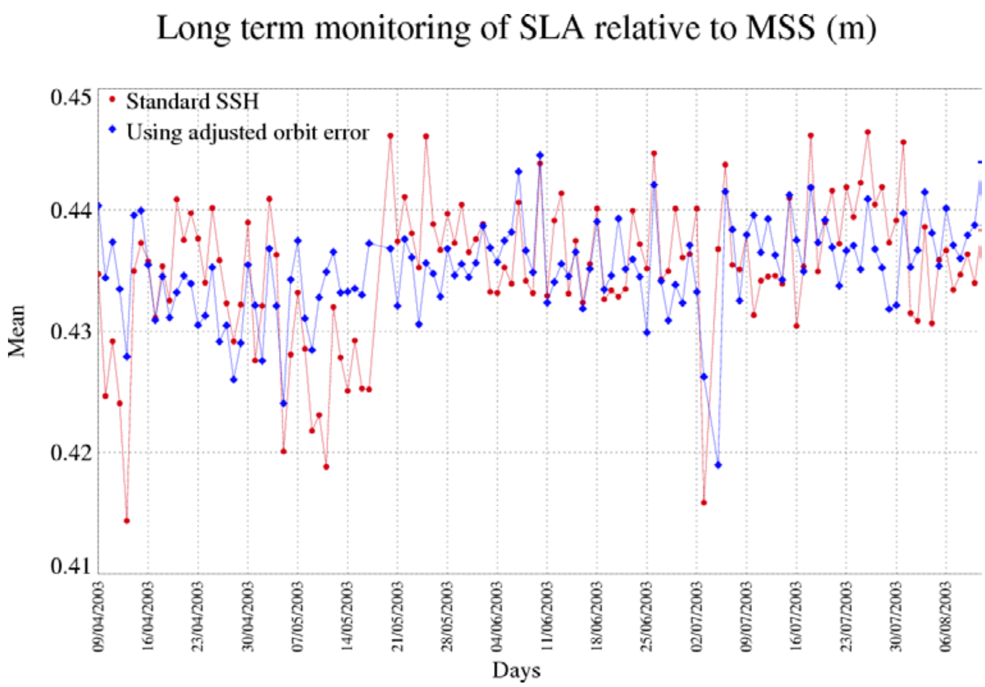

Figure 36 : Mean of SSH-MSS

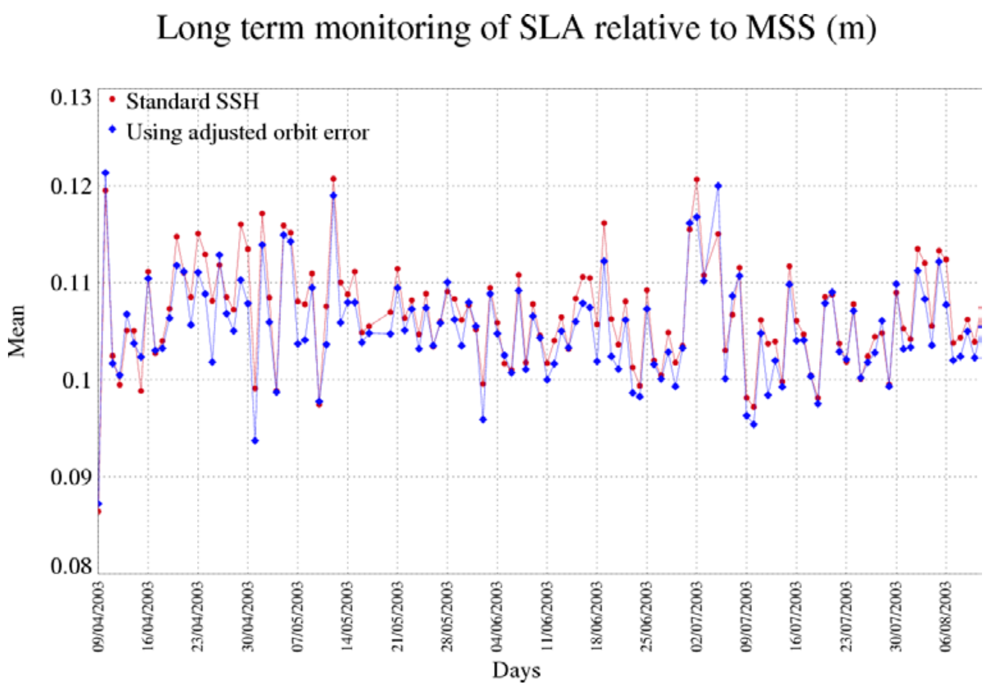

Figure 37 Standard deviation of SSH-MSS

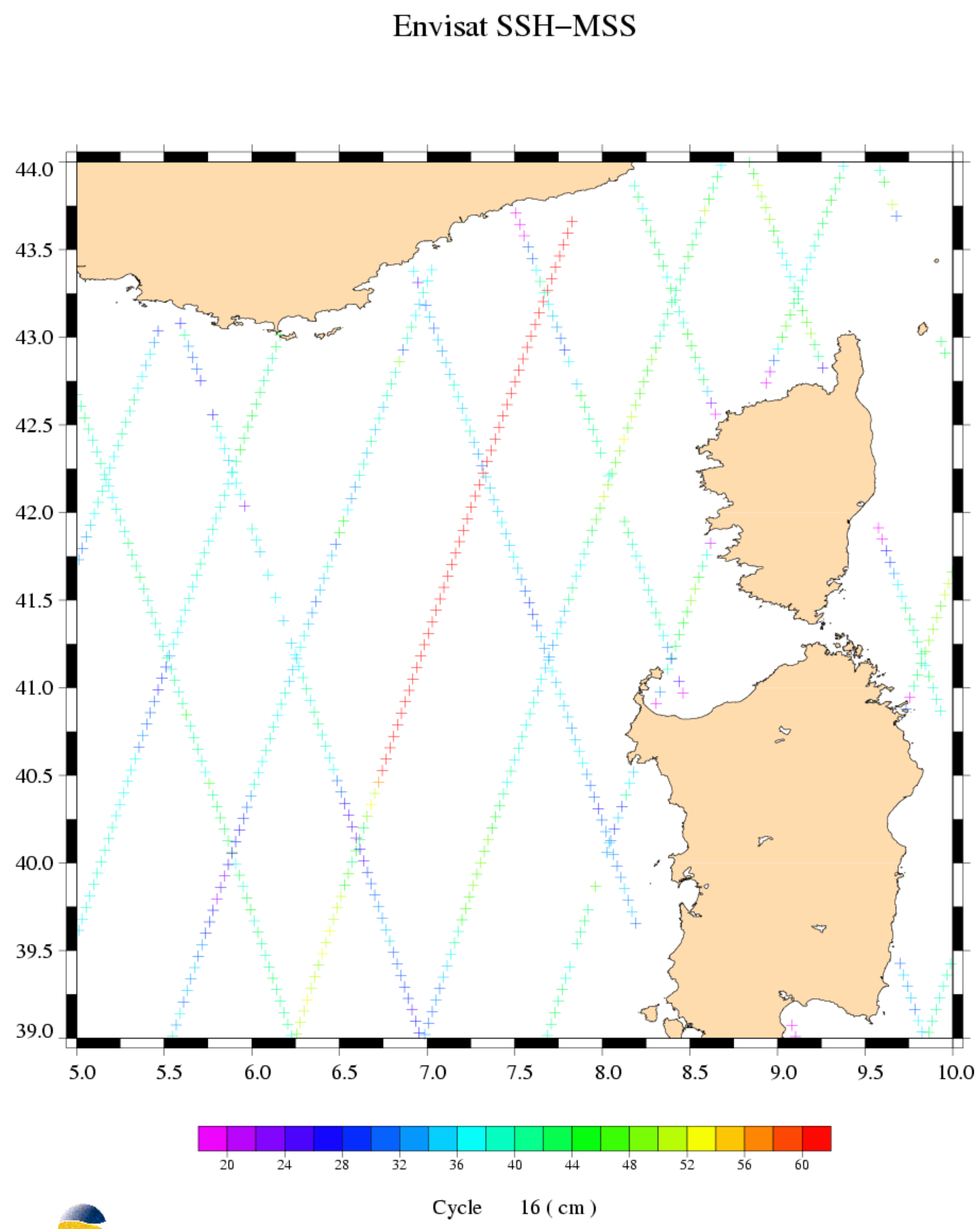

Figure 38 : SSH-MSS on Cycle 16 over the Mediterranean sea (Pass 216 in red)

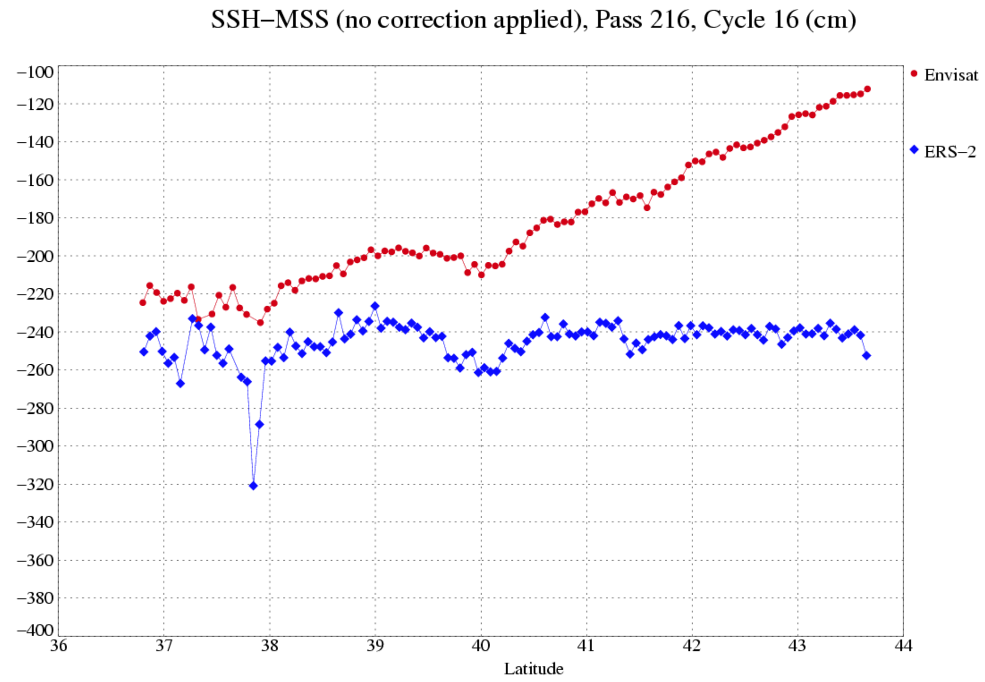

Figure 39 : SSH-MSS on cycle 16, pass 216

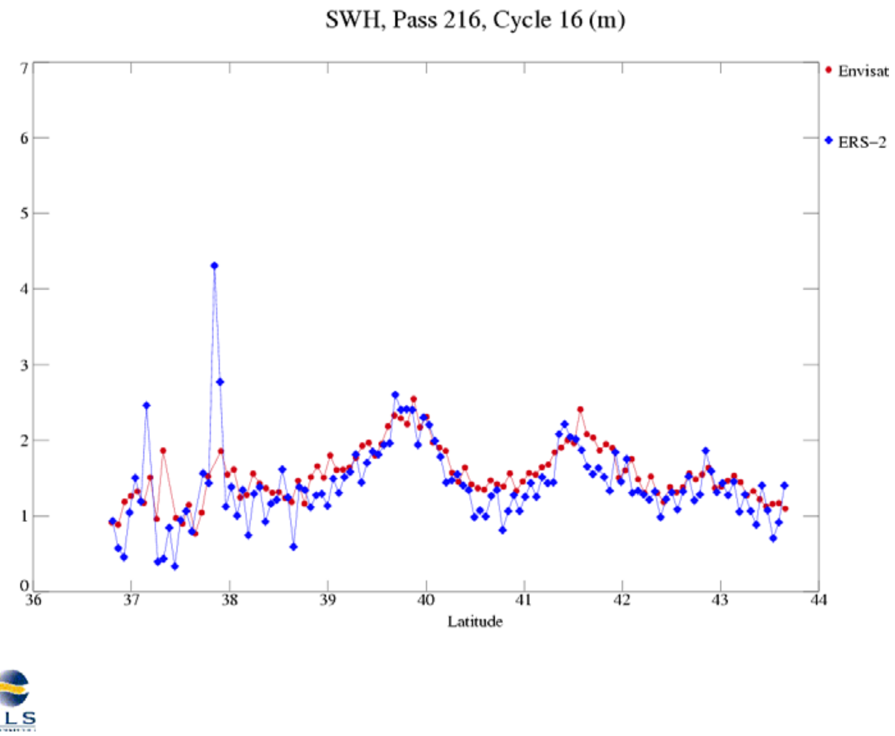

Figure 40 : SWH on cycle 16, pass 216

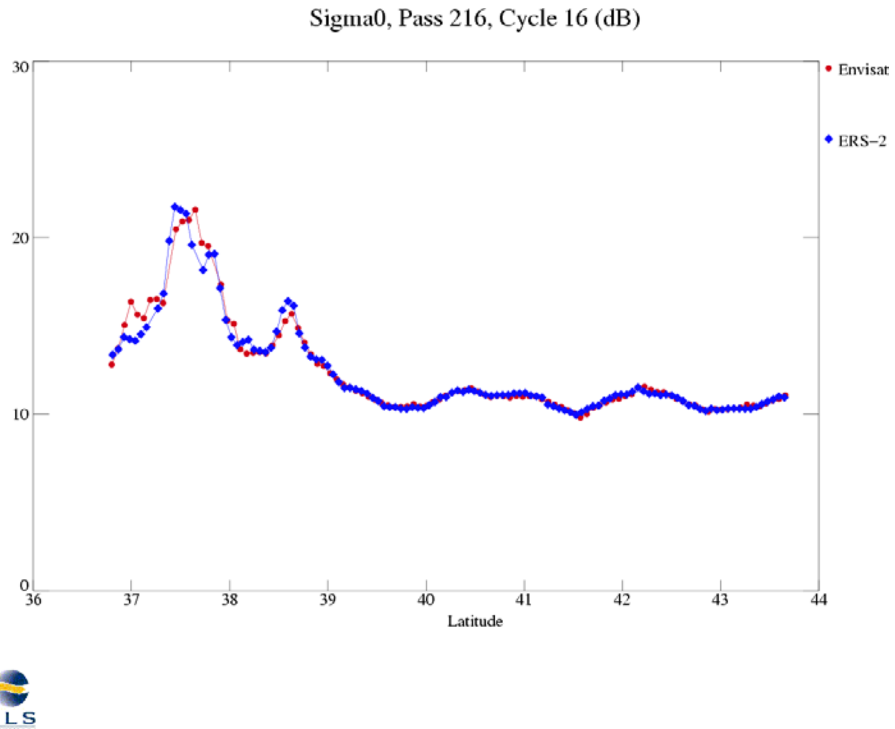

Figure 41 : Sigma0 on cycle 16, pass 216

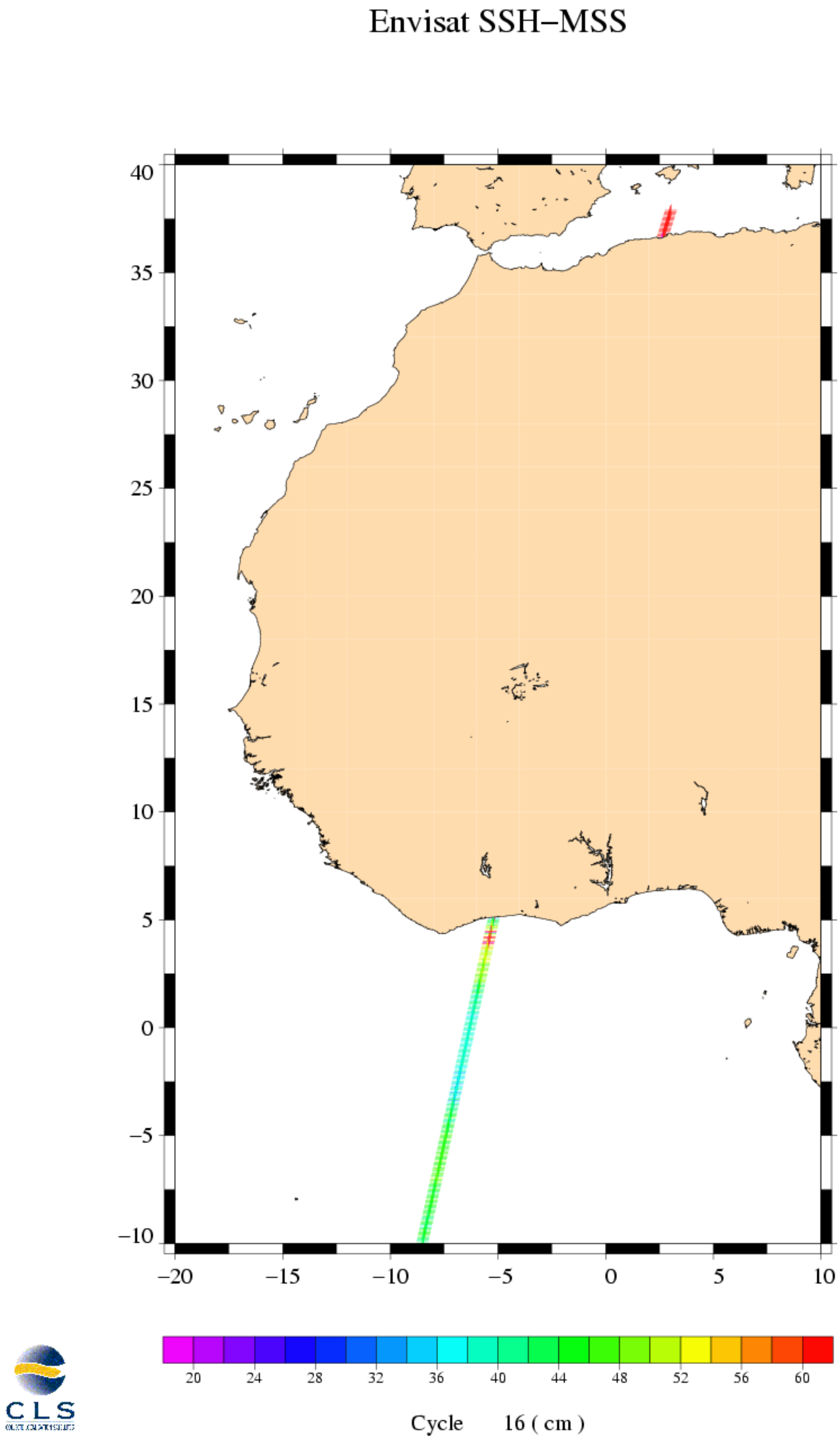

Figure 42 : SSH-MSS on cycle 16 pass 388

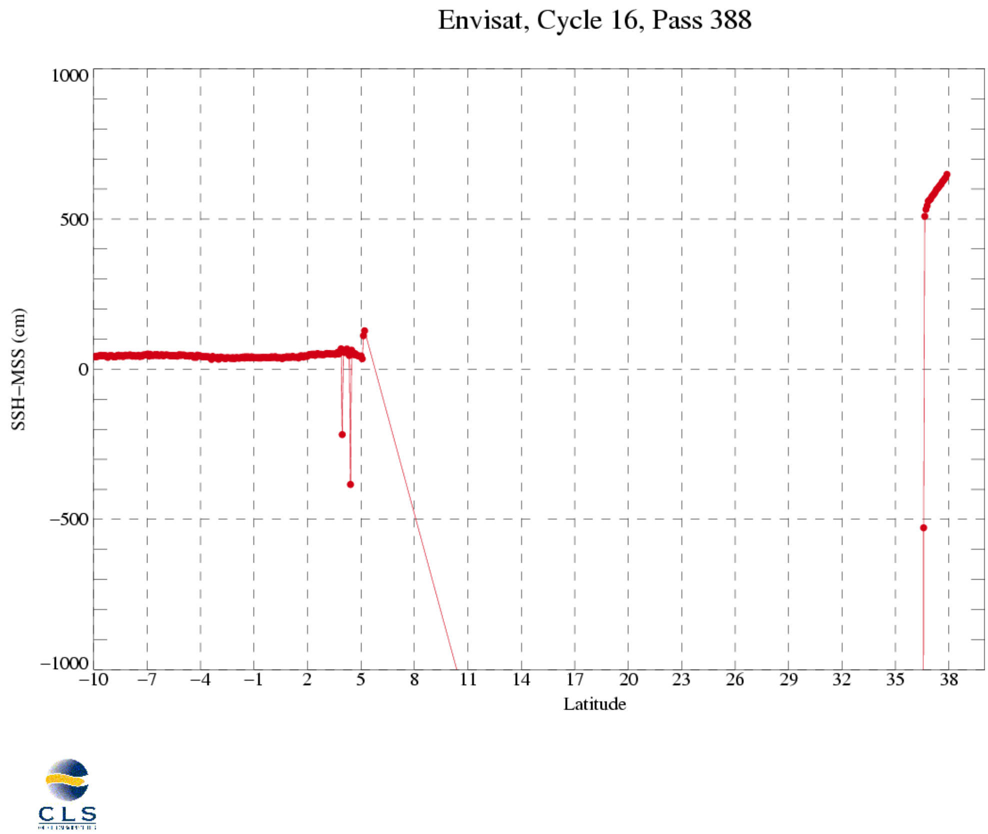

Figure 43 : SSH-MSS on cycle 16, pass 388

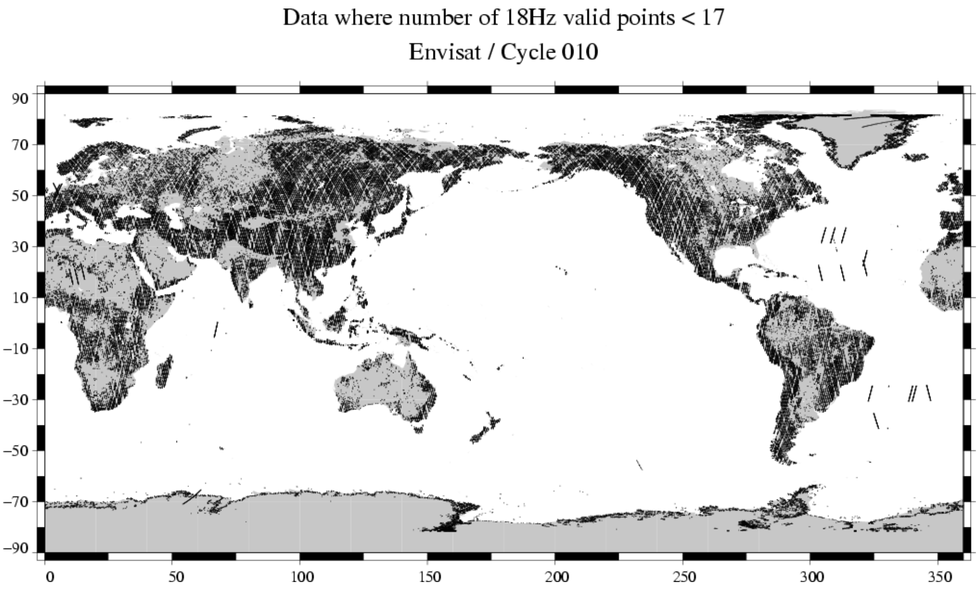

Figure 44 : Locations of measurements with number of Ku Band elementary valid ranges <17, cycle 10

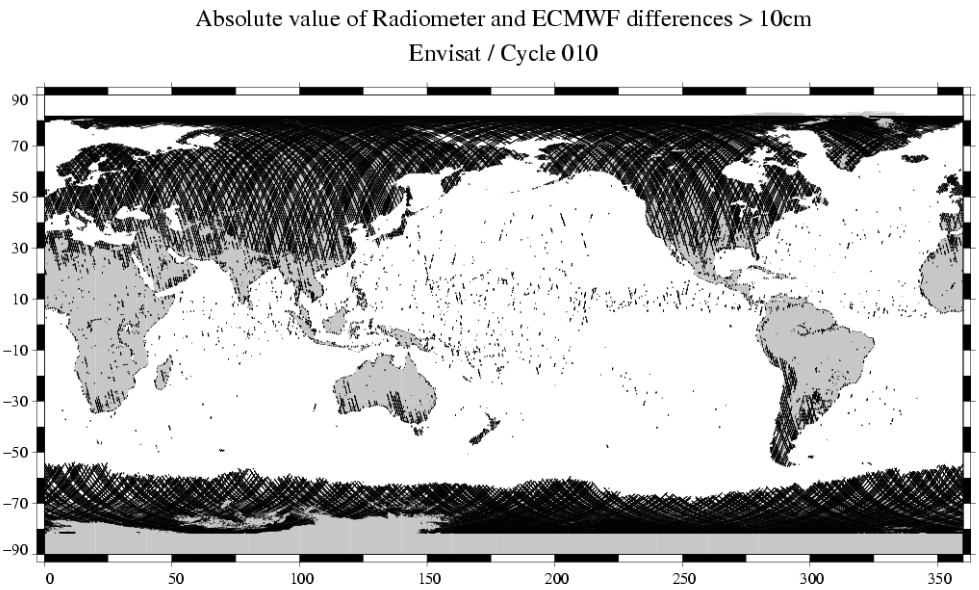

Figure 45 : Measurements for which |MWR-CMWF|>10cm, cycle 10

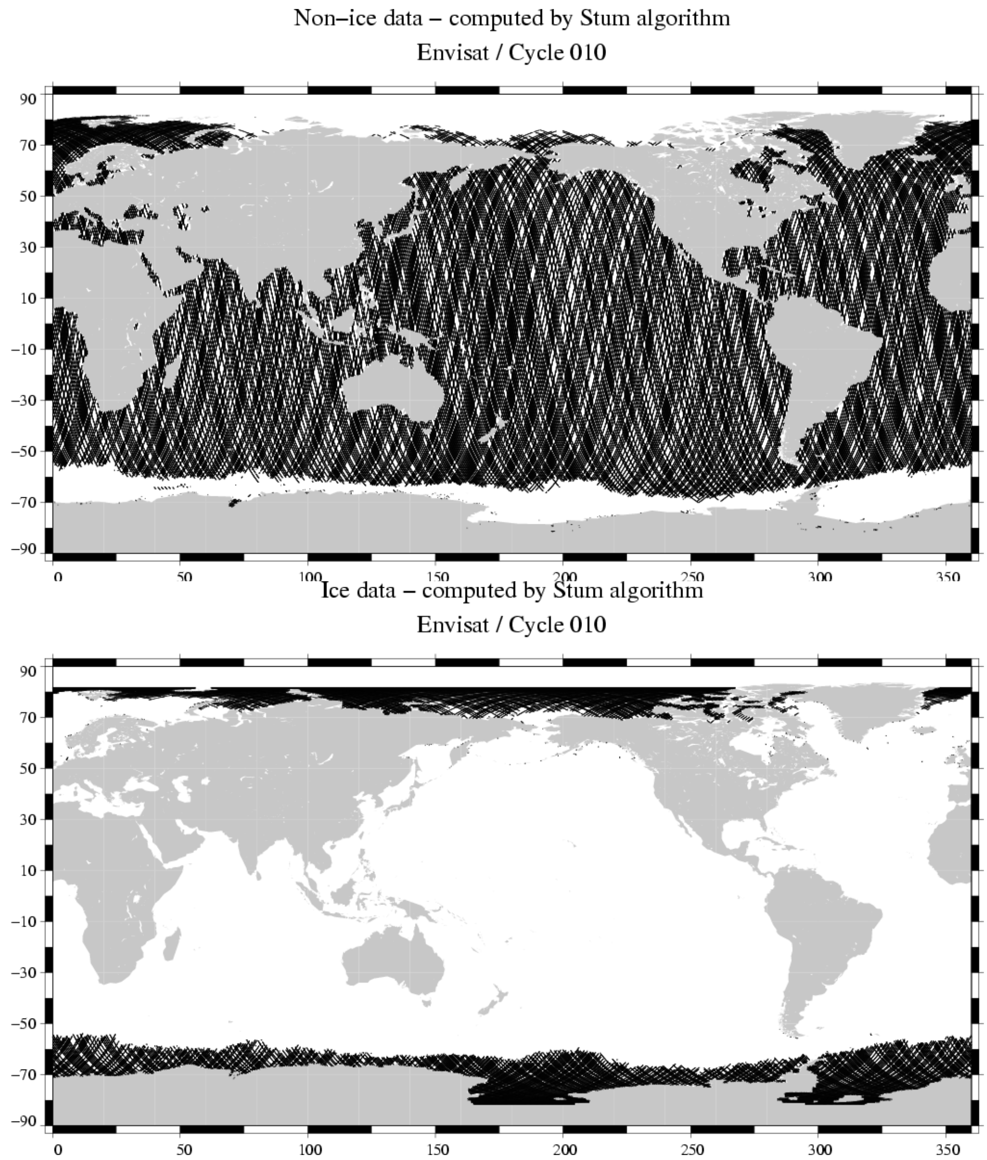

Figure 46 : Ocean (top) and ice (bottom) data using ERS-2 method, cycle 10

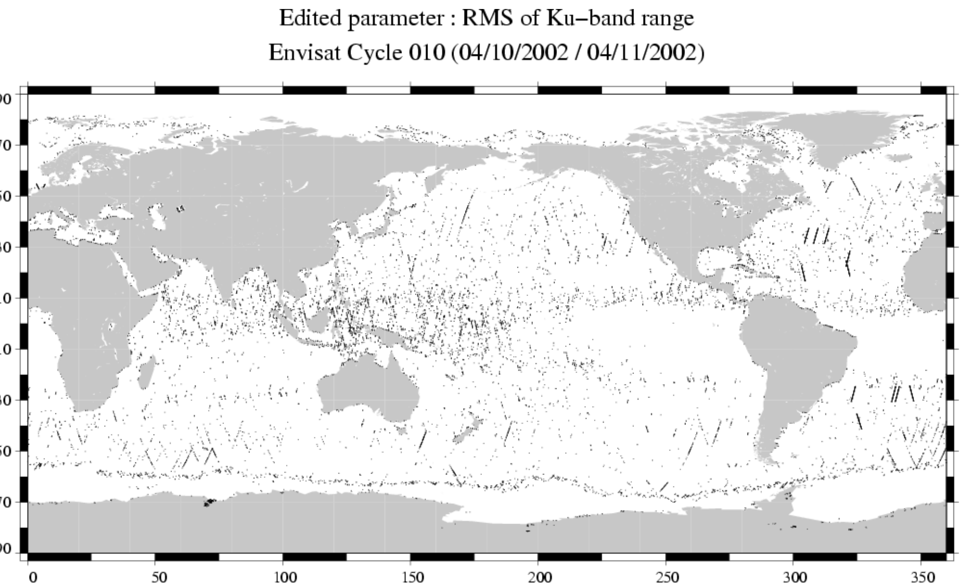

Figure 47 : RMS of Ku range>20cm over open ocean

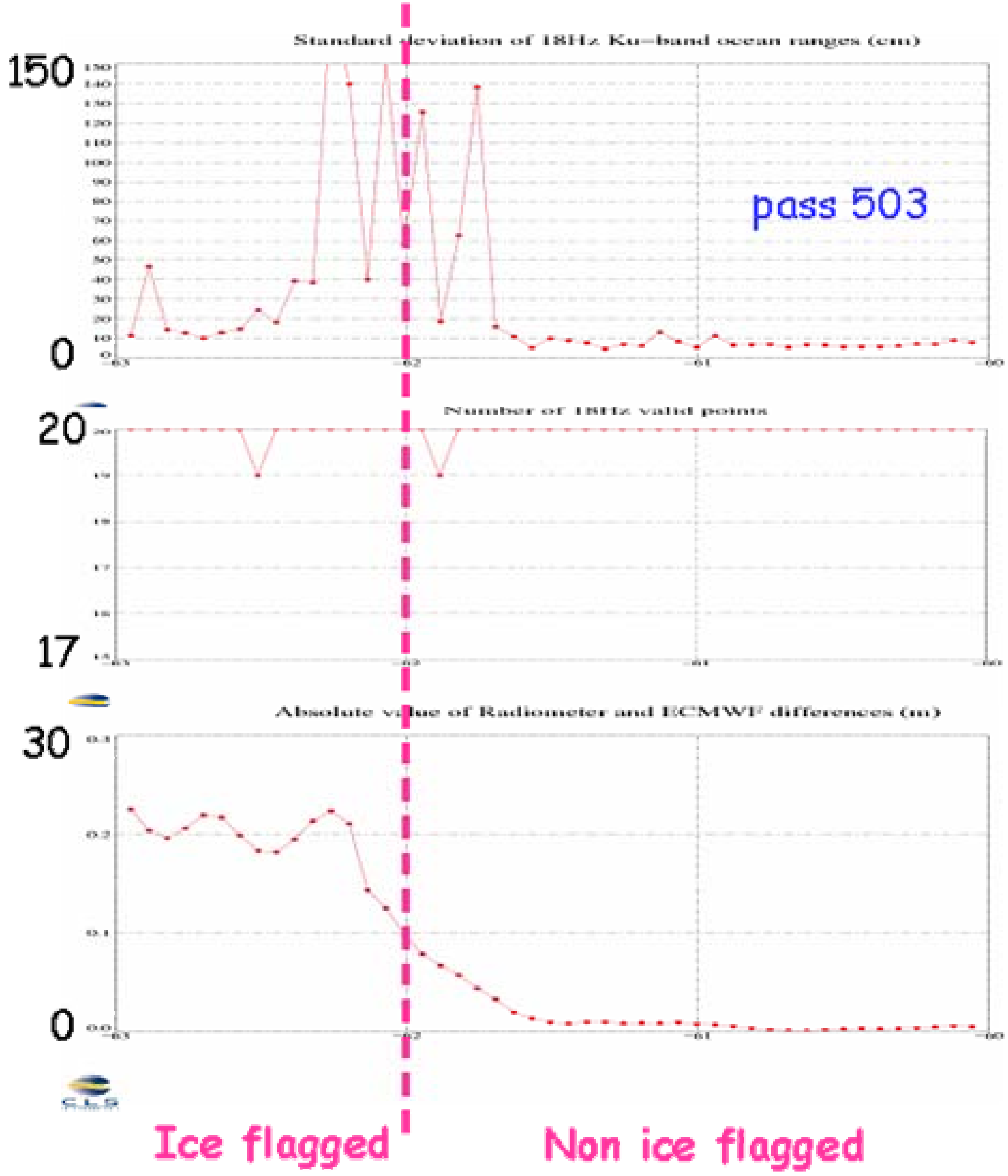

Figure 48 : RMS of Ku-band range, number of elementary measurements, and |MWR-ECMWF| on pass 503

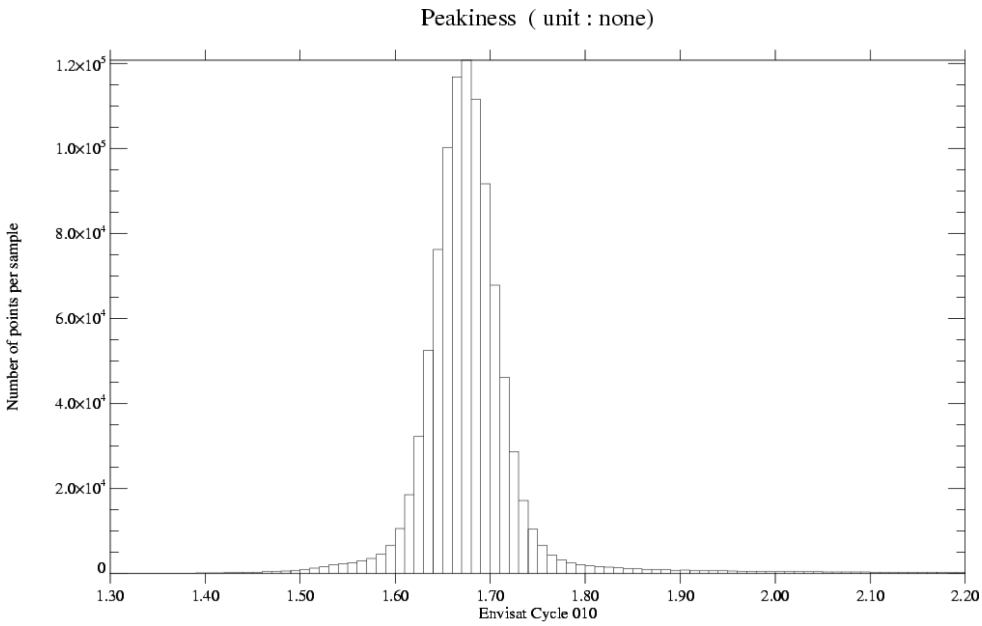

Global nb of points	:	1172316	Sel. nb of points	:	974628	Sample interval	:	0.010
Global mean	:	4.399	Selected mean	:	1.678	Maximum value	:	65.526
Global Std	:	7.647	Selected std	:	0.058	Minimum value	:	0.850

Figure 49 : Histogram of peakiness, cycle 10

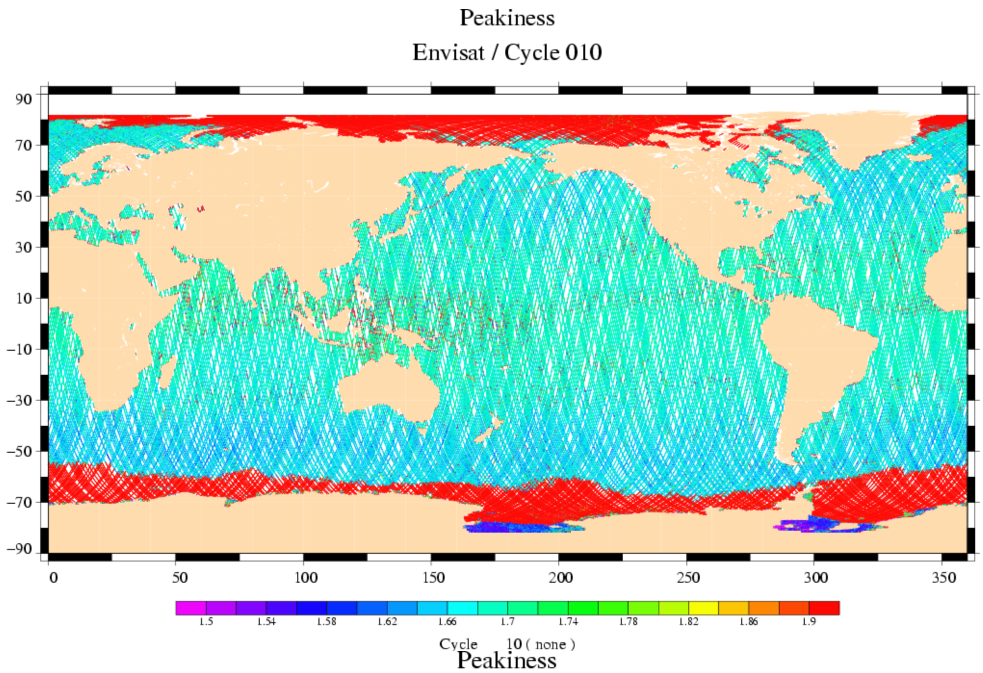

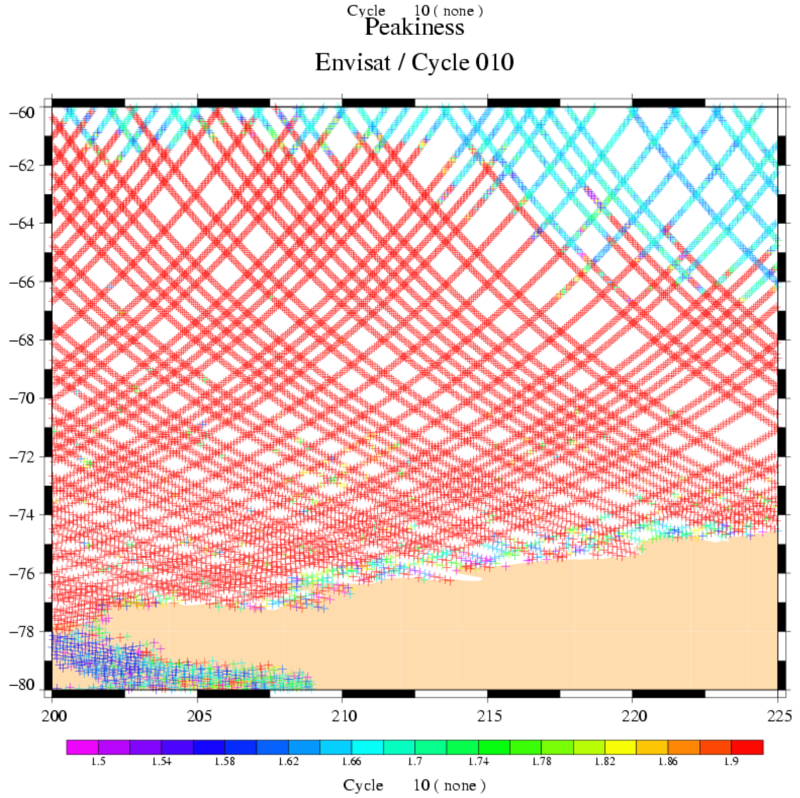

Figure 50 : Map of peakiness (top), zoom on Antarctica (bottom), cycle 10

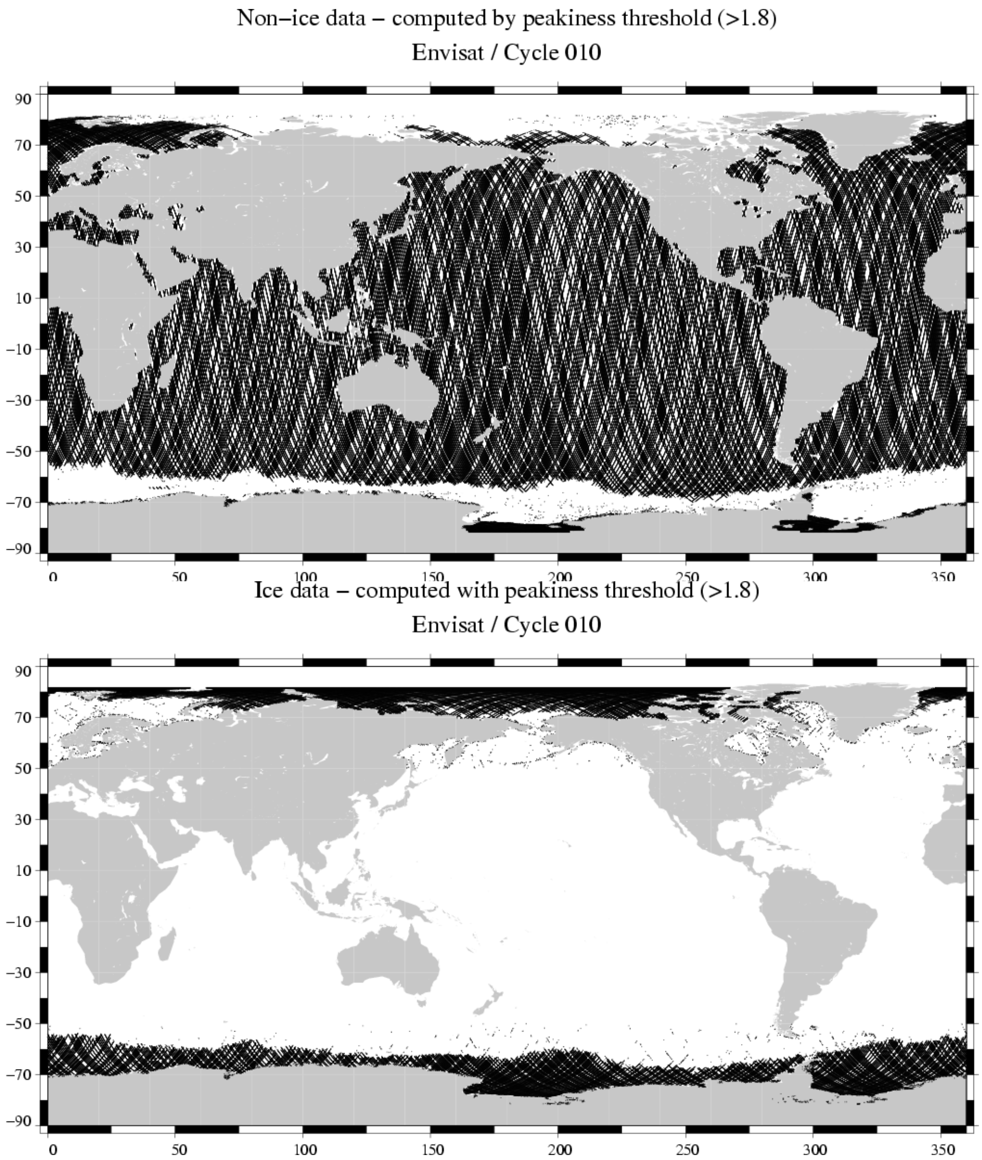

Figure 51 : Ocean (top) and ice (bottom) data using a 1.8 threshold on peakiness, cycle 10

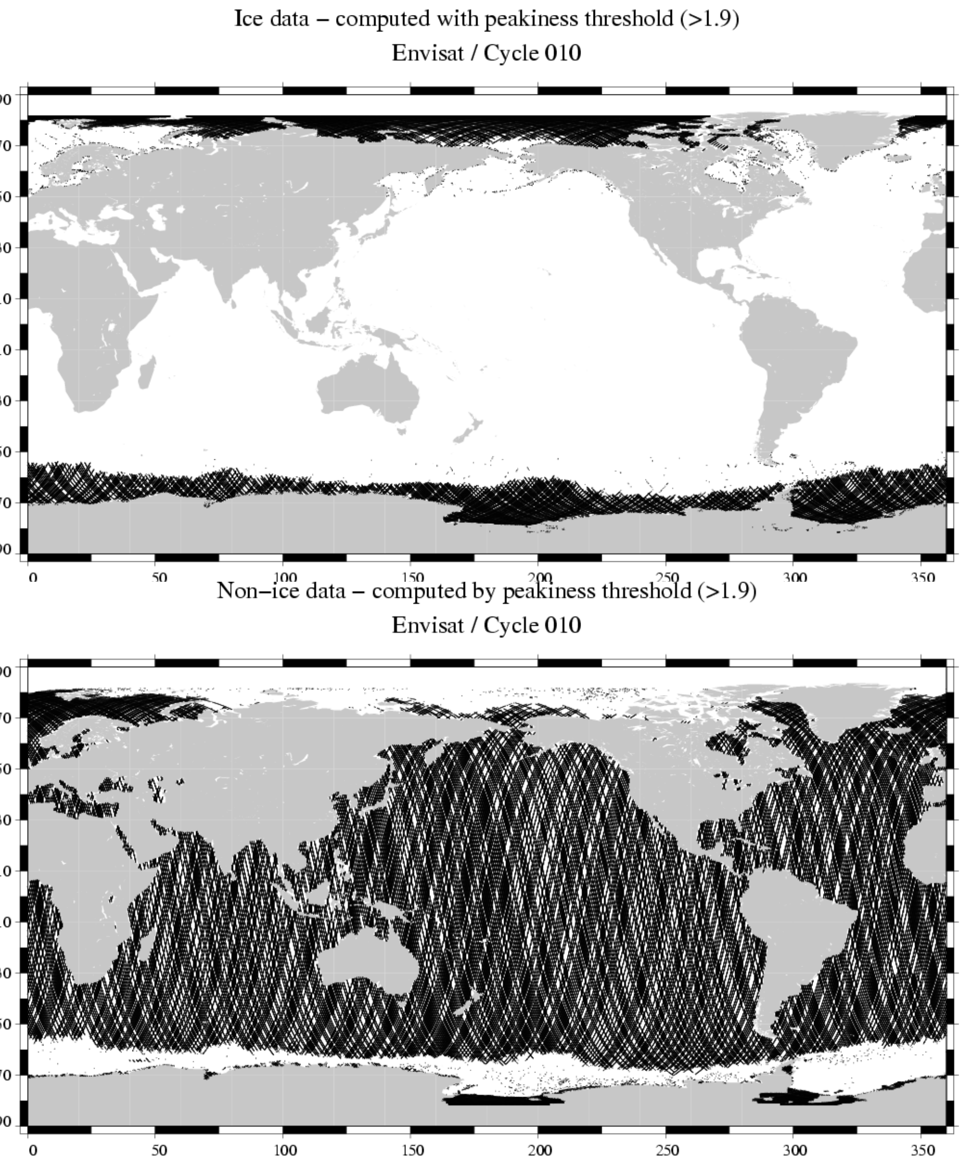

Figure 52 : Ocean (top) and ice (bottom) data using a 1.9 threshold on peakiness, cycle 10

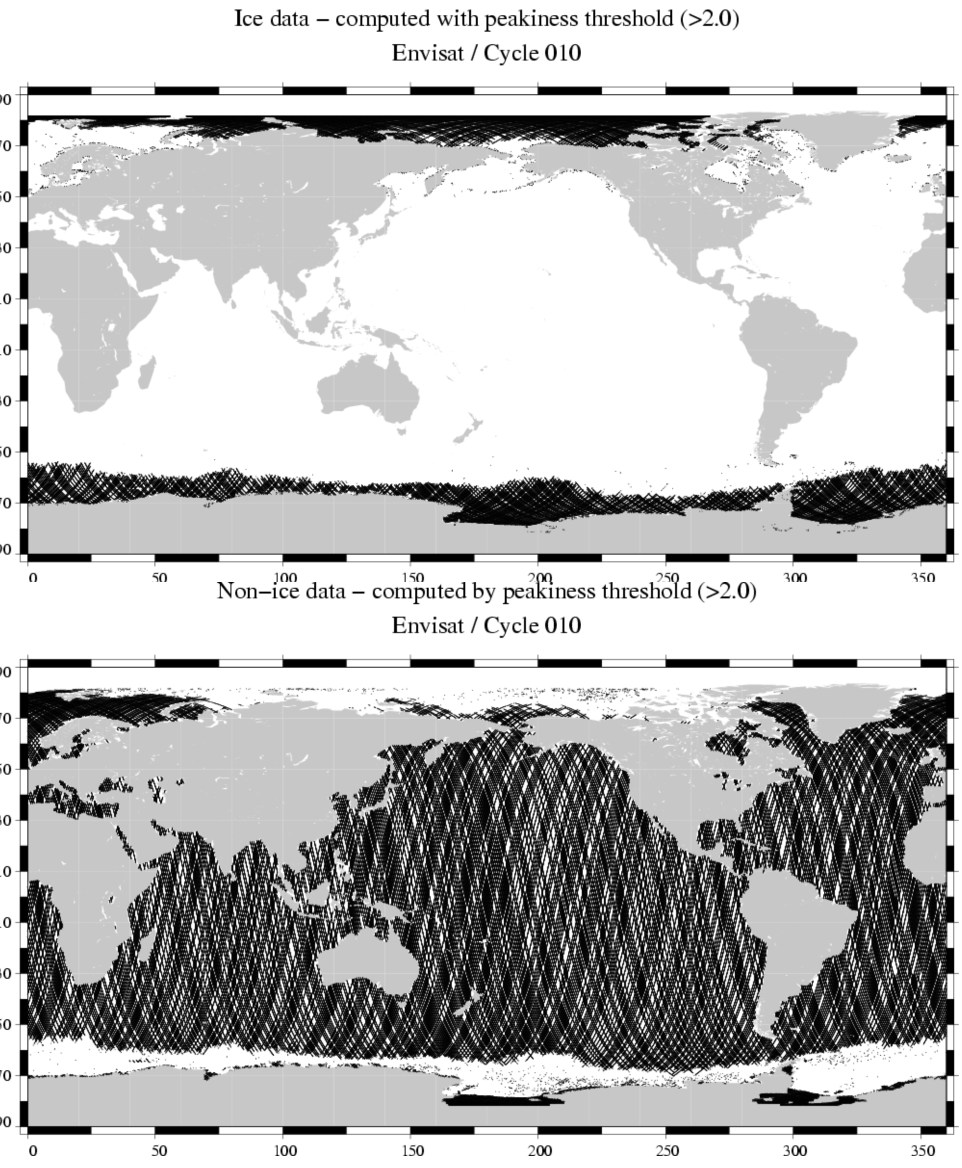

Figure 53 : Ocean (top) and ice (bottom) data using a 2.0 threshold on peakiness, cycle 10

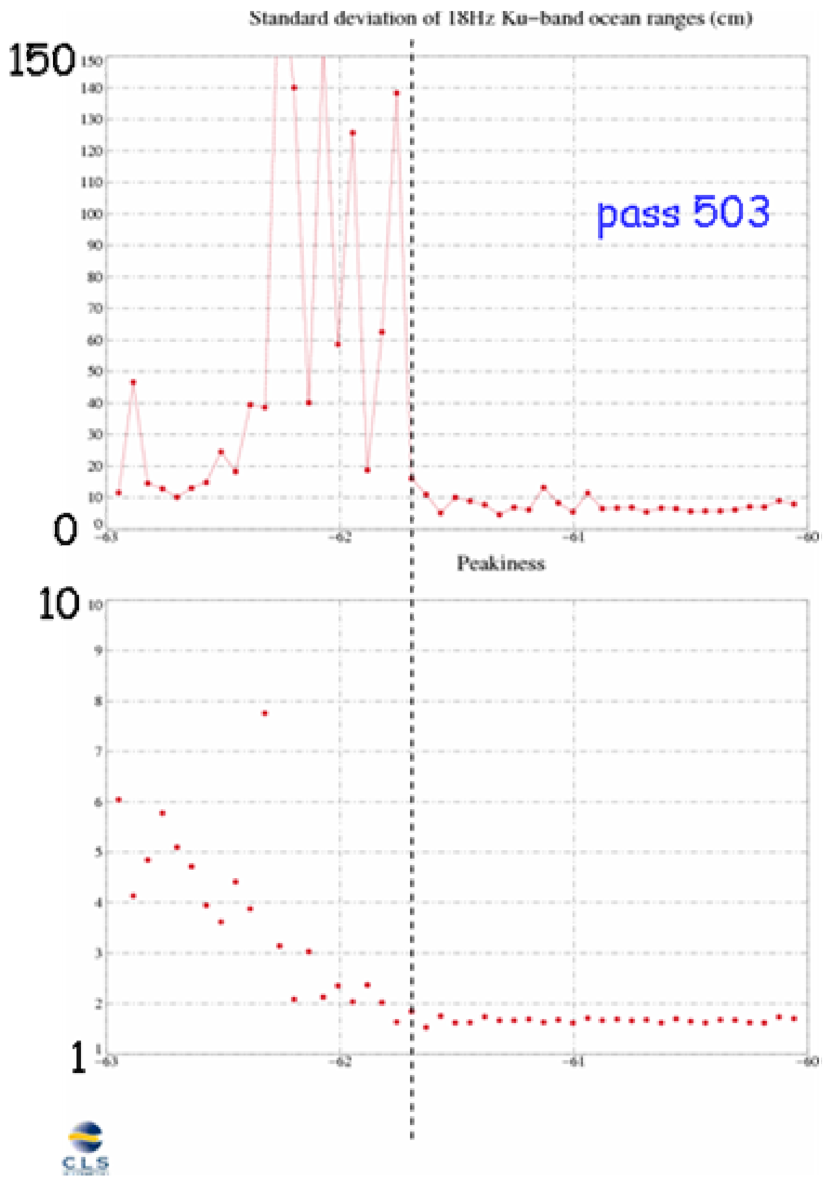

Figure 54 : RMS of Ku range, number of elementary data, |MWR-ECMWF| on pass 503

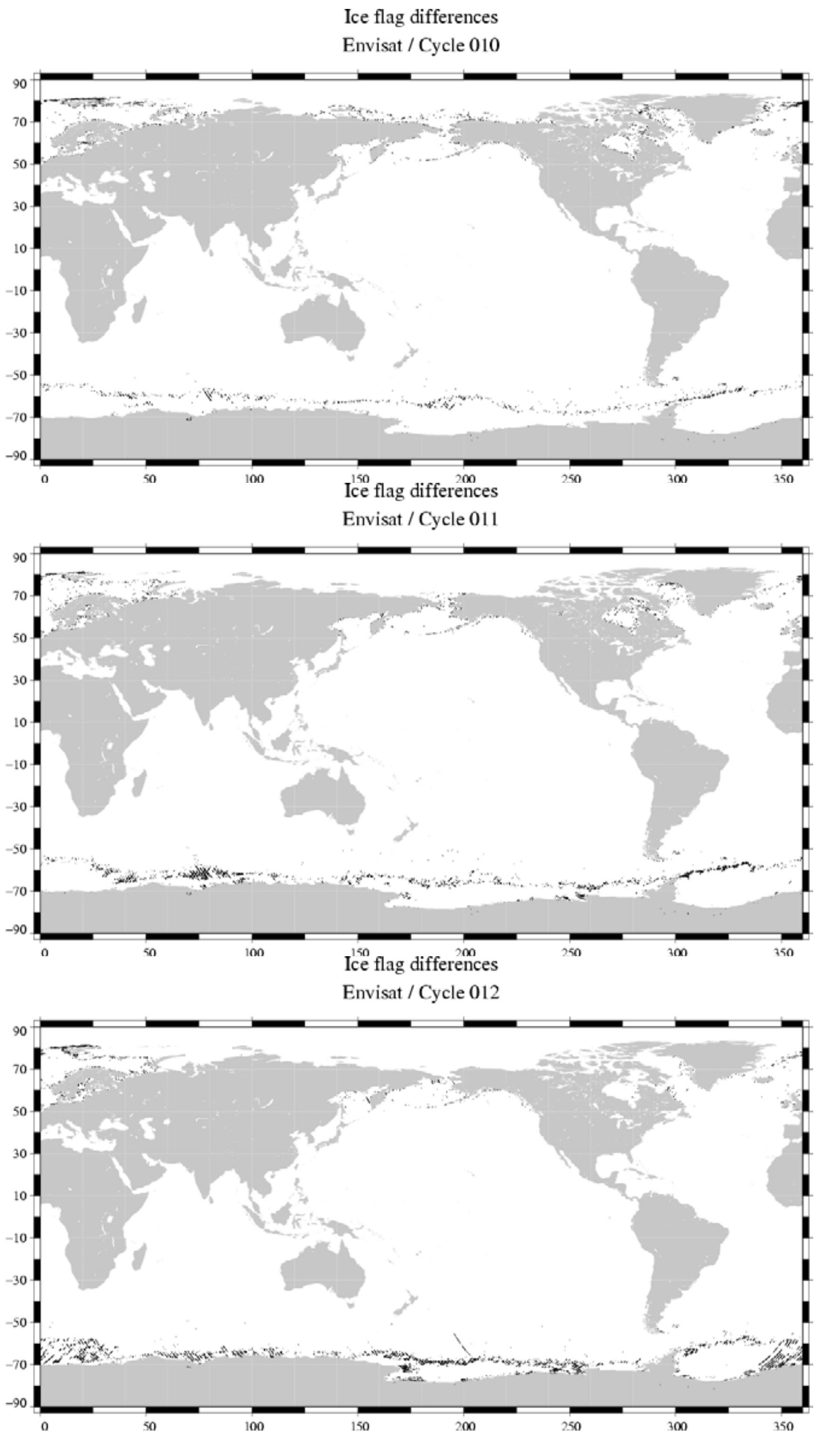

Figure 55 : Points detected as ice by a 2.0 threshold on peakiness, but seen as ocean data by the ERS-2 method, cycles 10, 11 and 12

: NX_TabUnix19304SshMssNonCorr/

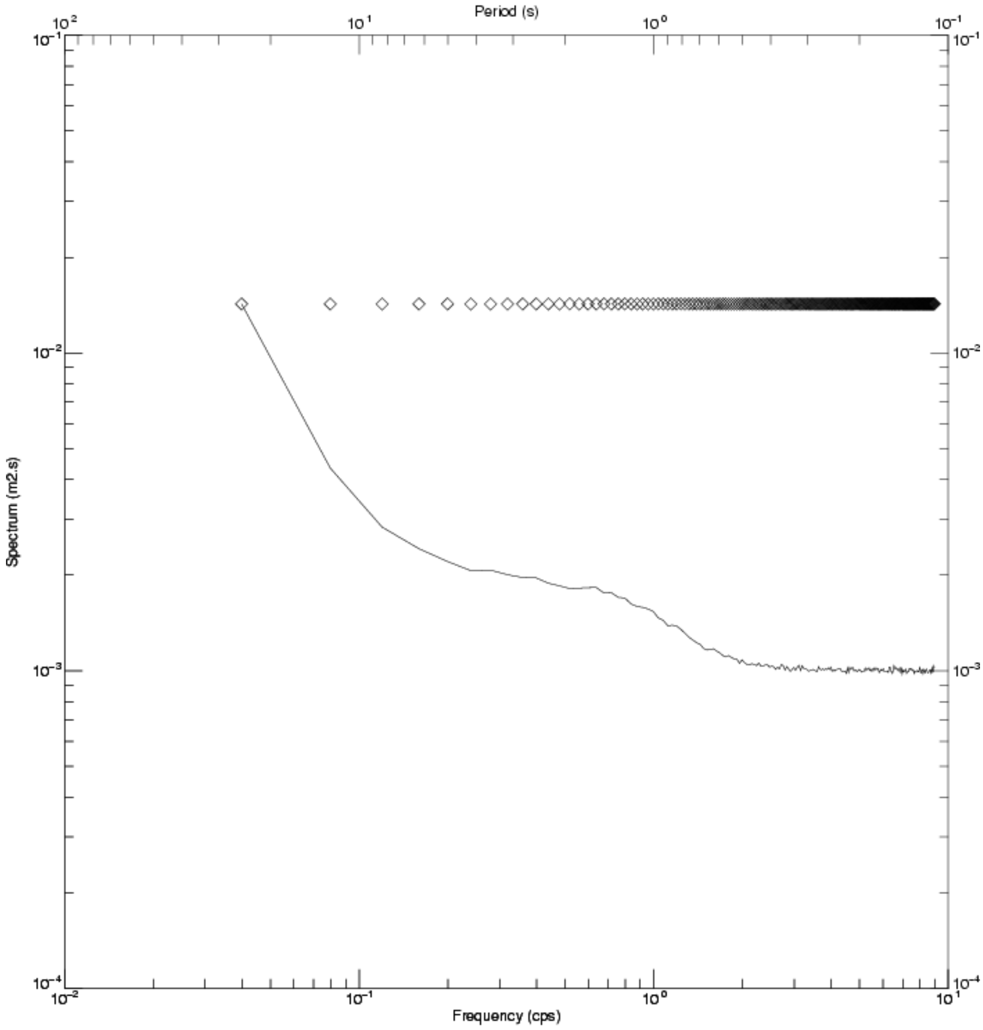

Frequency spectrum (m2.s)

Figure 56 : Power spectrum of Envisat SLA$_{nc/mss}$ at 20Hz

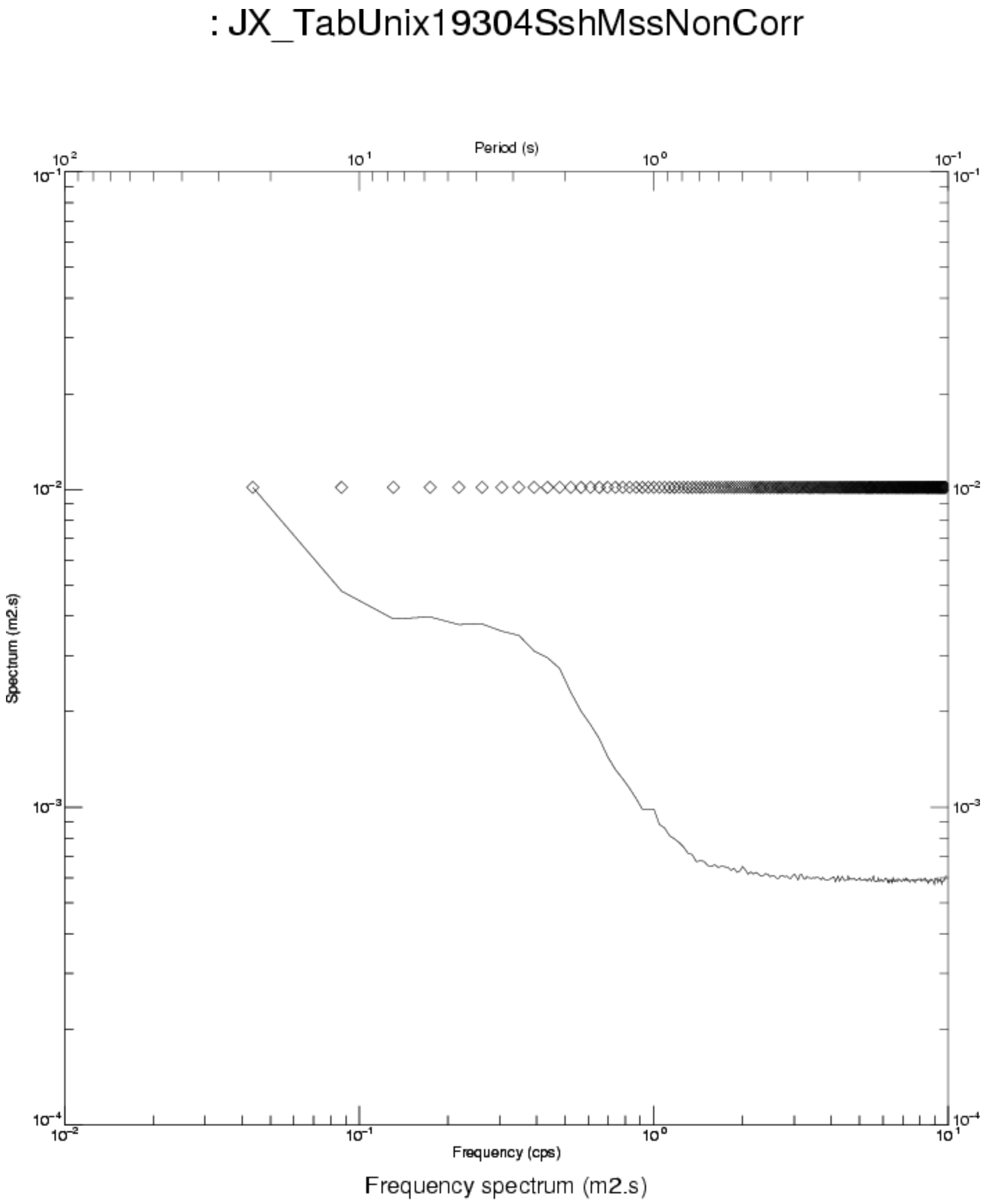

Figure 57 : Power spectrum of Jason SLA$_{nc/mss}$ at 20Hz

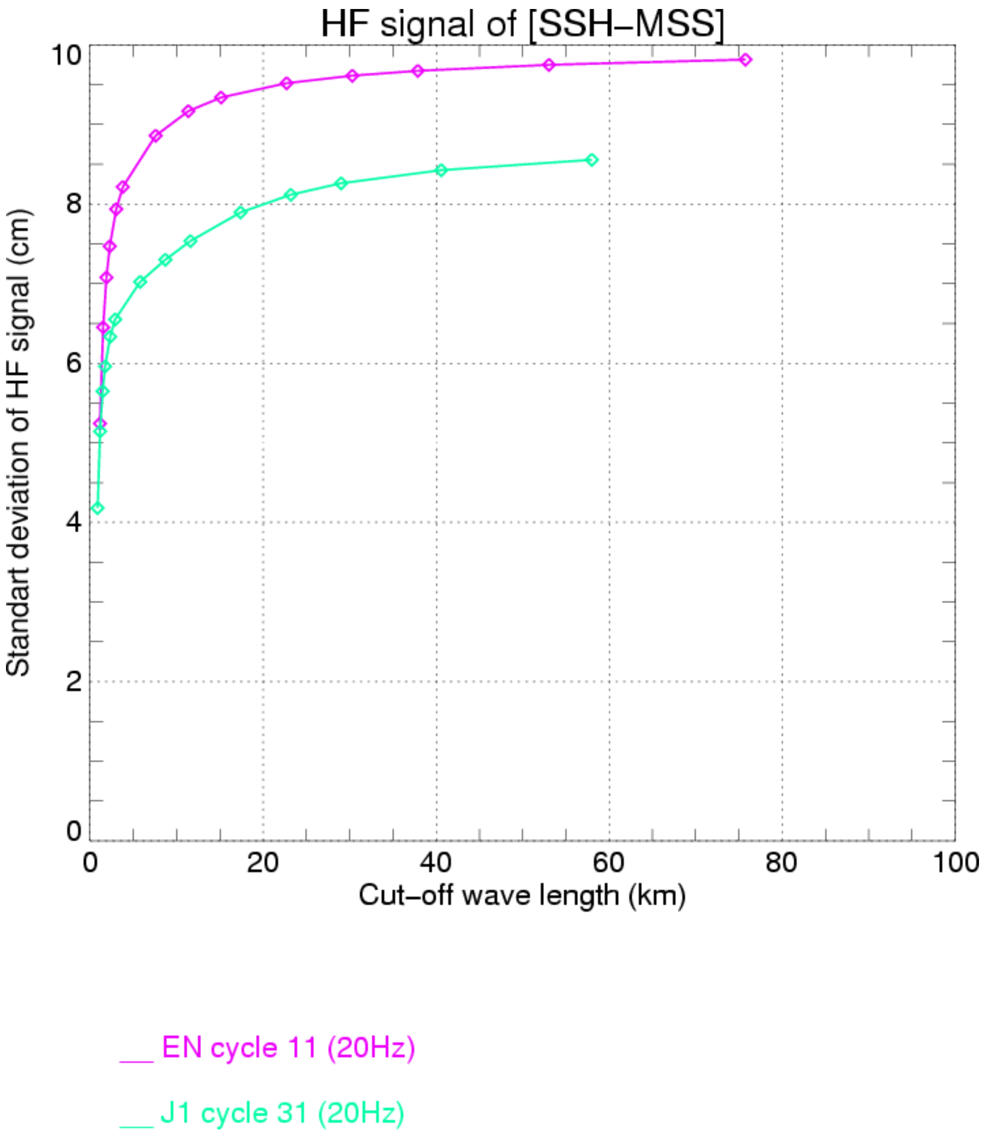

Figure 58 : Standard deviation of HF[SLA$_{nc/mss}$] at 20Hz according to cut-off wave-length

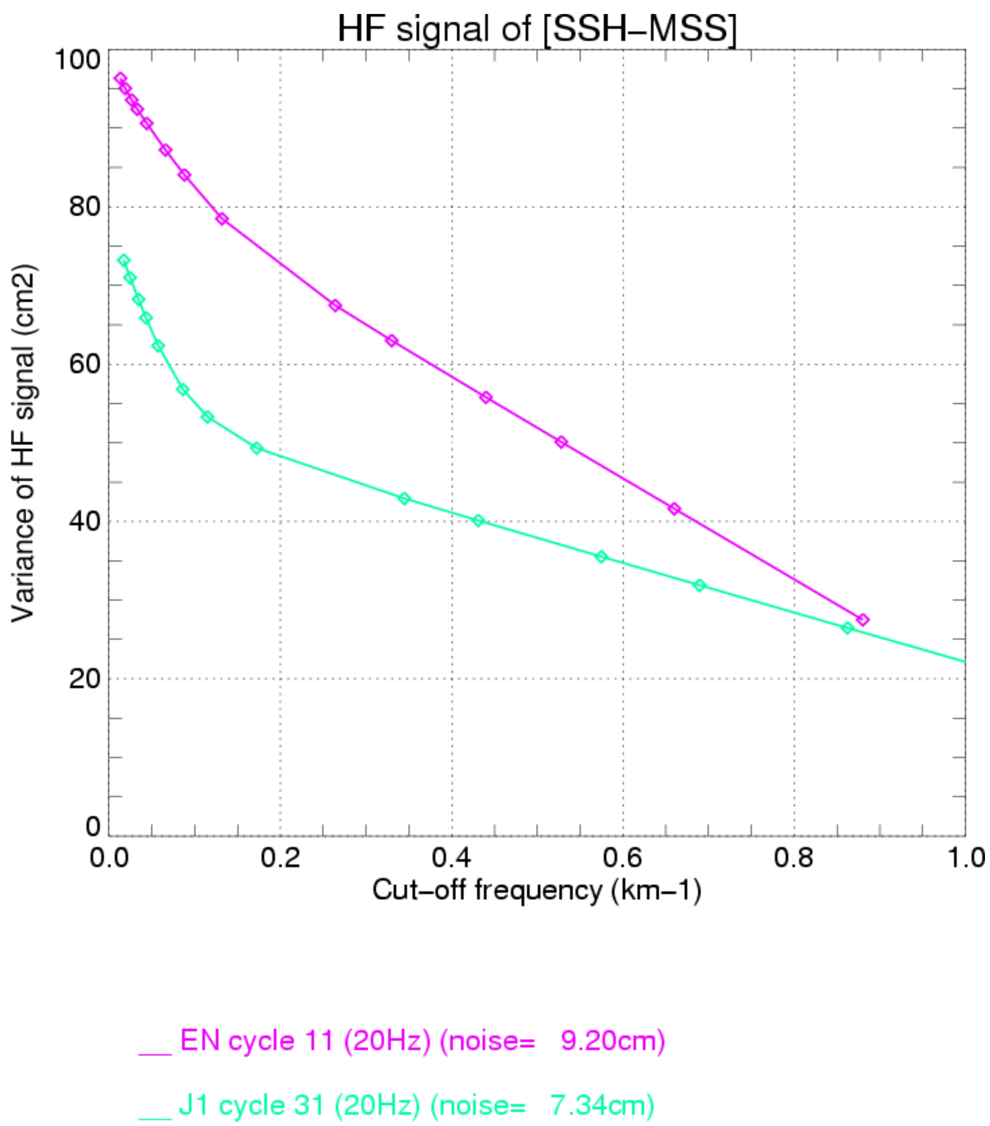

Figure 59 : Standard deviation of HF[$SLA_{nc/mss}$] at 20Hz according to the cut-off frequency

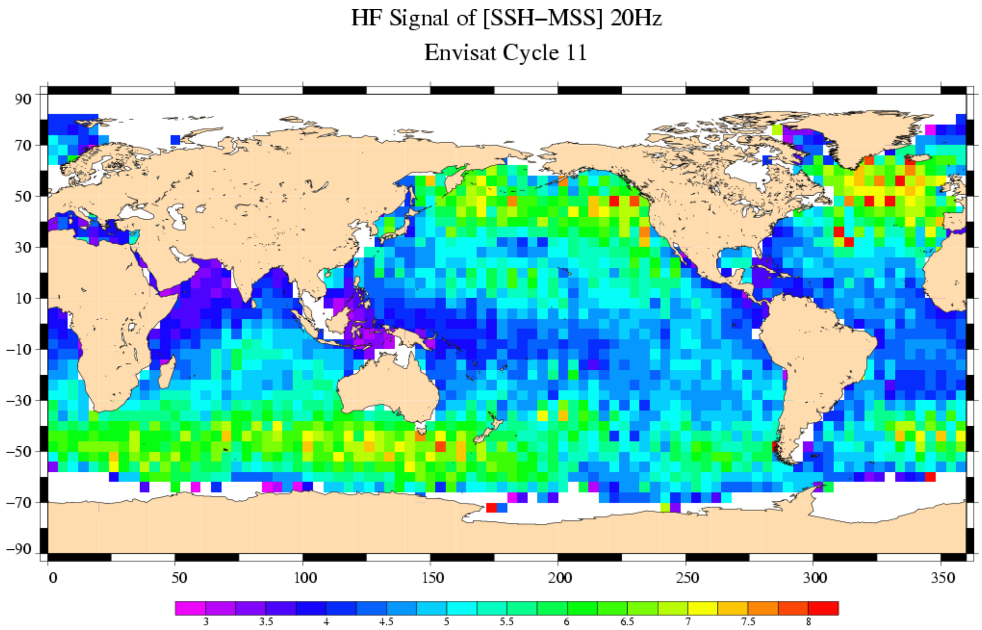

Figure 60 : Standard deviation of ENVISAT High Frequency signal, using 20Hz data

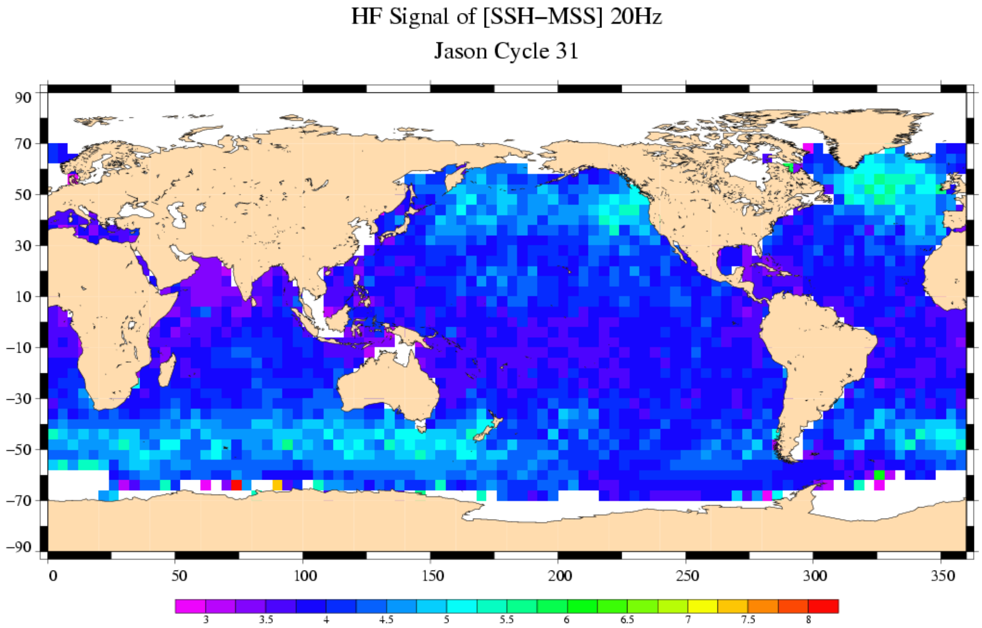

Figure 61 : Standard deviation of Jason-1 High Frequency signal, using 20Hz data

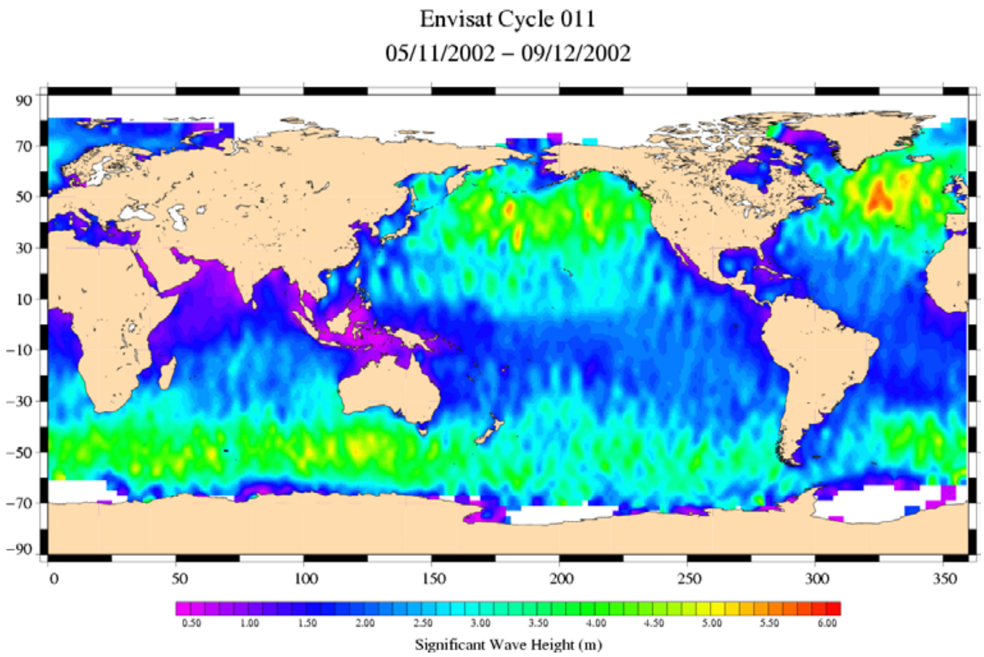

Figure 62 : ENVISAT SWH

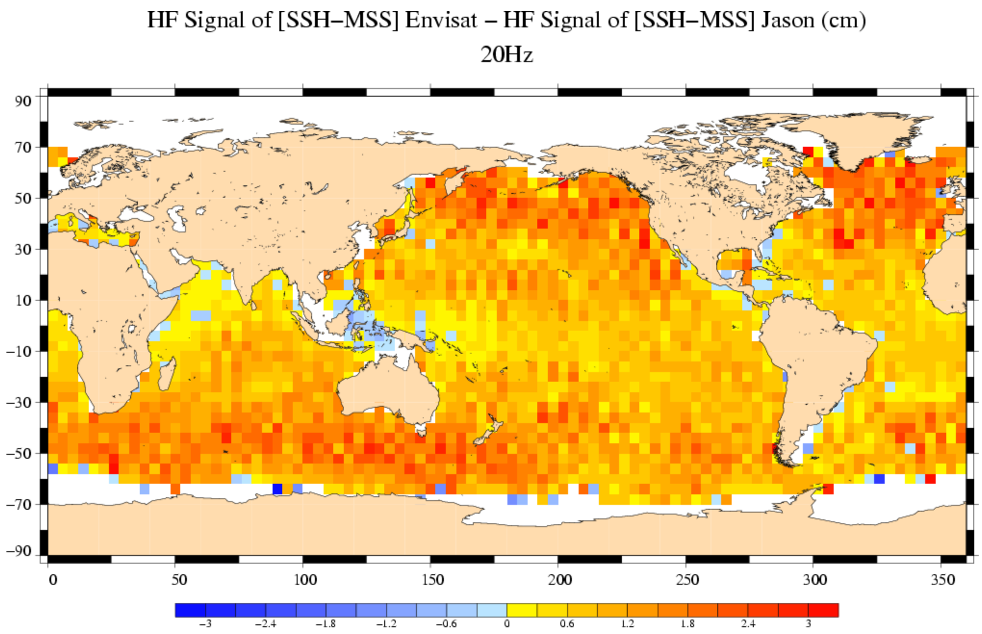

Figure 63 : Difference [Figure 61 - Figure 60]

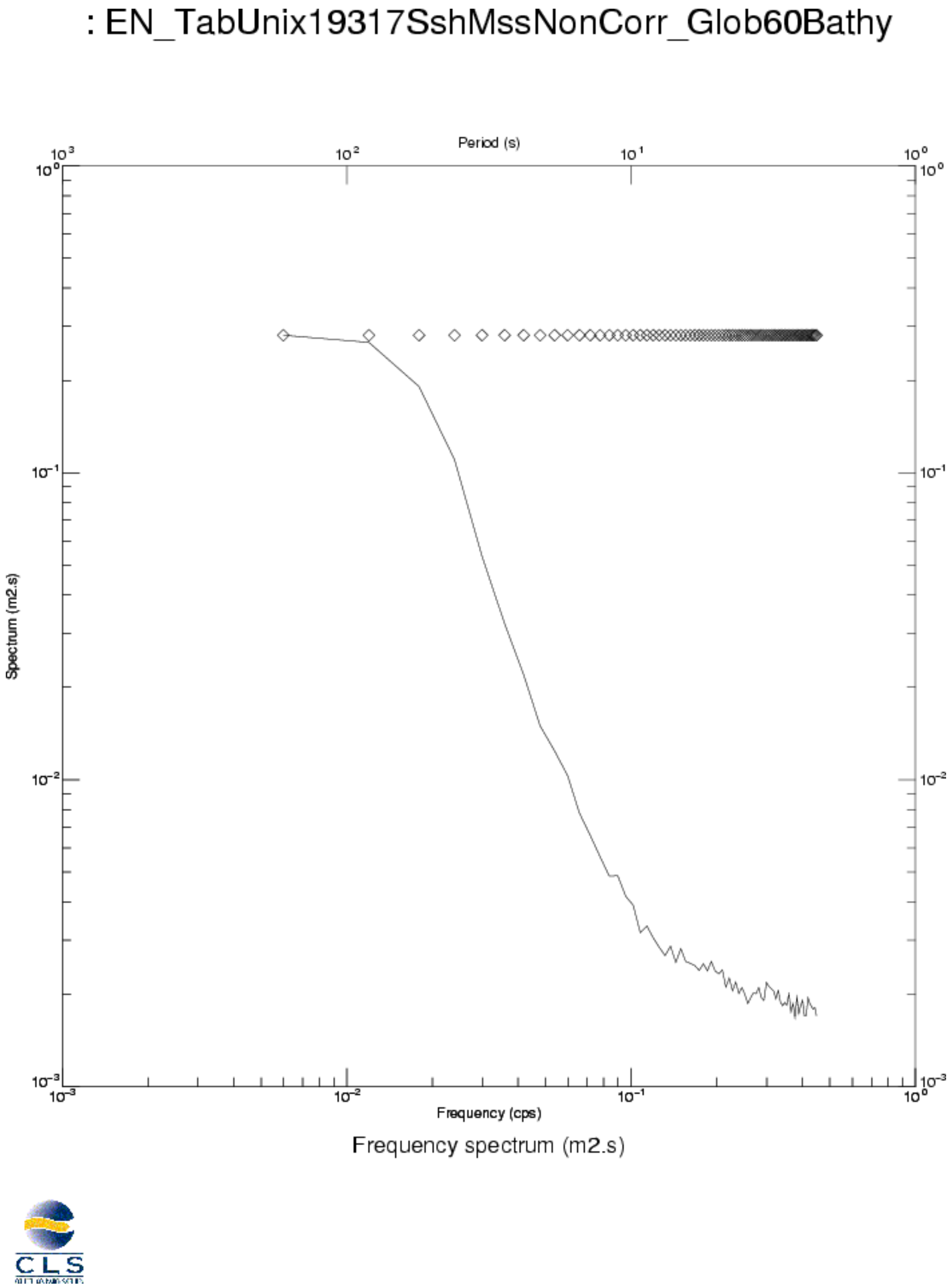

Figure 64 : Power spectrum of Envisat SLA$_{nc/mss}$, using 1Hz data

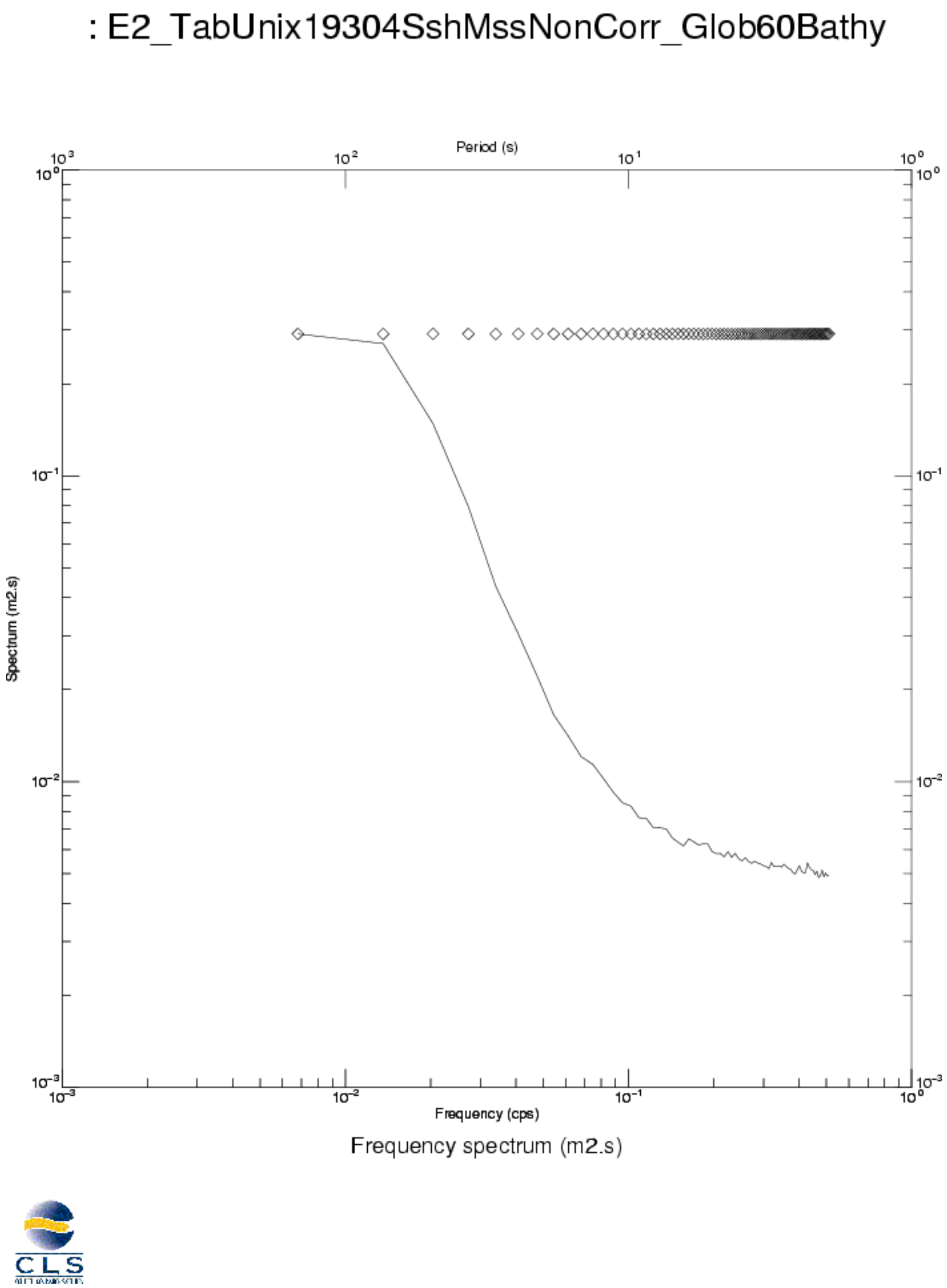

Figure 65 : Power spectrum of ERS-2 SLA$_{nc/mss}$, using 1Hz data

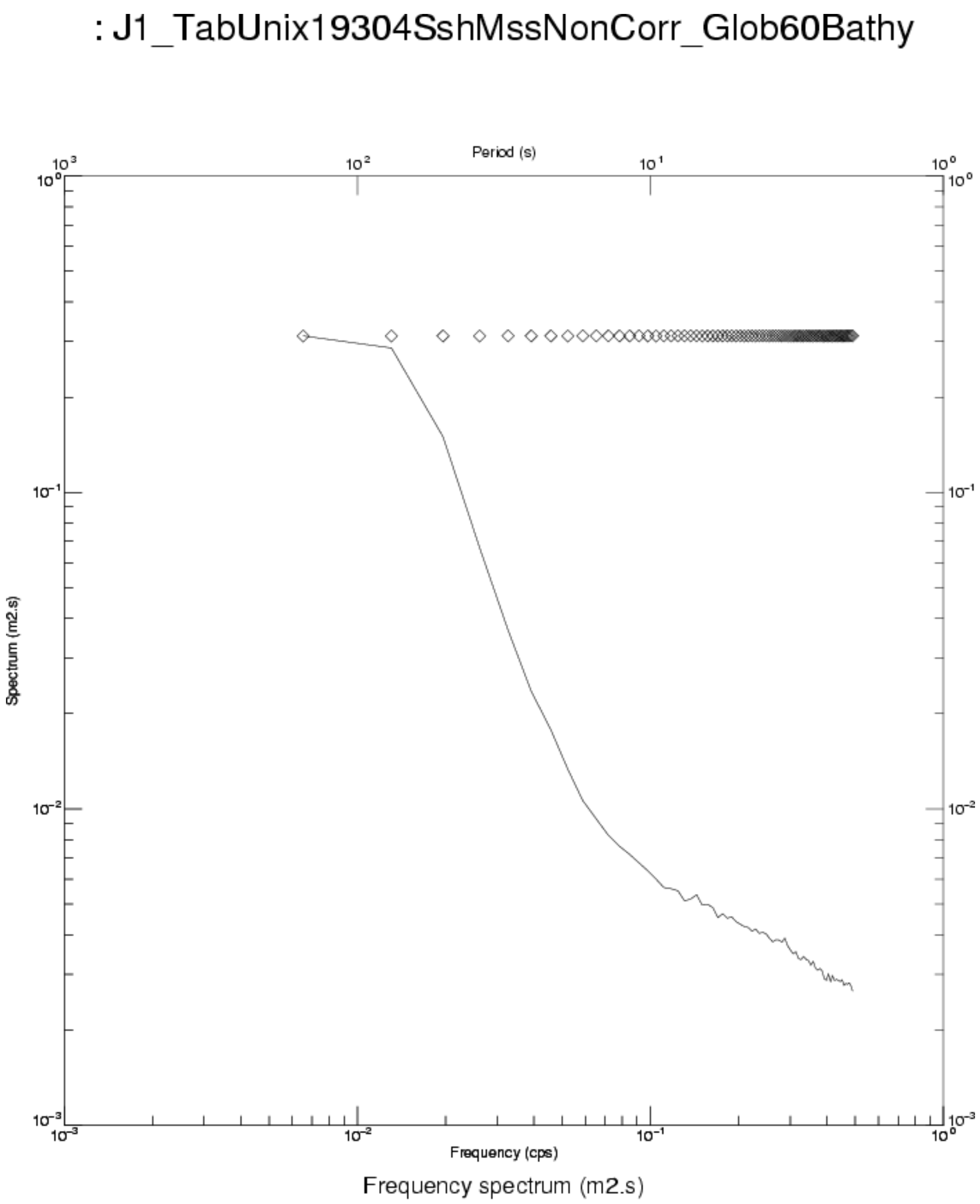

Figure 66 : Power spectrum of J1 $SLA_{nc/mss}$ using 1Hz data

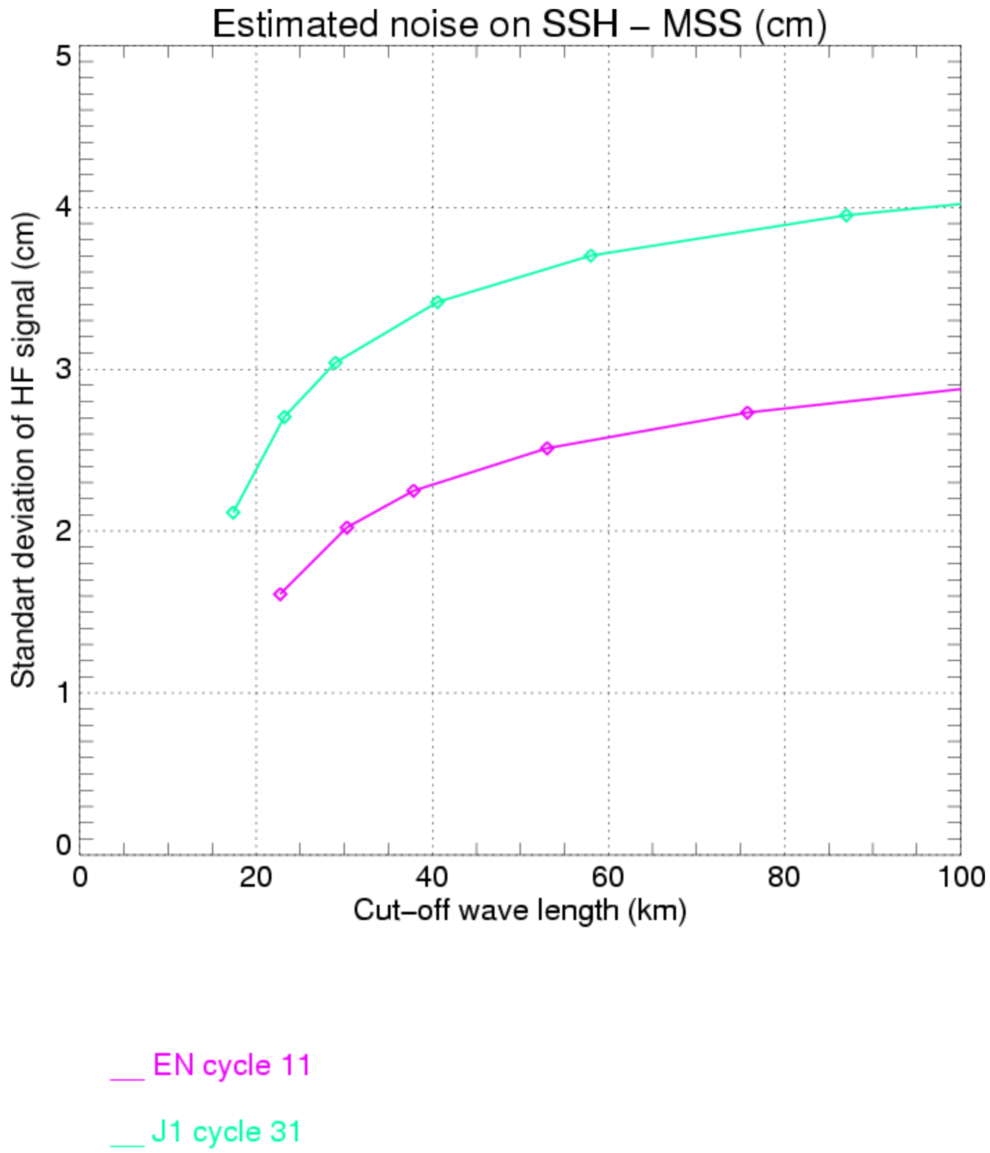

Figure 67 : Standard deviation of High Frequency signal as a function of the cut-off wave-length, using 1Hz data

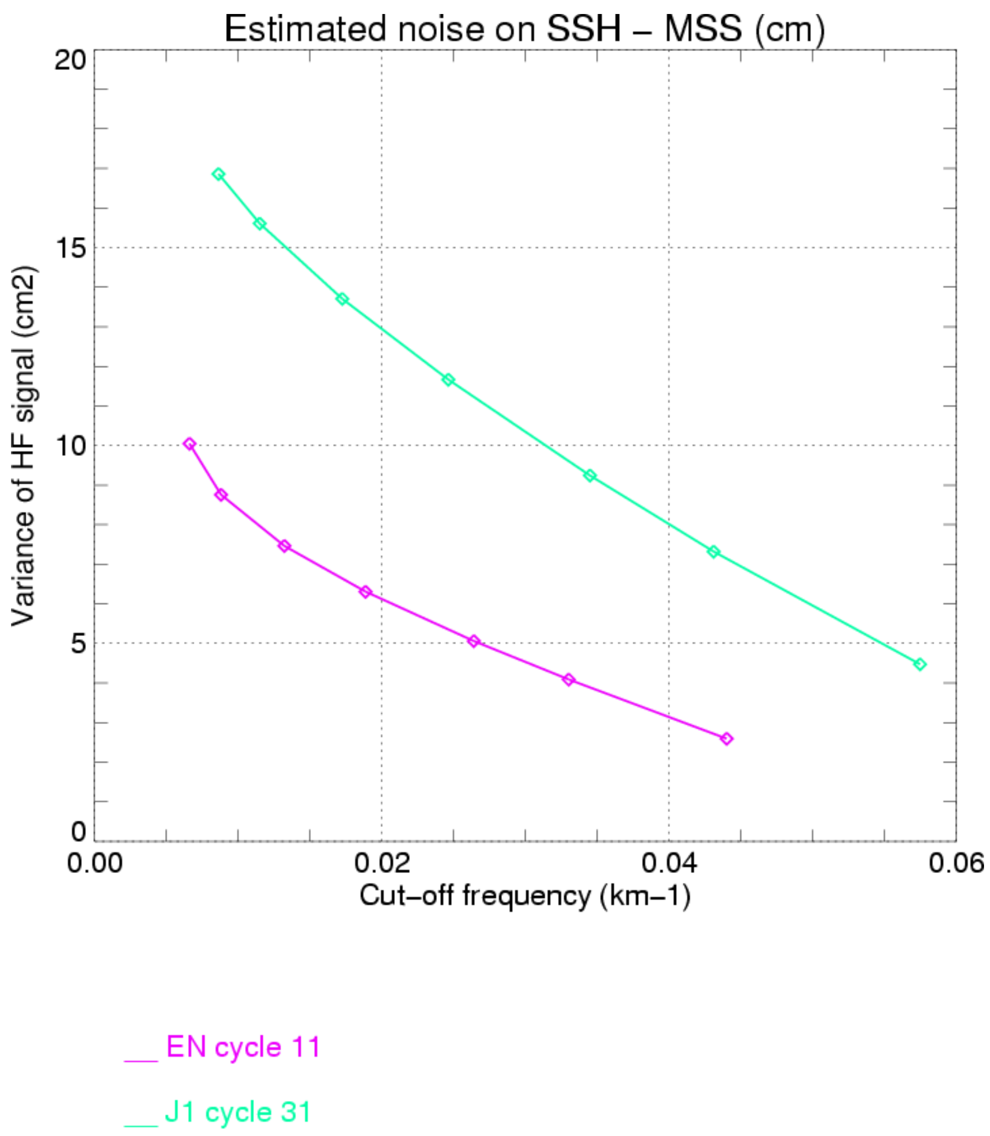

Figure 68 : Standard deviation of High Frequency signal as a function of the cut-off frequency, using 1Hz data

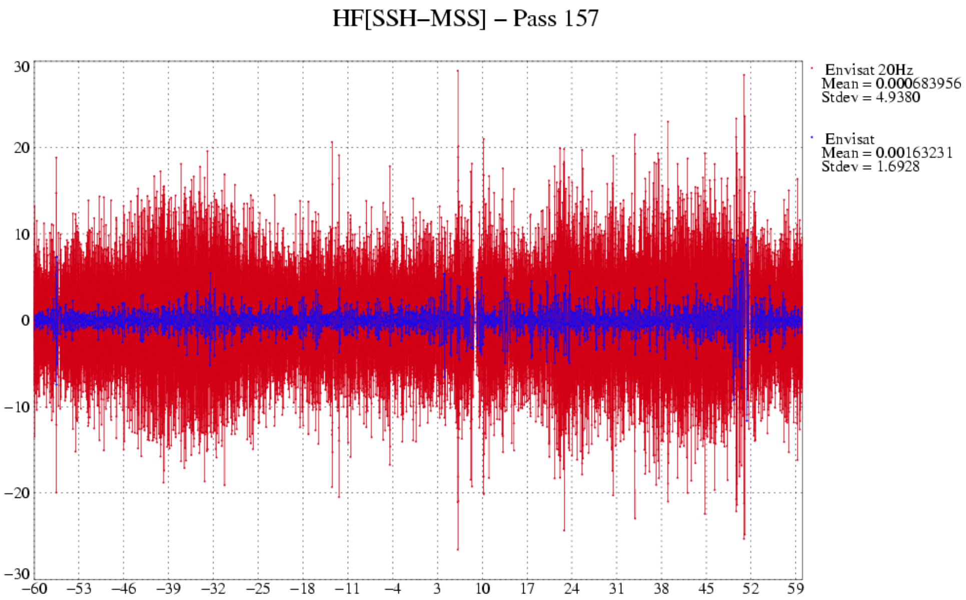

Figure 69 : HF signals, red: 20 Hz data, blue: 1 Hz data, on a particular ENVISAT pass

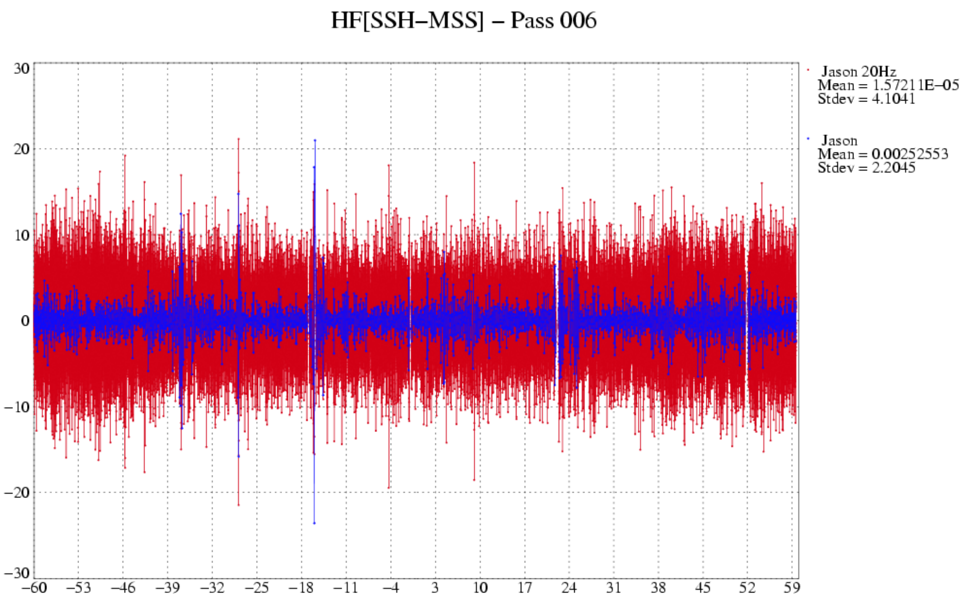

Figure 70 : HF signals, red: 20 Hz data, blue: 1 Hz data, on a particular Jason-1 pass

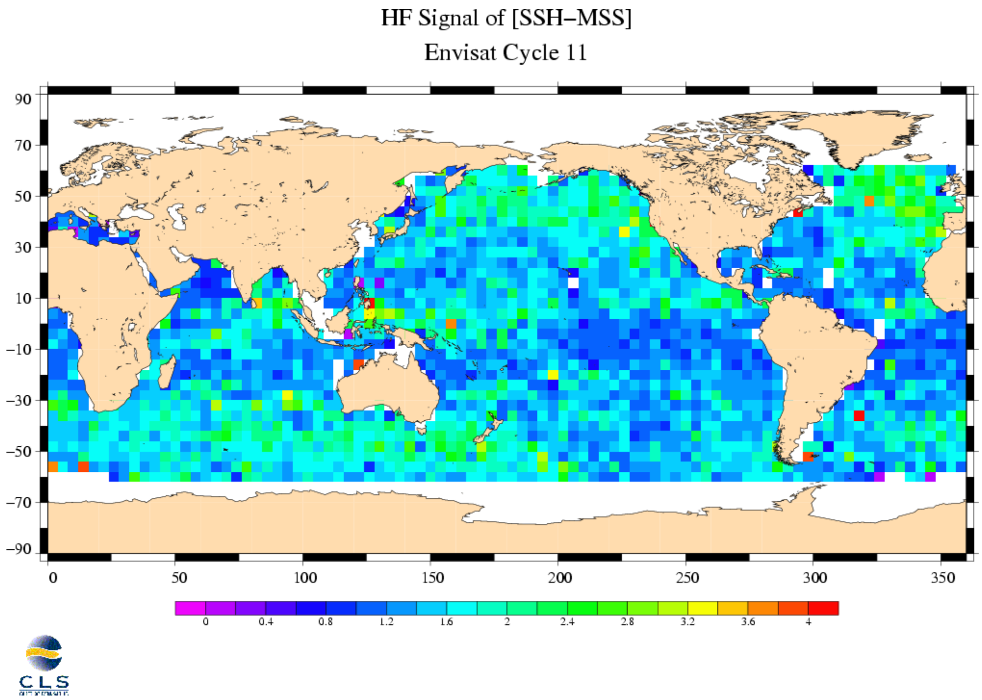

Figure 71 : Standard deviation of ENVISAT HF[$SLA_{nc/mss}$] at 1Hz

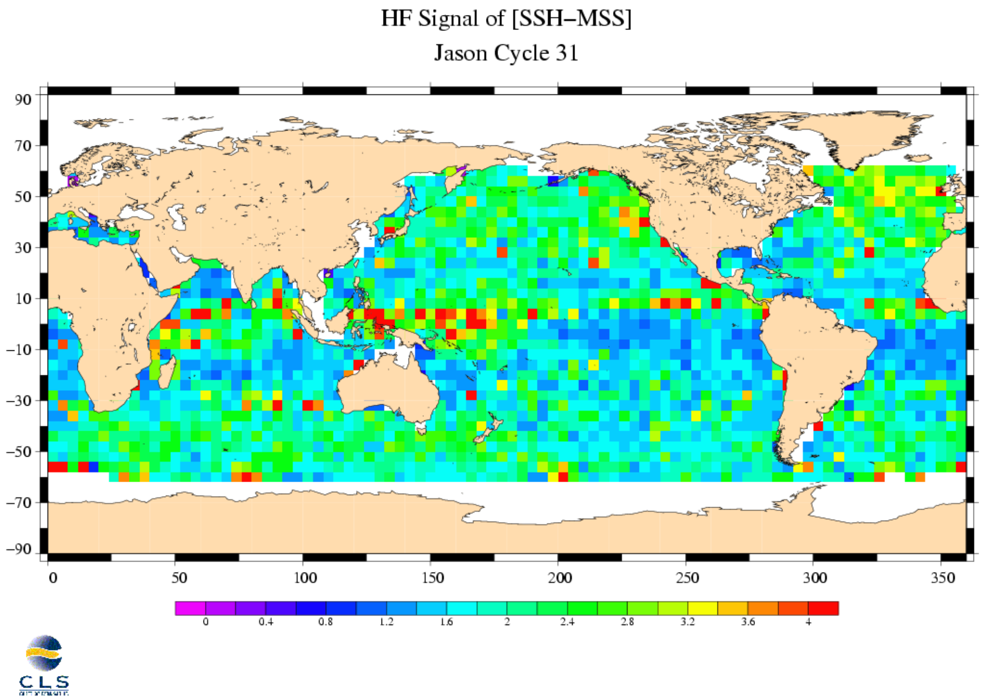

Figure 72 : Standard deviation of Jason-1 HF[$SLA_{nc/mss}$] at 1Hz

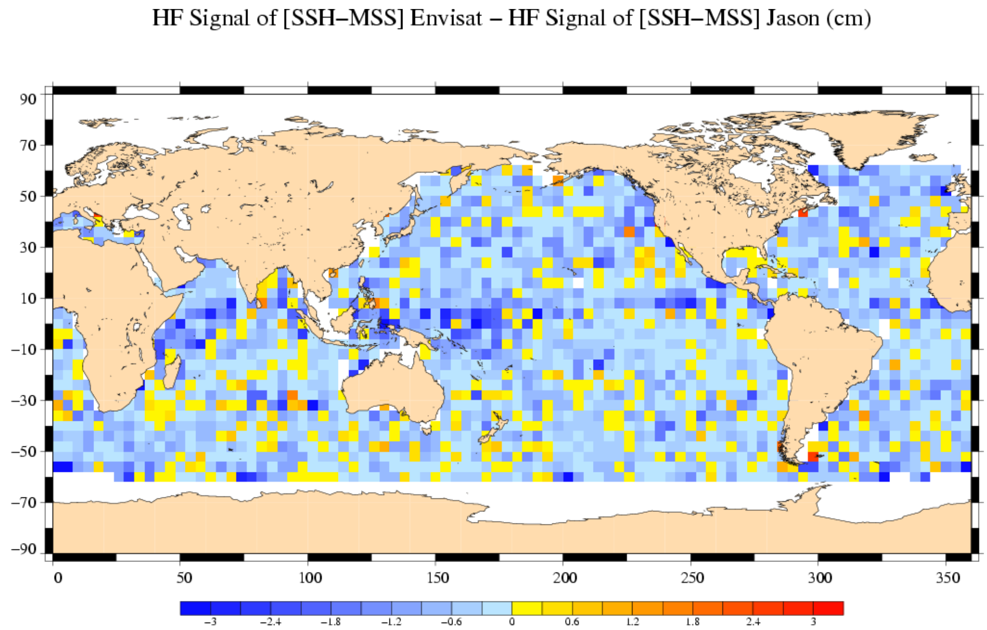

Figure 73 : Difference [Figure 72 - Figure 71]

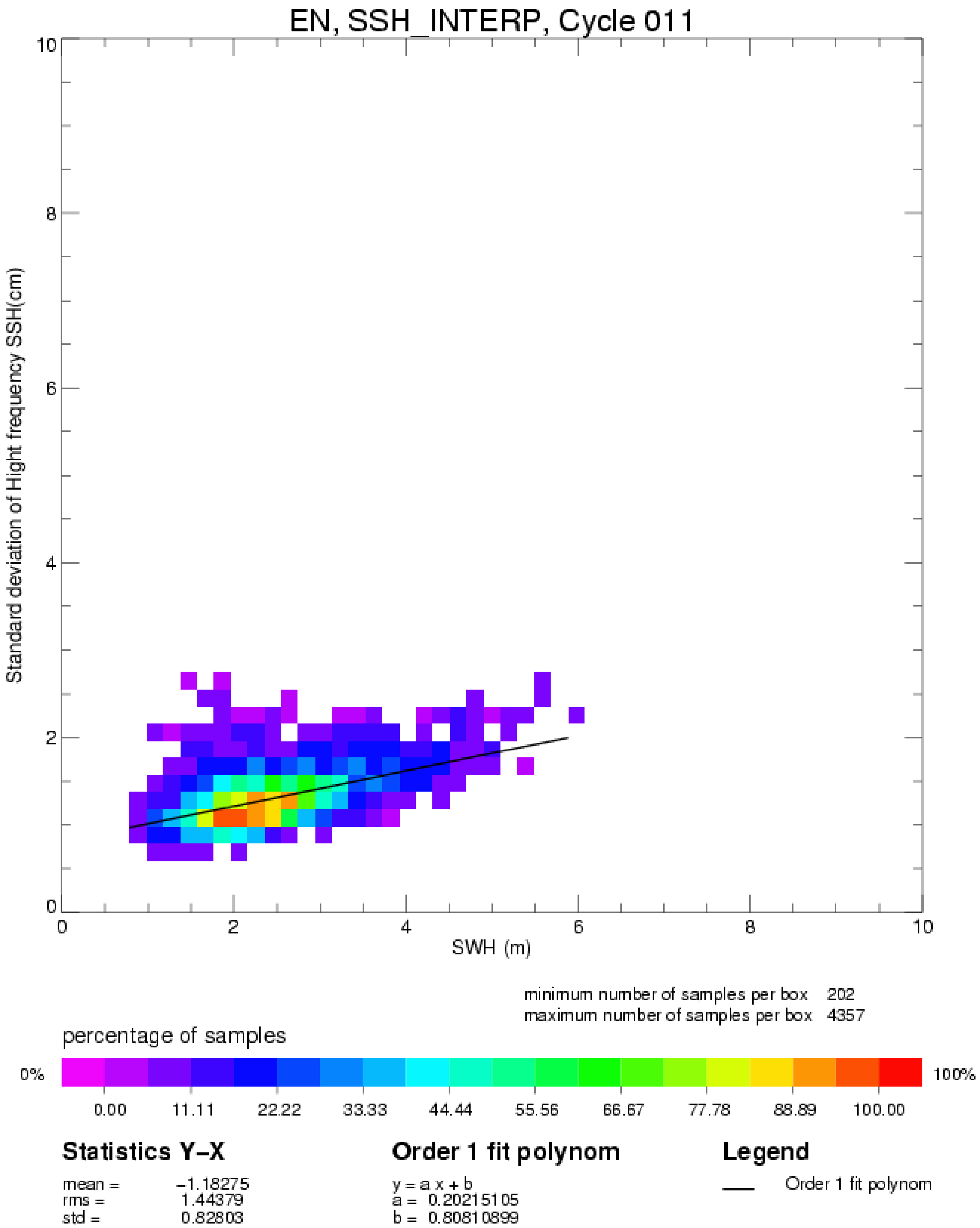

Figure 74 : Scatter plot of the standard deviation of Envisat HF[SLA$_{nc/mss}$] at 1Hz according to waves

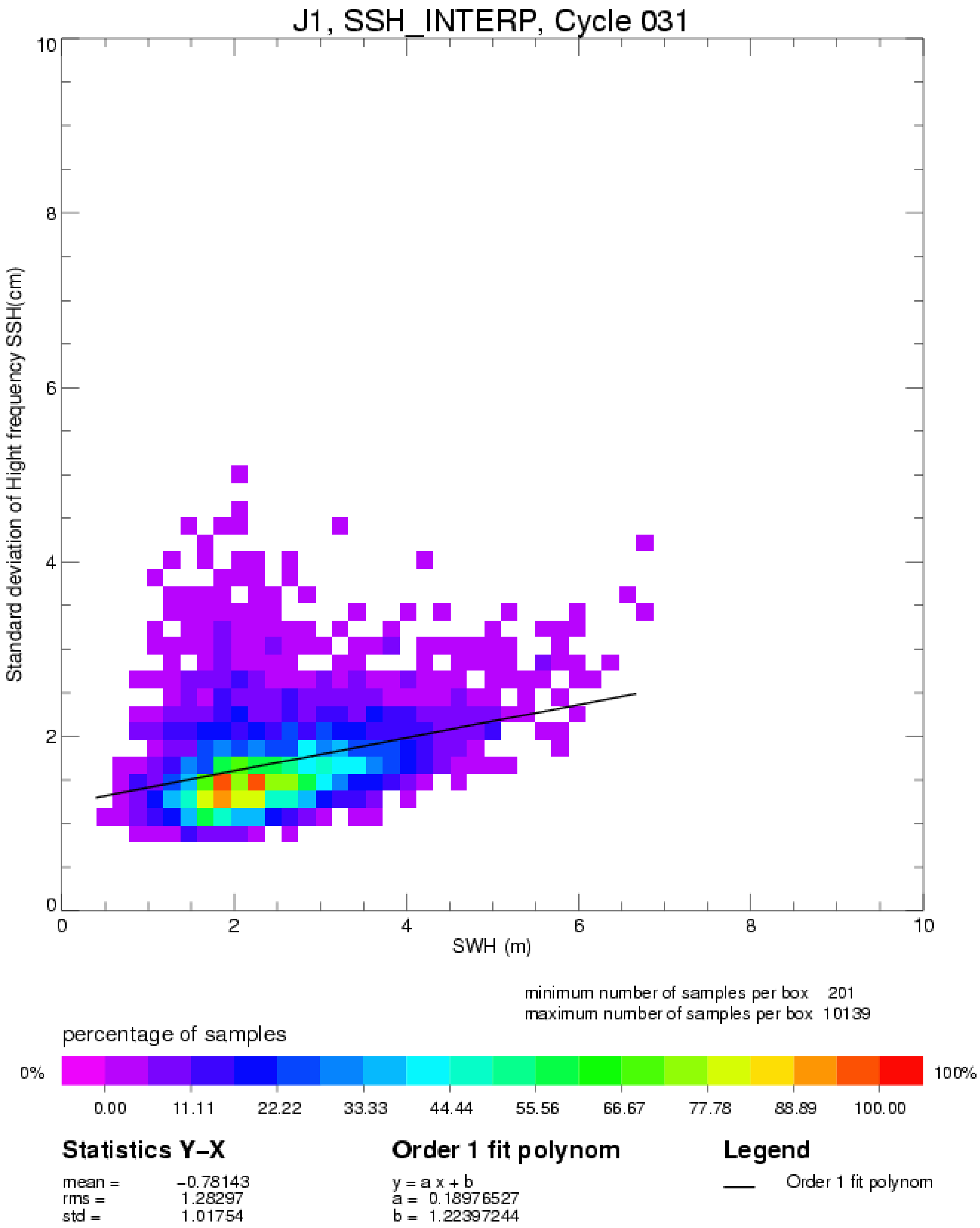

Figure 75 : Scatter plot of the standard deviation of Jason HF[$SLA_{nc/mss}$] at 1Hz according to waves

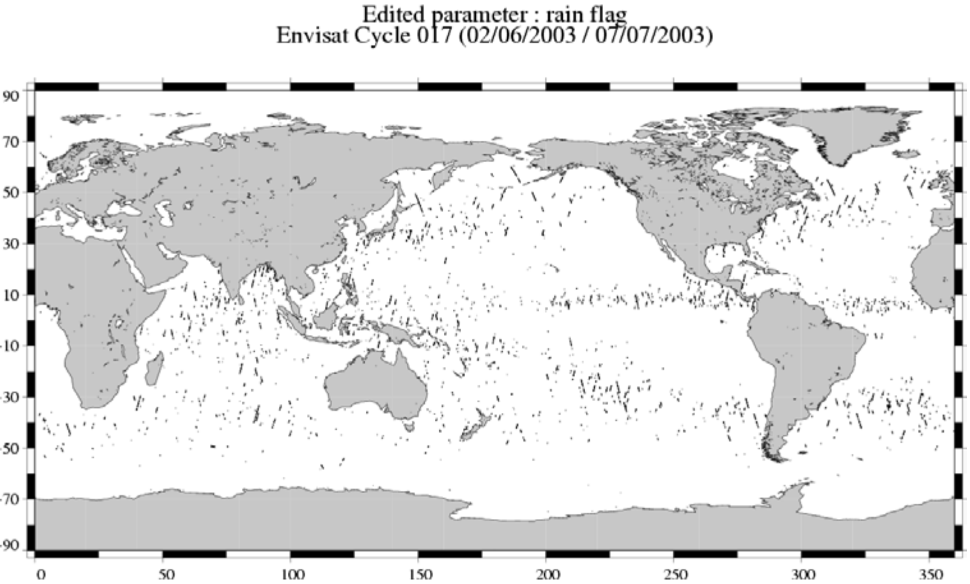

Figure 76 : Map of rain flagged points, Cycle 17

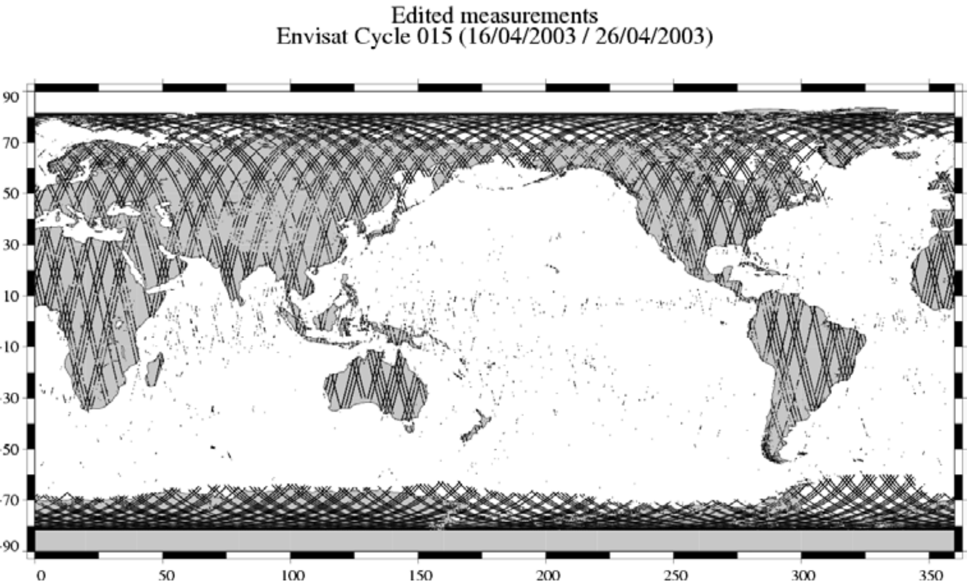

Figure 77 : Map of edited measurements, Cycle 17

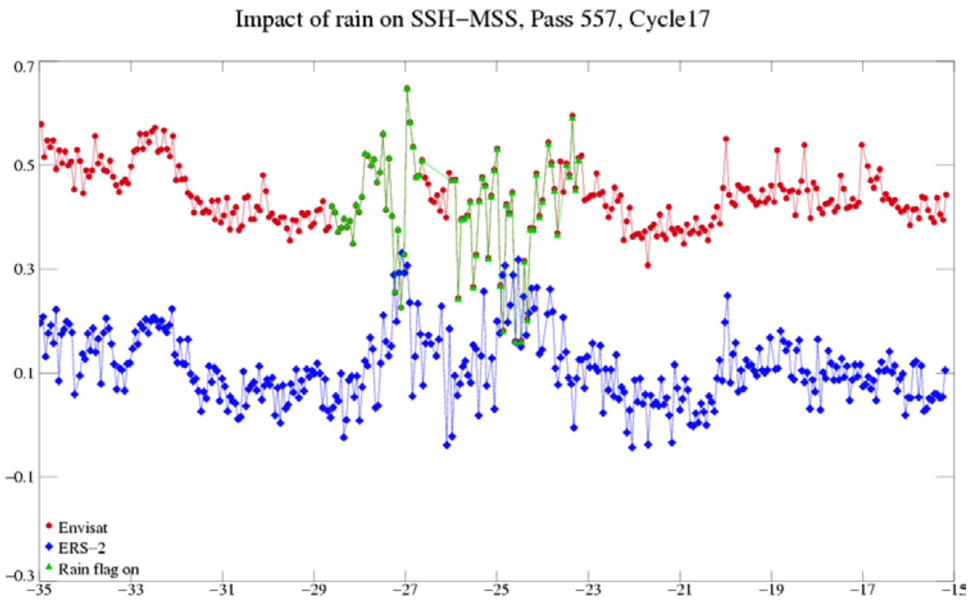

Figure 78 : Impact of rain on SSH-MSS, Pass 557, Cycle 17

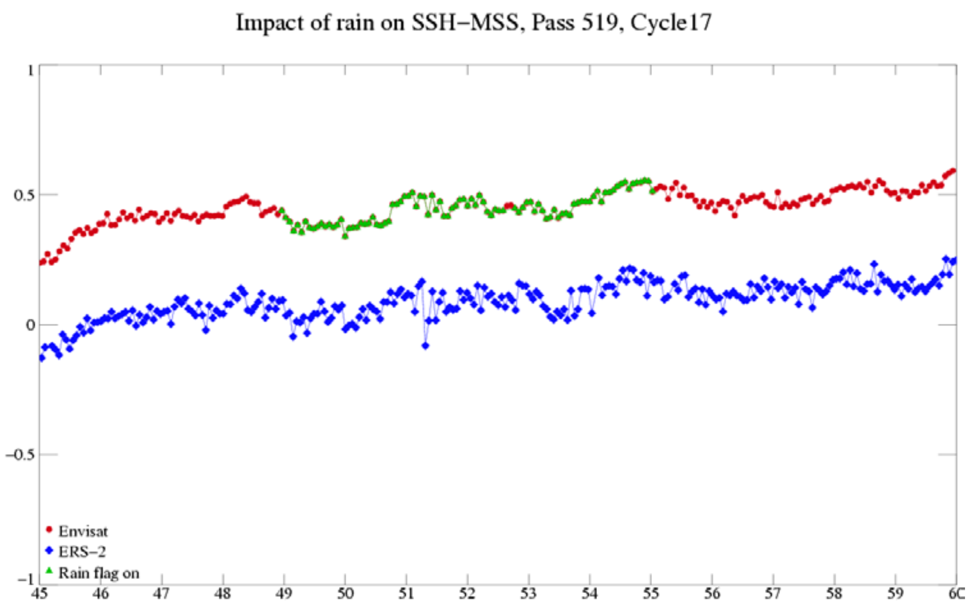

Figure 79 : Impact of rain on SSH-MSS, Pass 519, Cycle 17

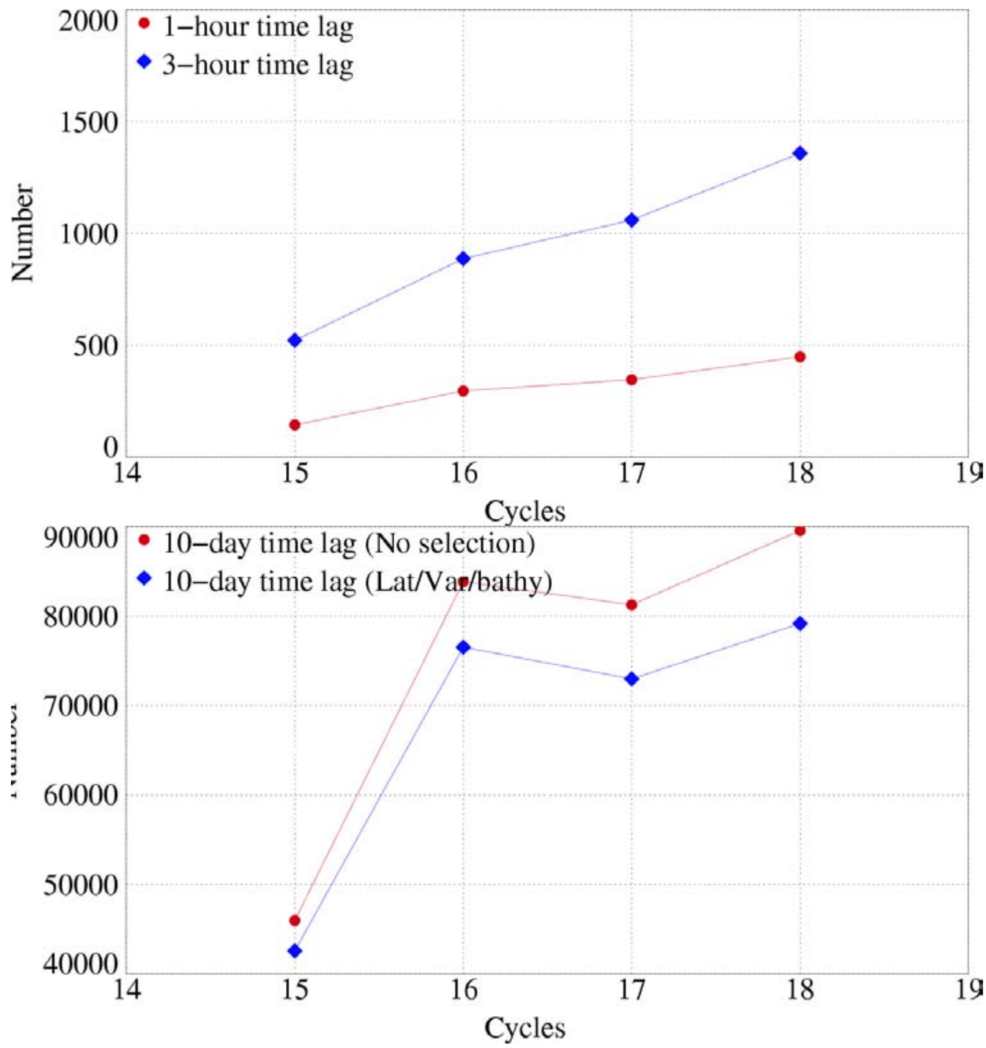

Figure 80 : Number of Jason-1/Envisat 1 hour, 3 hour and 10 days time lag dual crossover

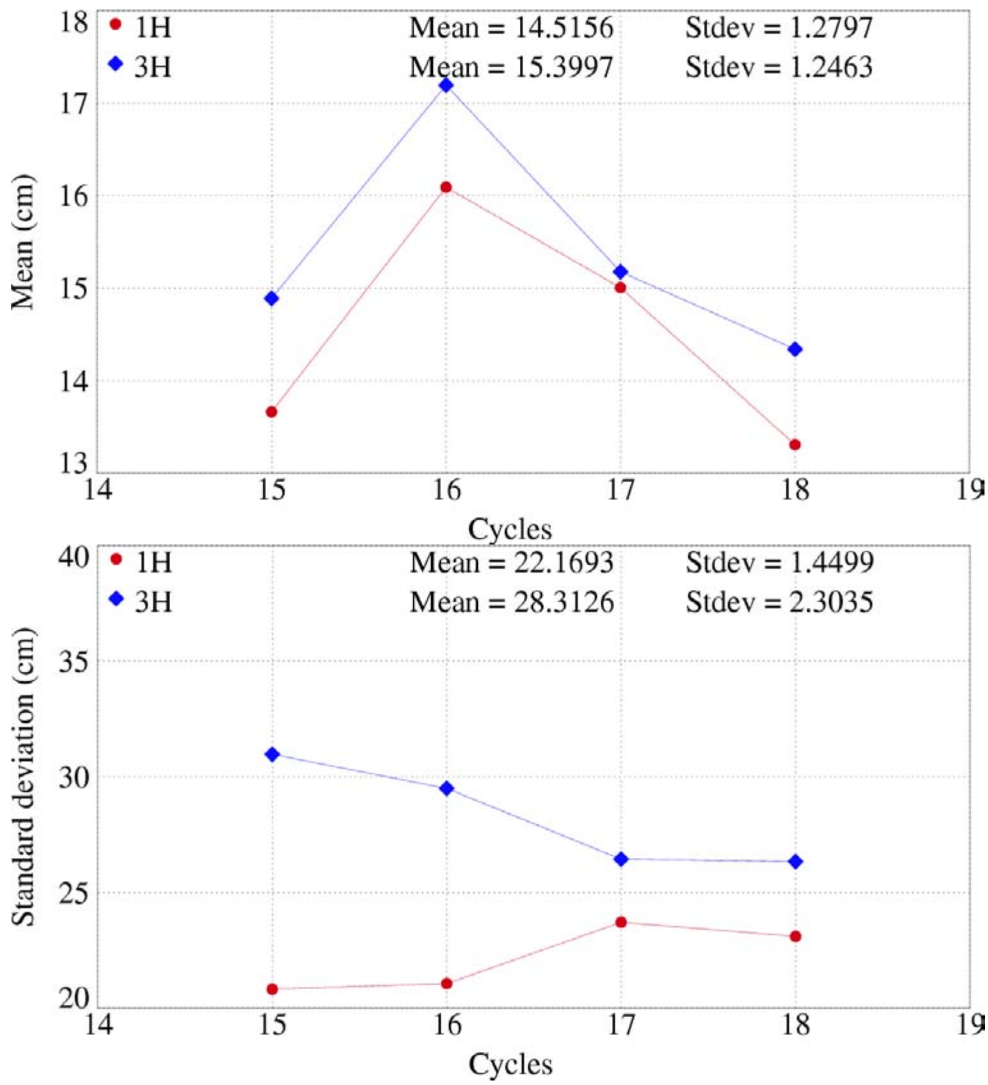

Figure 81 : Mean and standard deviation of [Envisat – Jason-1] Ku SWH differences at crossover (cm)

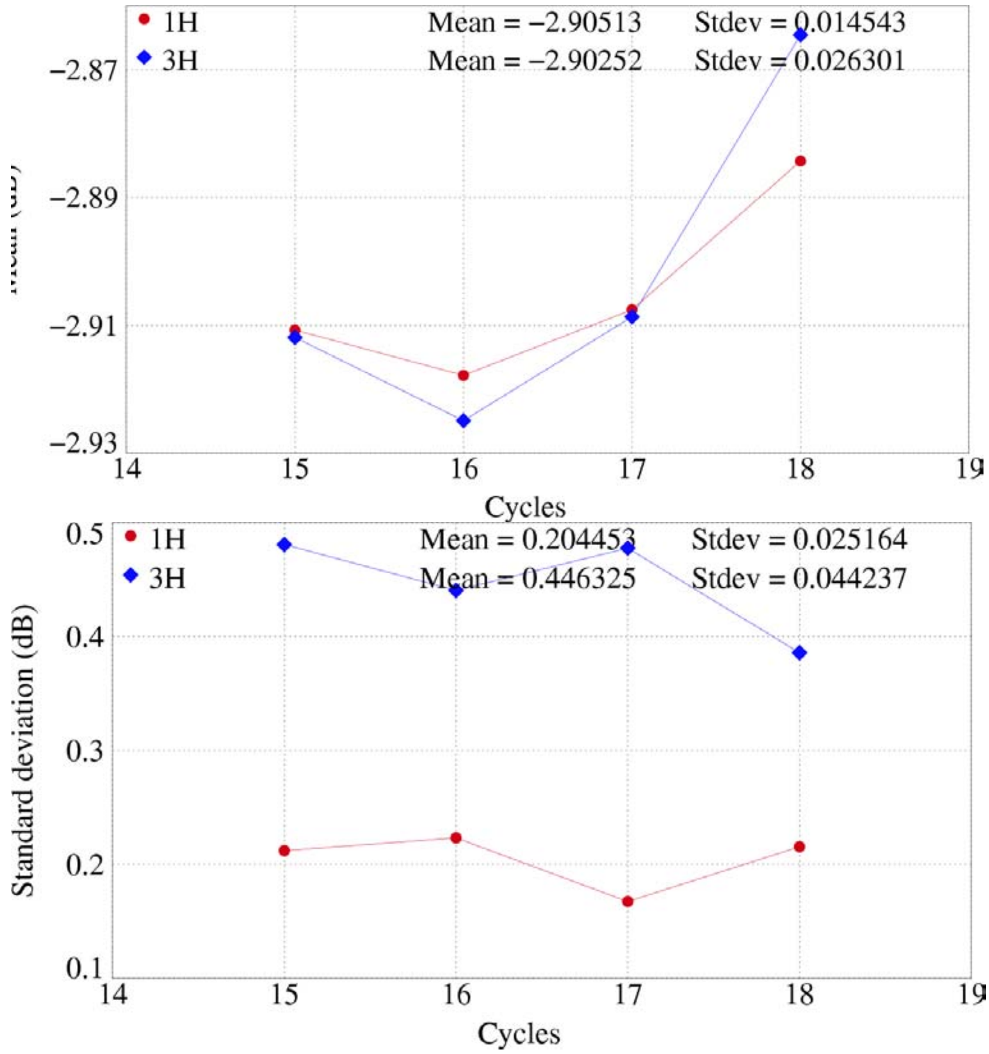

Figure 82 : Mean and standard deviation of [Envisat – Jason-1] Ku Sigma0 differences at crossover (dB)

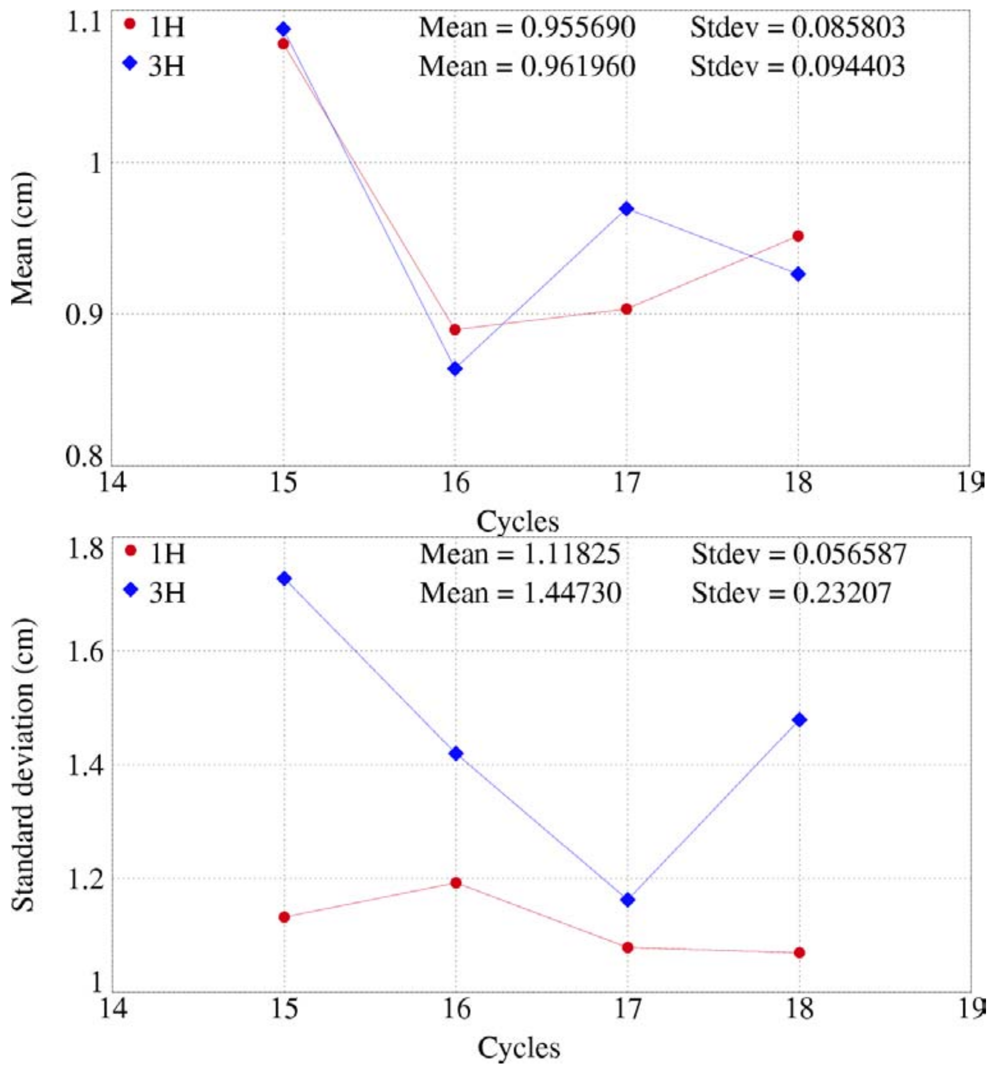

Figure 83 : Mean and standard deviation of [Envisat – Jason-1] dual frequency ionosphere correction differences at crossover (cm)

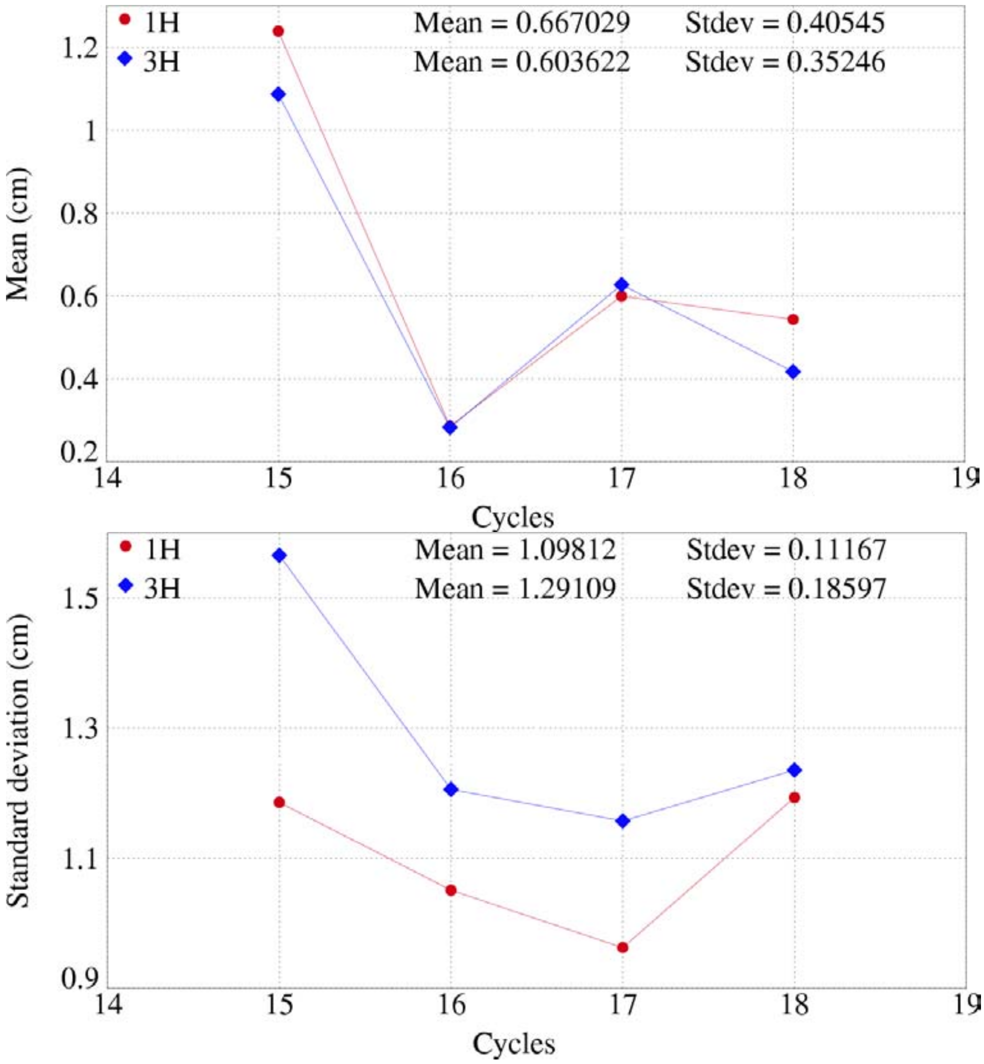

Figure 84 : Mean and standard deviation of [Envisat – Jason-1] DORIS ionosphere correction differences at crossover (cm)

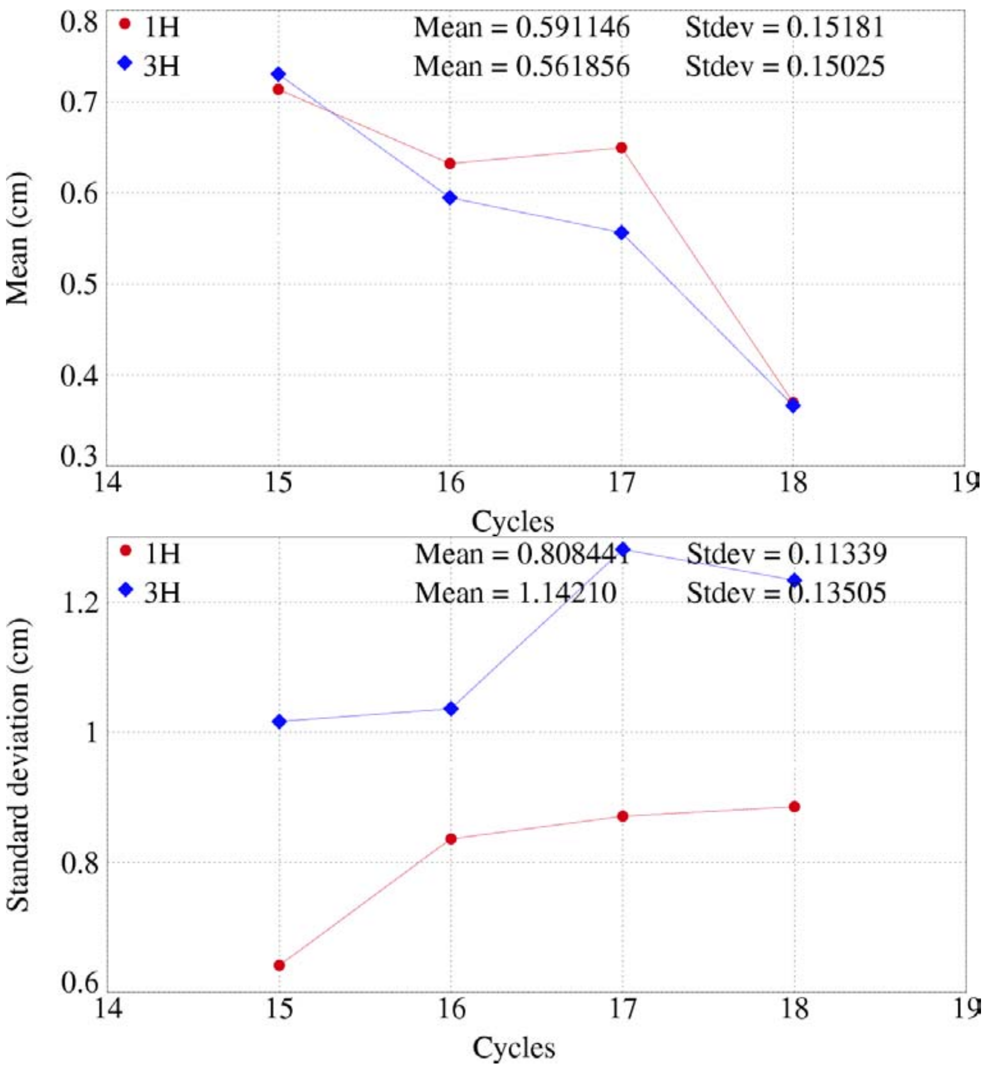

Figure 85 : Mean and standard deviation of [Envisat – Jason-1] Radiometer wet troposphere correction differences at crossover (cm)

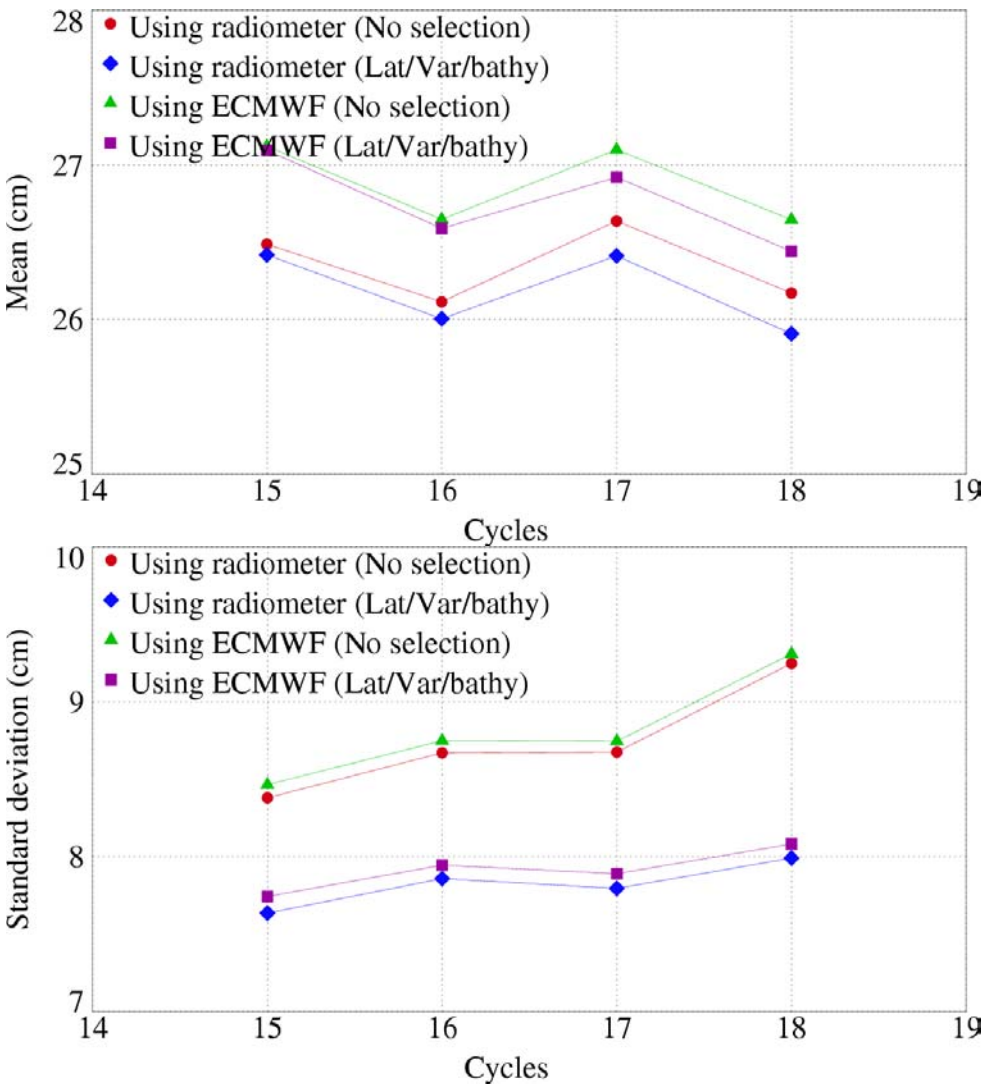

Figure 86 : Number, mean and standard deviation of [Envisat – Jason-1] SSH differences at crossover (cm)

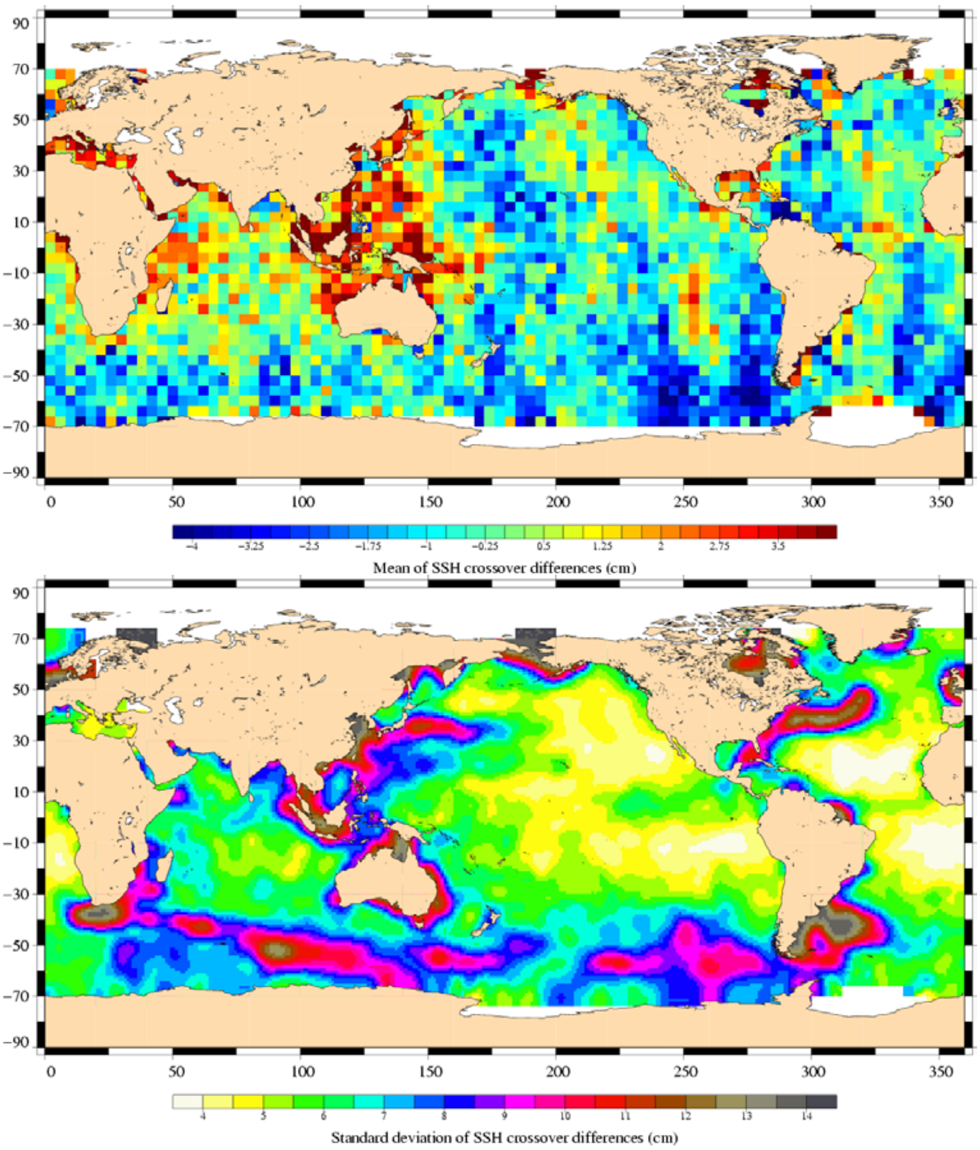

Figure 87 : Geographical pattern (4x4 degree bins) of crossover [Envisat – Jason-1] mean and standard deviation SSH differences (cm), from cycle 15 to cycle 18

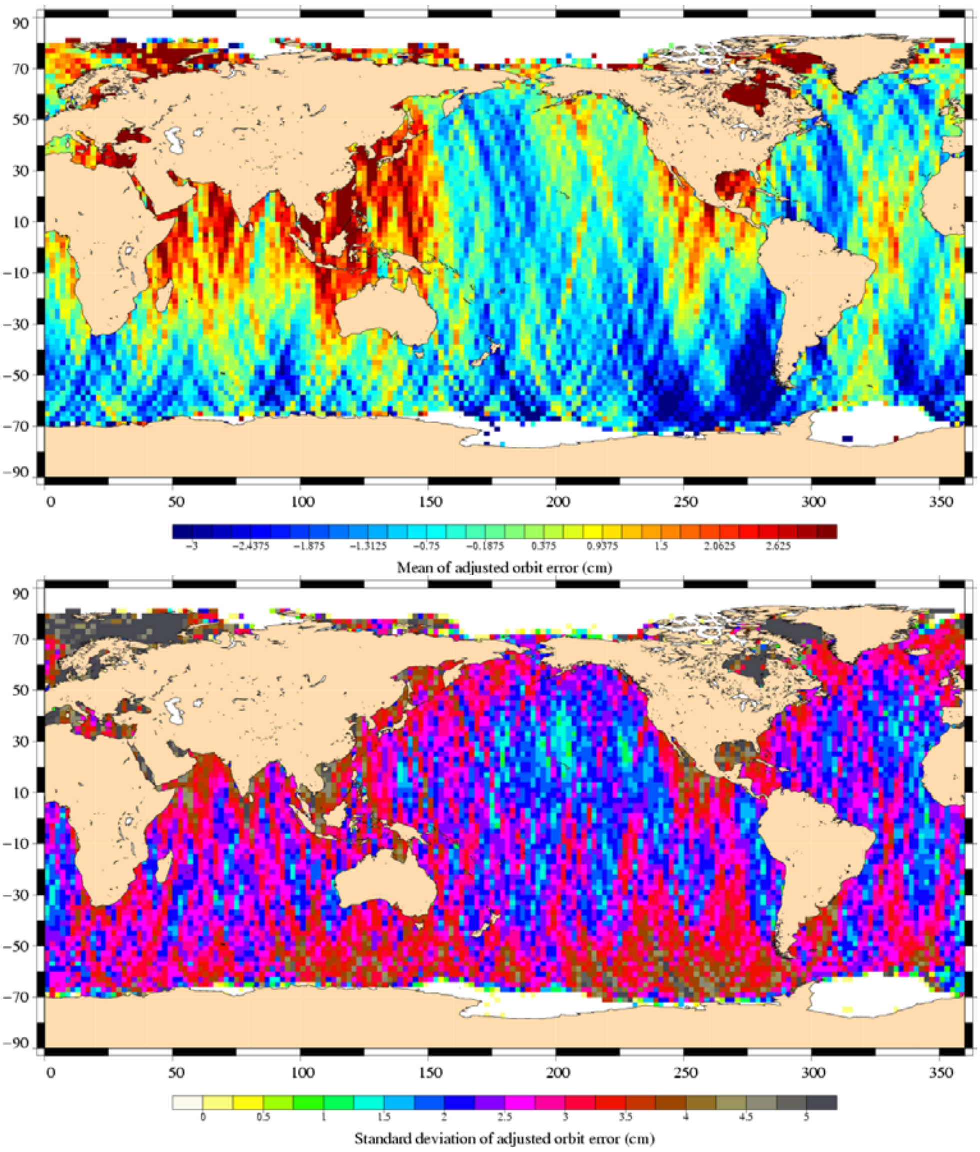

Figure 88 : Geographical pattern (2x2 degree bins) of mean (centred about the Global mean value) and standard deviation of the Envisat adjusted long wave length error (cm), from cycle 15 to cycle 18

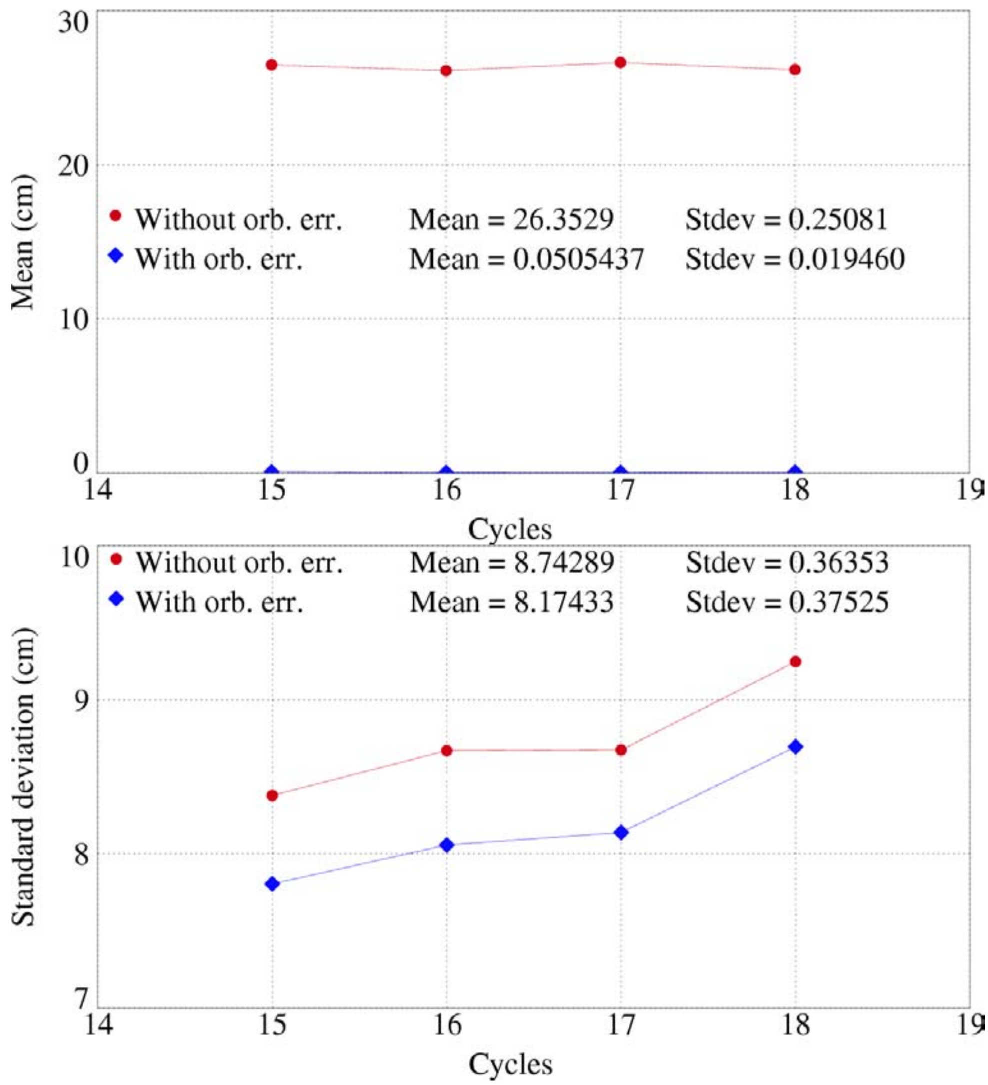

Figure 89 : Mean and standard deviation of [Envisat – Jason-1] SSH differences at crossover using adjusted long wave length error (cm)

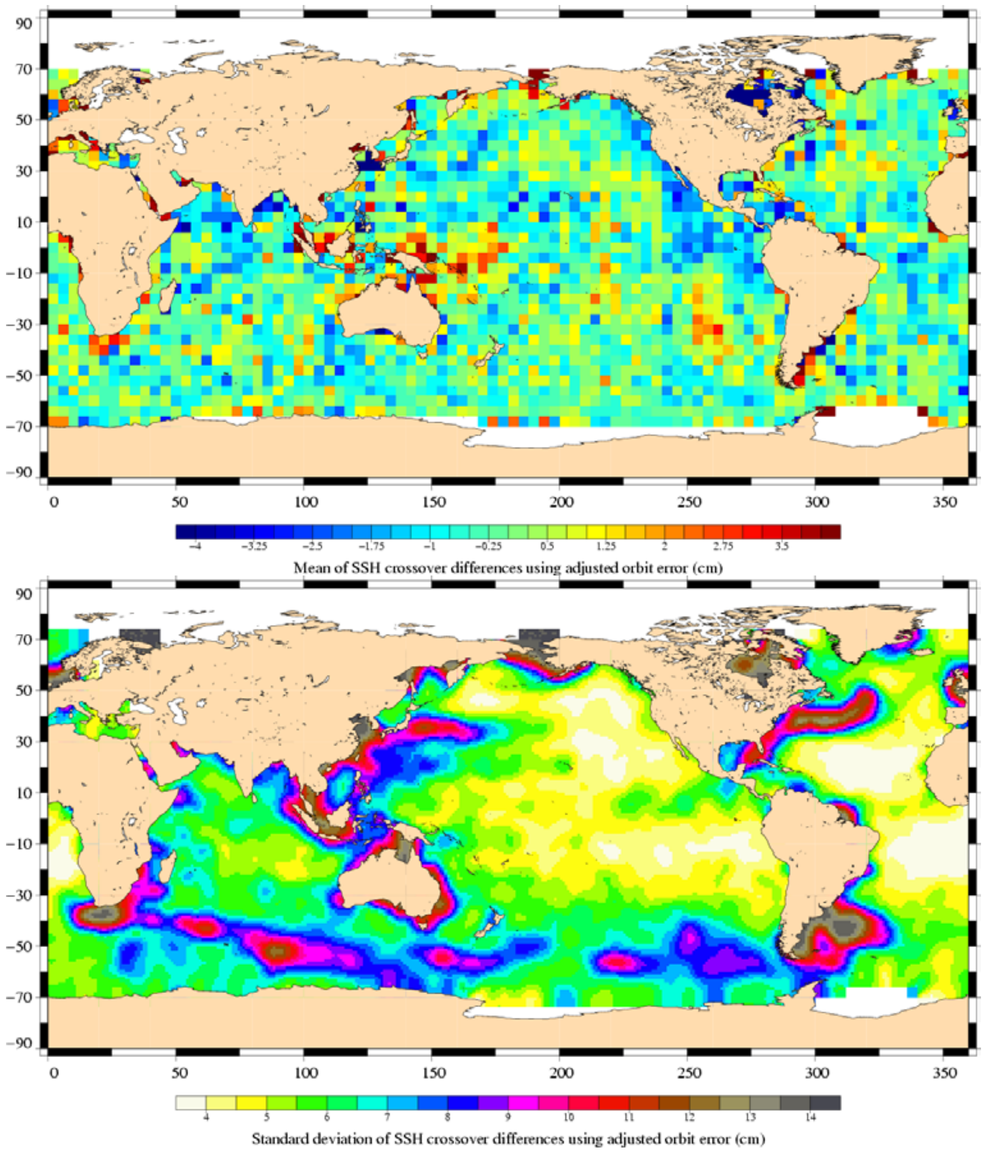

Figure 90 : Geographical pattern (4x4 degree bins) of crossover [Envisat – Jason-1] mean and standard deviation SSH differences using adjusted long wave length error (cm), from cycle 15 to cycle 18

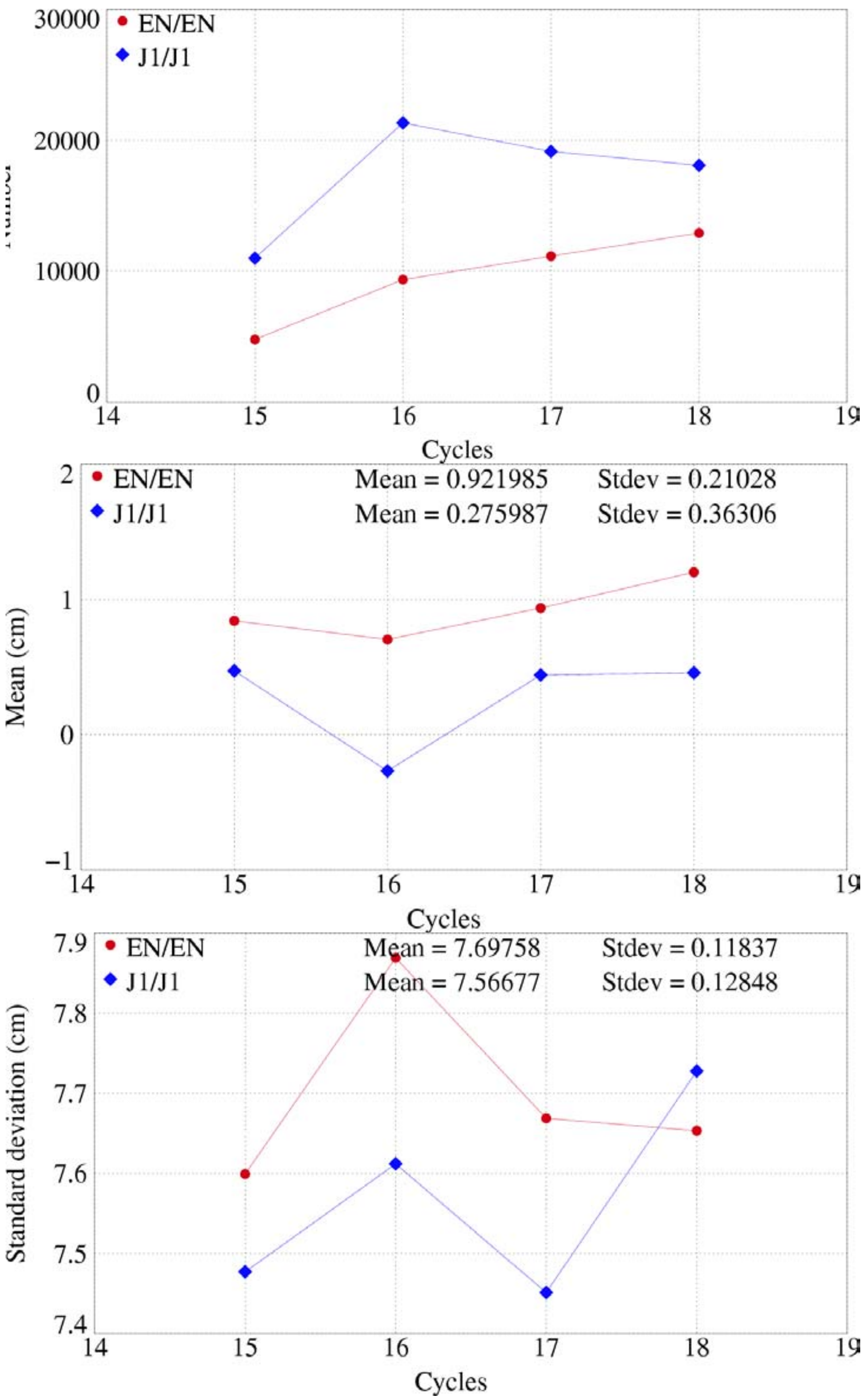

Figure 91 : Number, mean and standard deviation of SSH differences at crossover (cm), |latitude|<66°, Bathy<-1000m

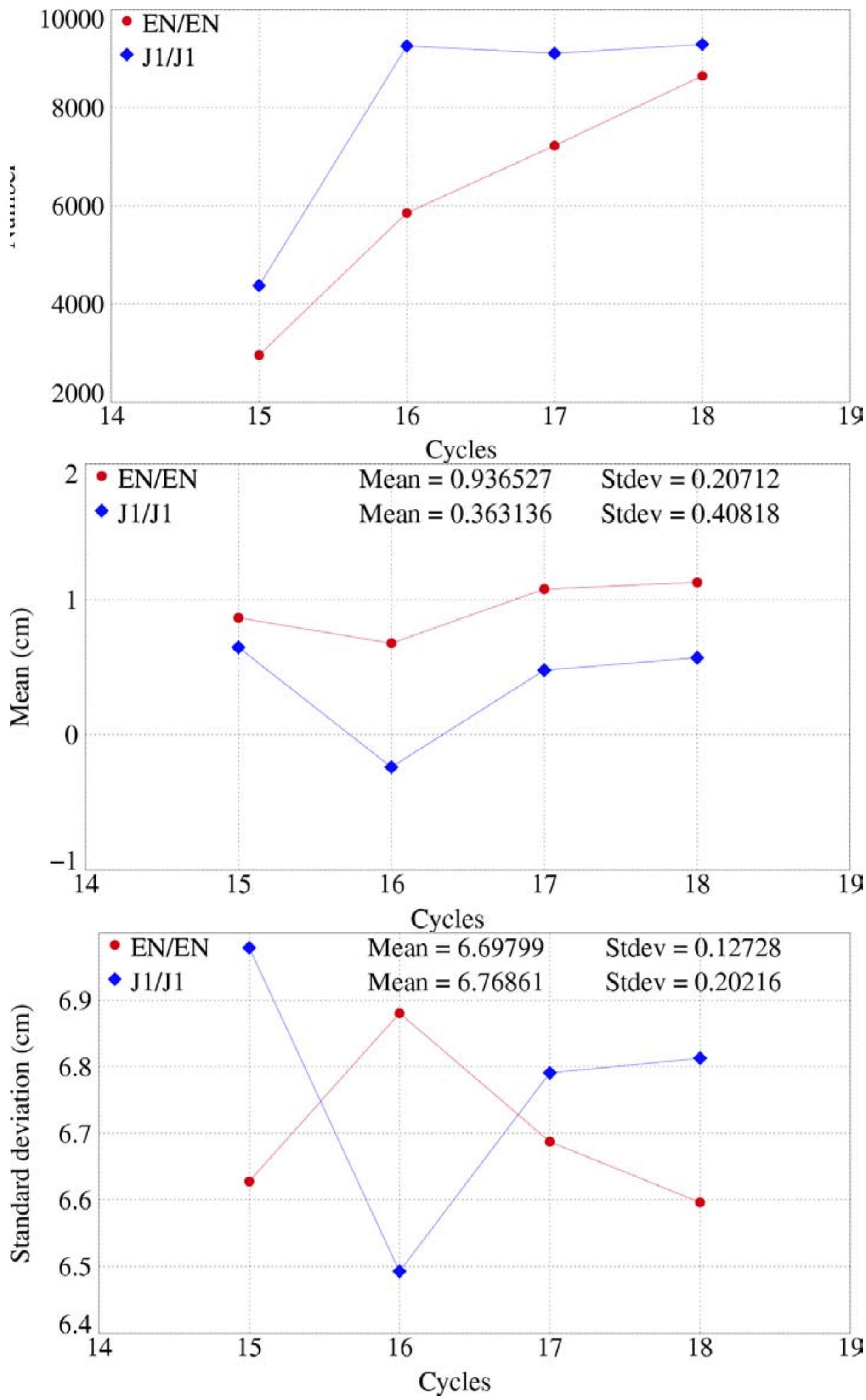

Figure 92 : Number, mean and standard deviation of SSH differences at crossover (cm), |latitude|<50°, Bathy<-1000m, Variability<20cm

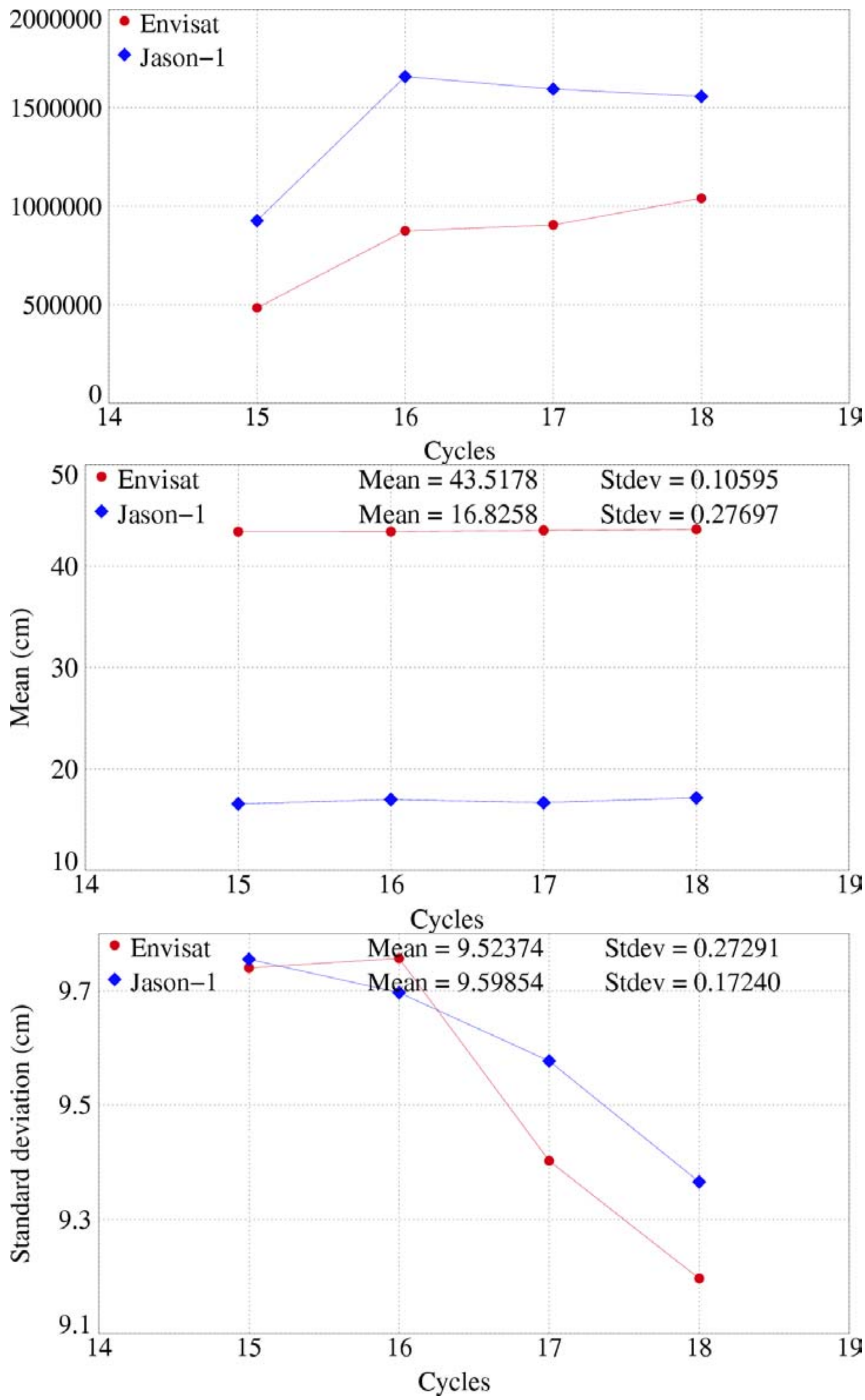

Figure 93 : Number, mean and standard deviation of SLA relative to MSS CLS01V1 (cm), |latitude|<66°, Bathy<-1000m, Variability<20cm

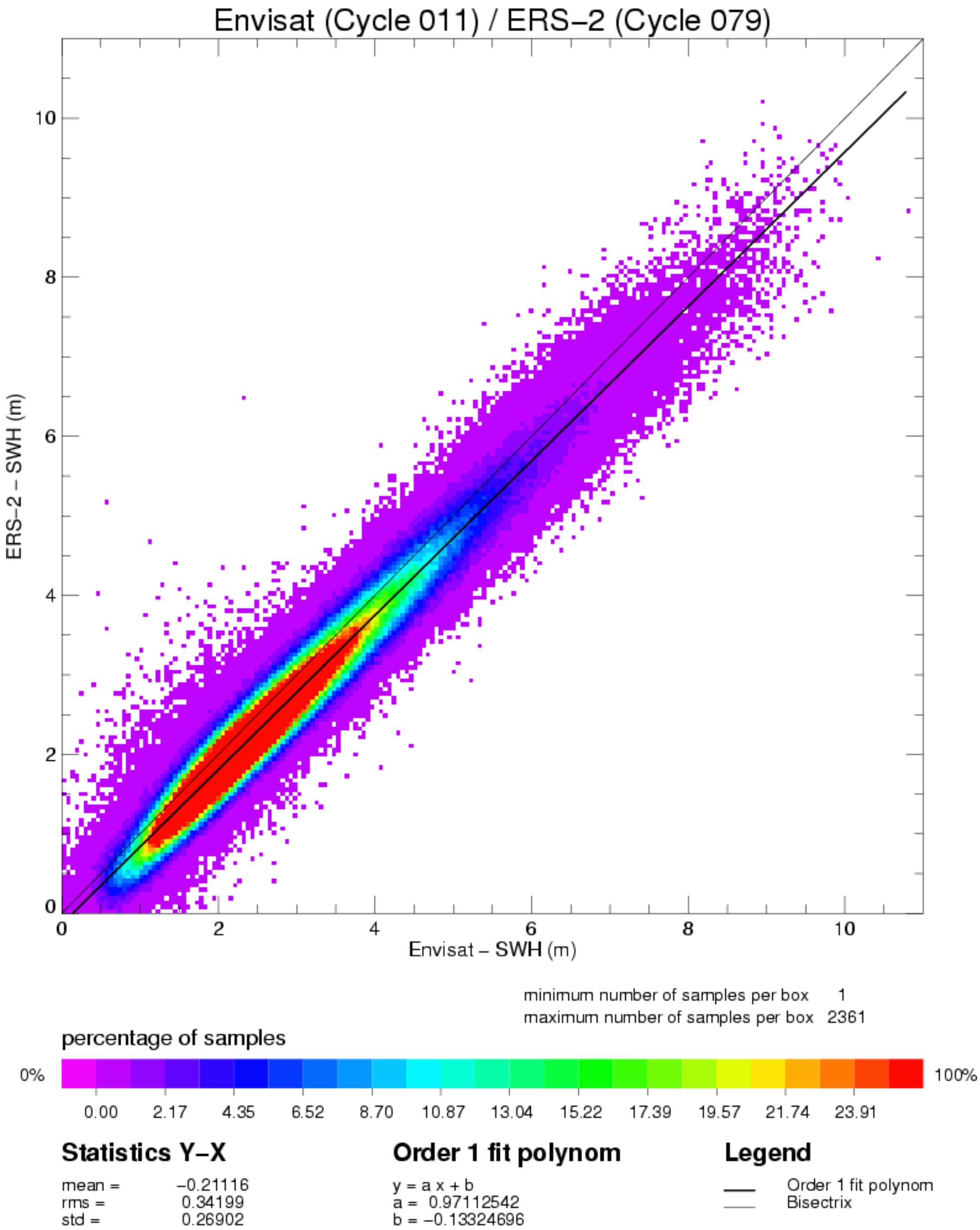

Figure 94 : **Scatter plot of ERS-2 SWH versus ENVISAT SWH in meters.**

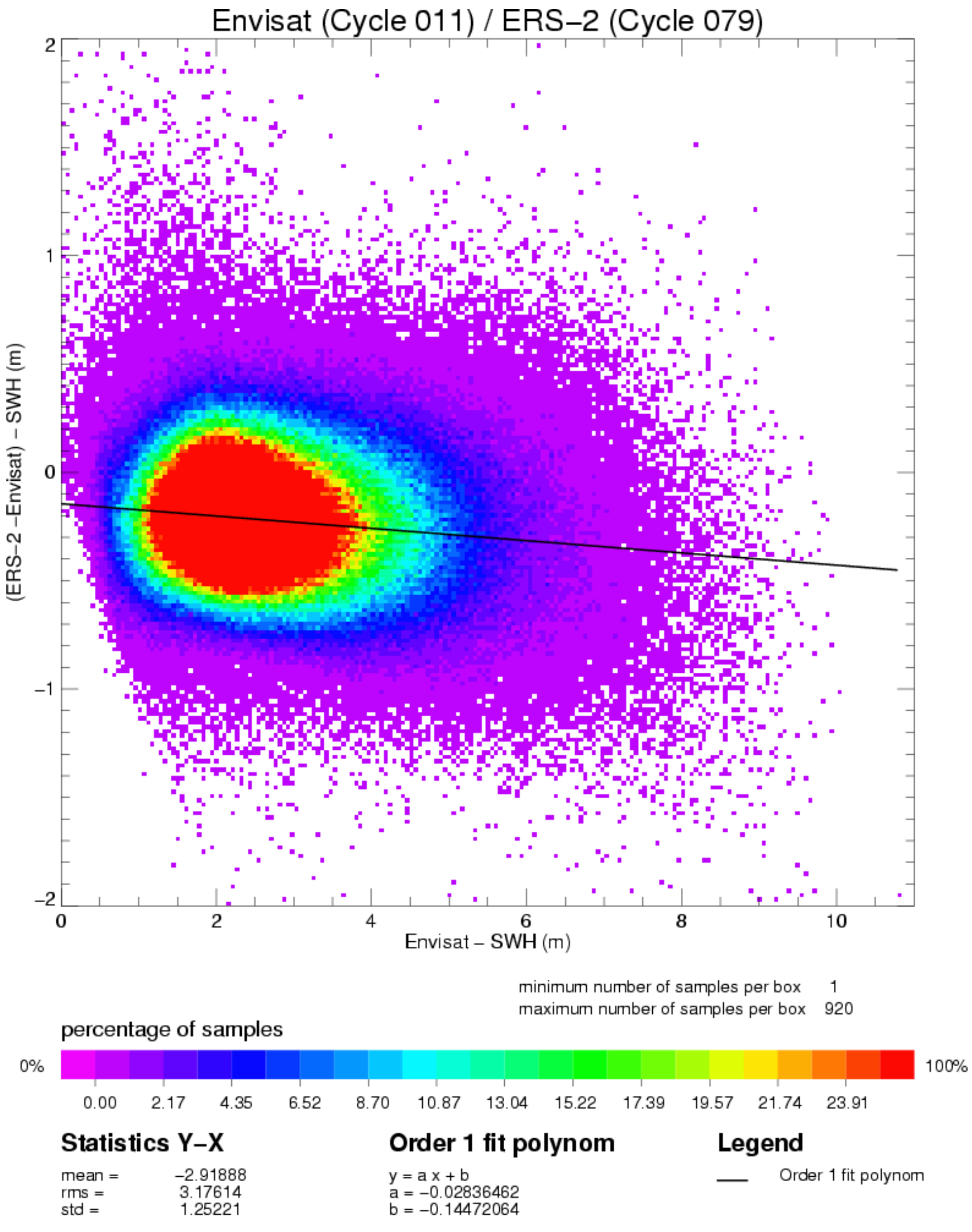

Figure 95 : Scatter plot of (ERS-2-ENVISAT) SWH differences (m) versus ENVISAT SWH.

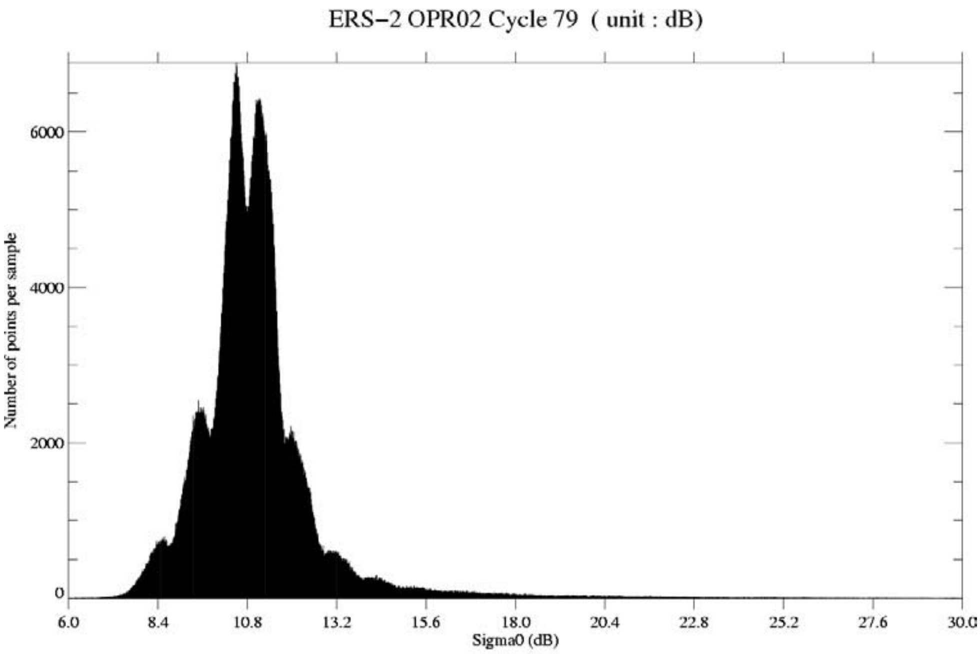

Global nb of points :	1480104	Sel. nb of points	:	1480104	Sample interval :	0.010
Global mean :	11.034	Selected mean	:	11.034	Maximum value :	30.000
Global Std :	1.718	Selected std	:	1.718	Minimum value :	6.000

Figure 96 : ERS-2 Sigma0 (dB) histogram for cycle 79.

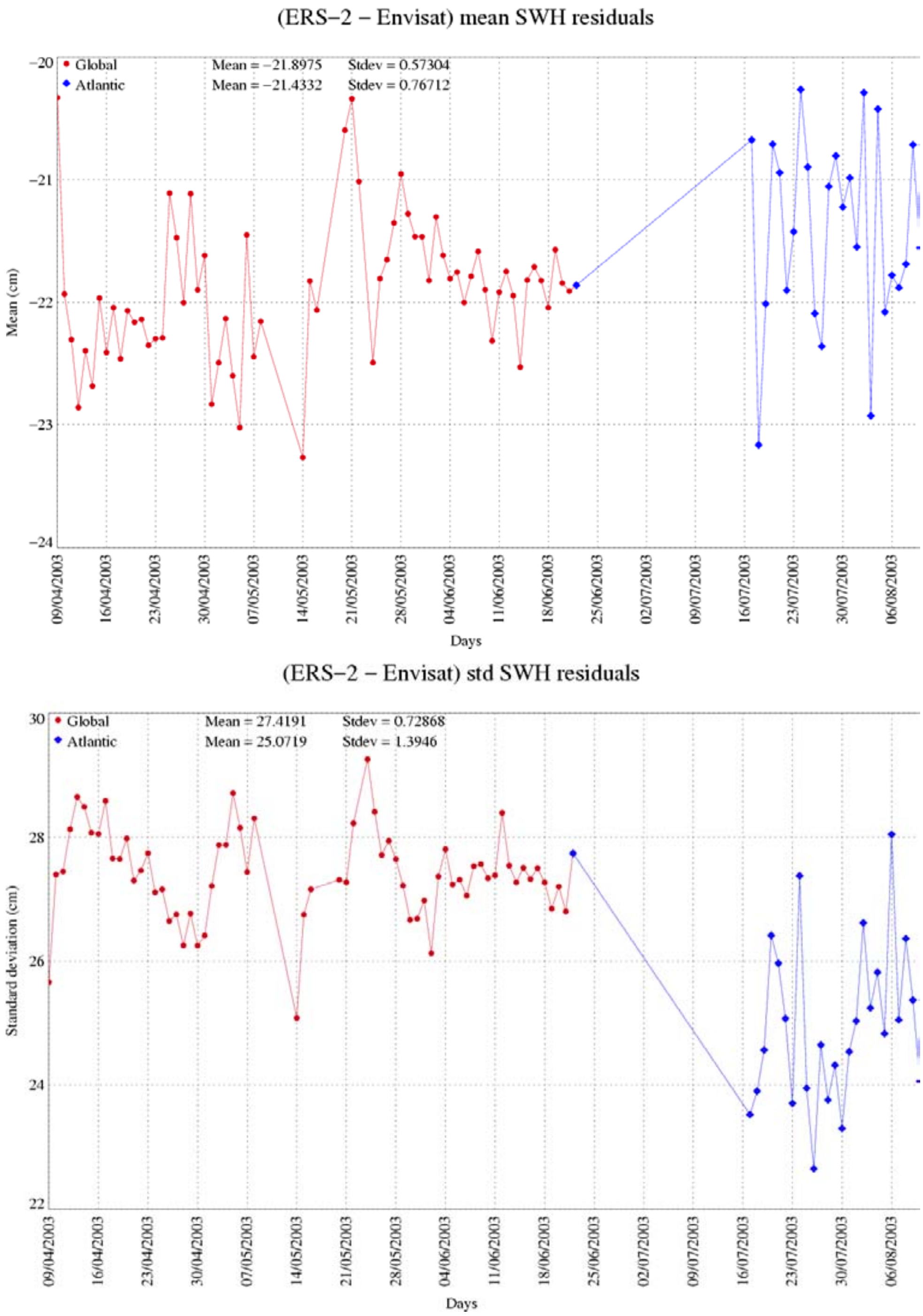

Figure 97 : **Mean and standard deviation of (ERS-2 – Envisat) SWH along track residuals for each day.**

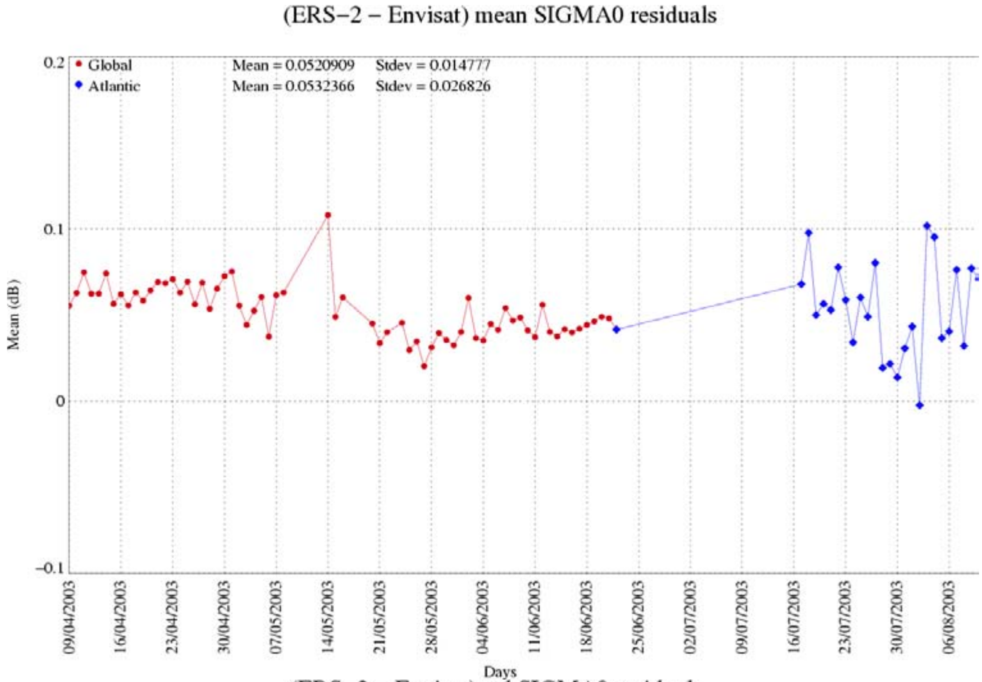

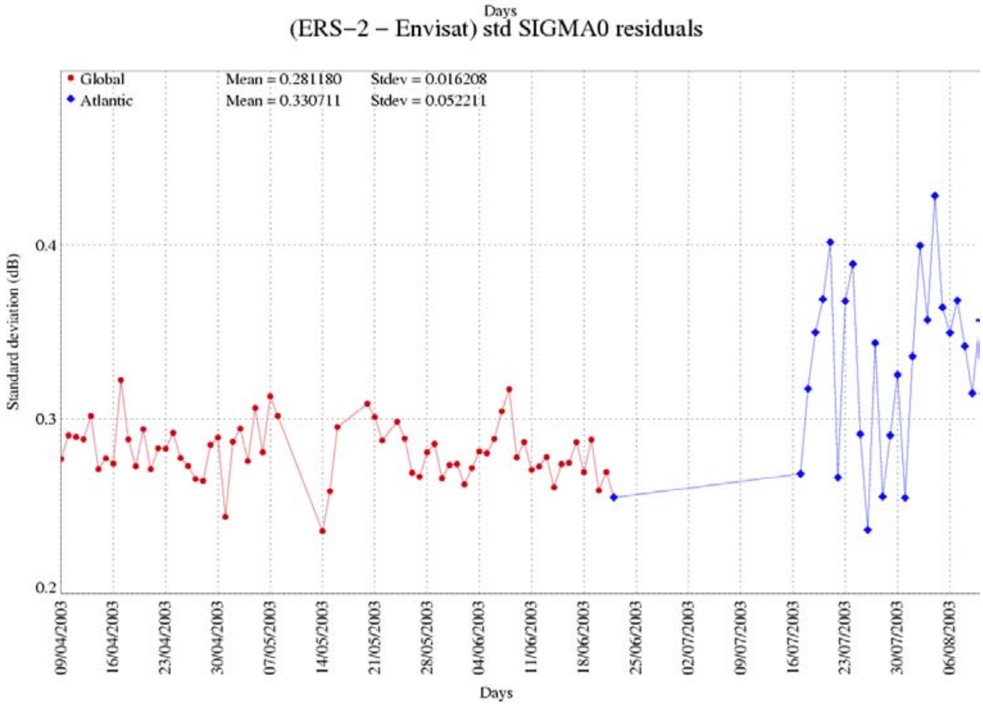

Figure 98 : Mean and standard deviation of (ERS-2 – Envisat) SIGMA-0 along track residuals for each day.

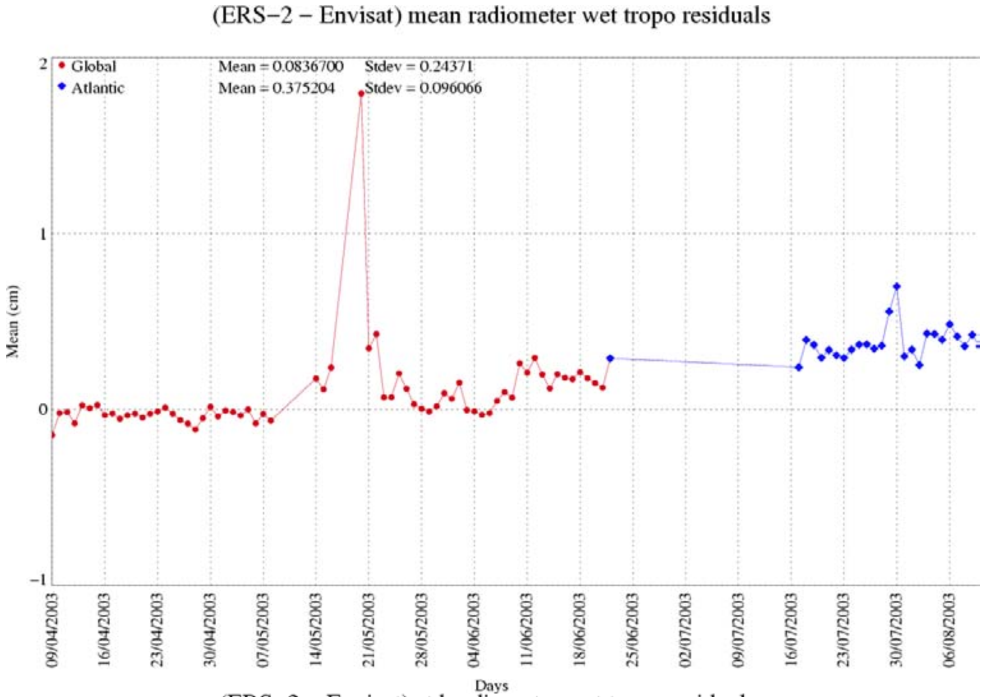

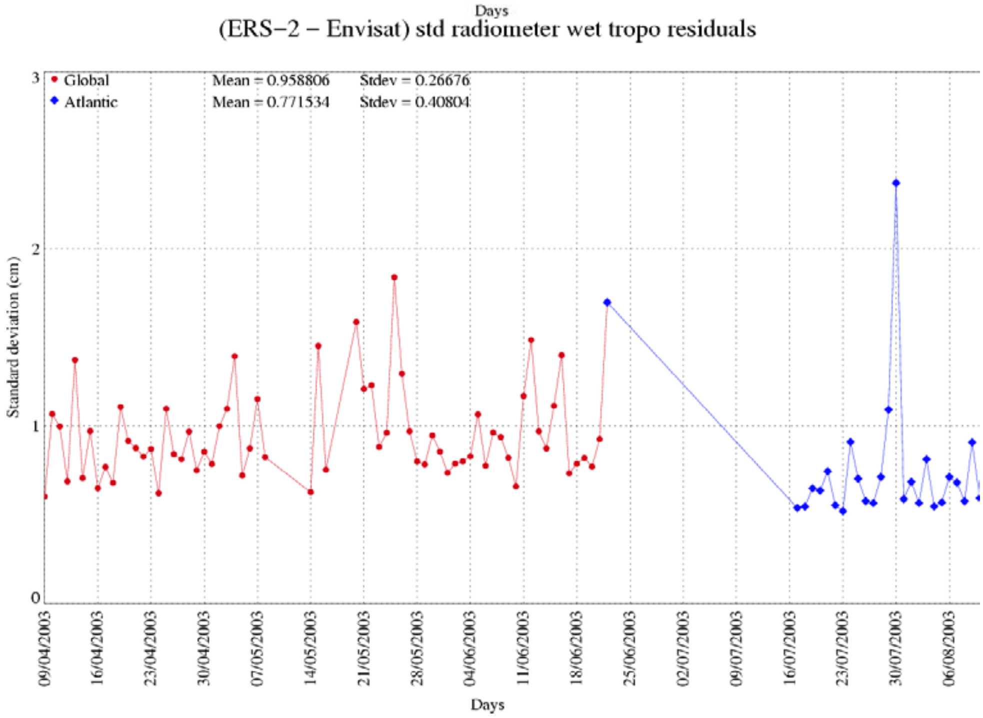

Figure 99 : **Mean and standard deviation of (ERS-2 – Envisat) Radiometer wet troposphere correction along track residuals for each day.**

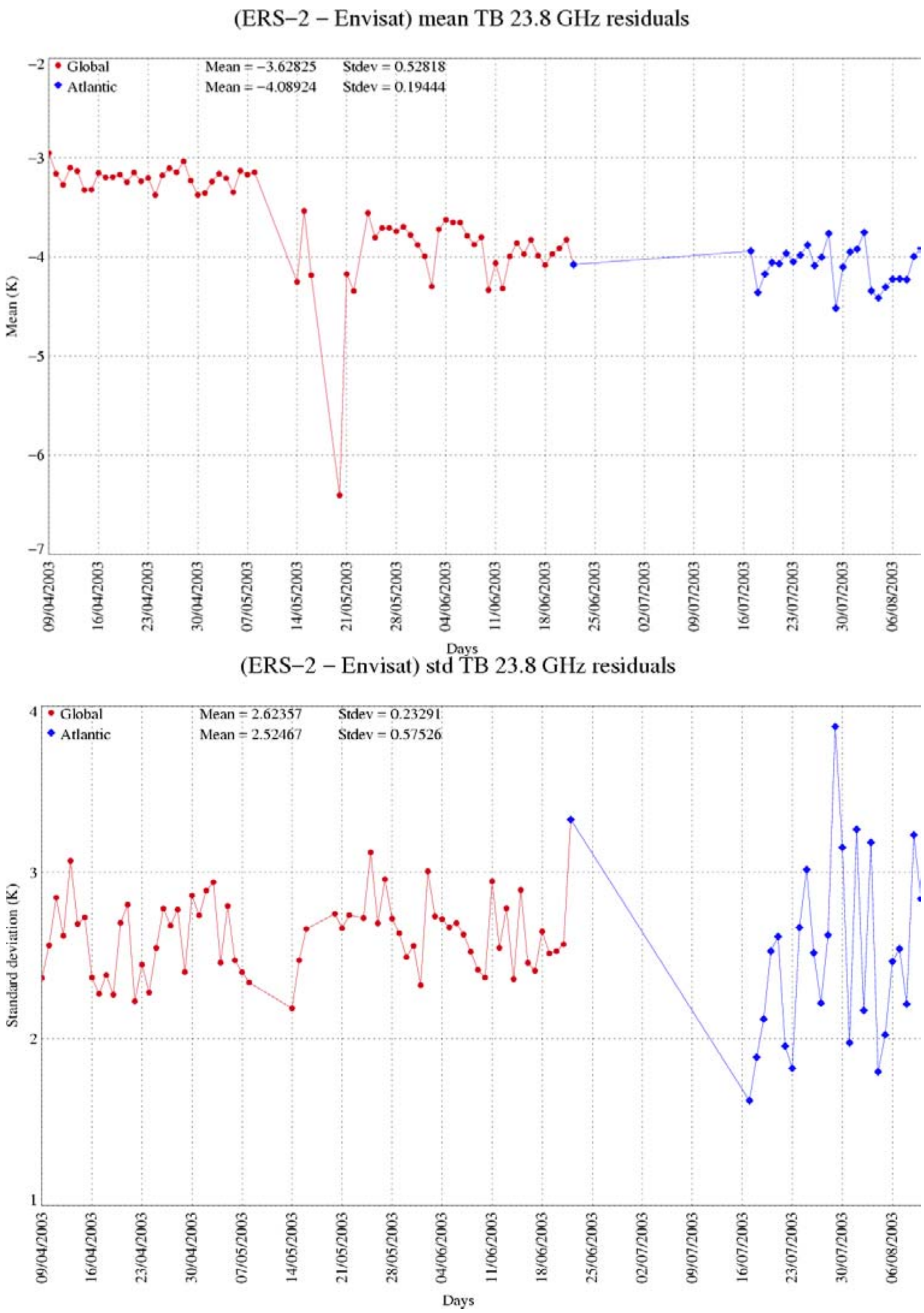

Figure 100 : Mean and standard deviation of (ERS-2 – Envisat) TB 23 GHz along track residuals for each day.

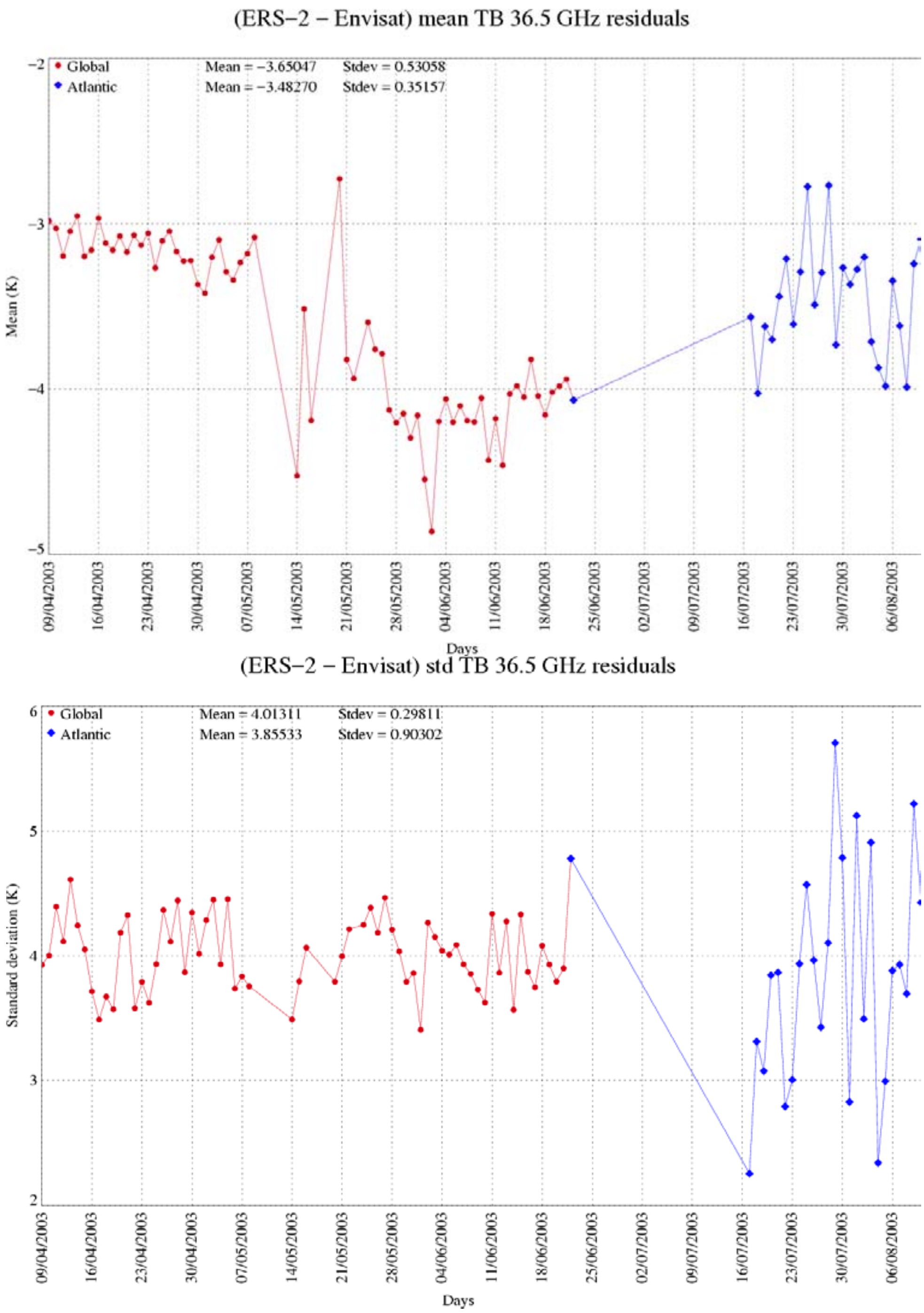

Figure 101 : Mean and standard deviation of (ERS-2 – Envisat) TB 36 GHz along track residuals for each day.

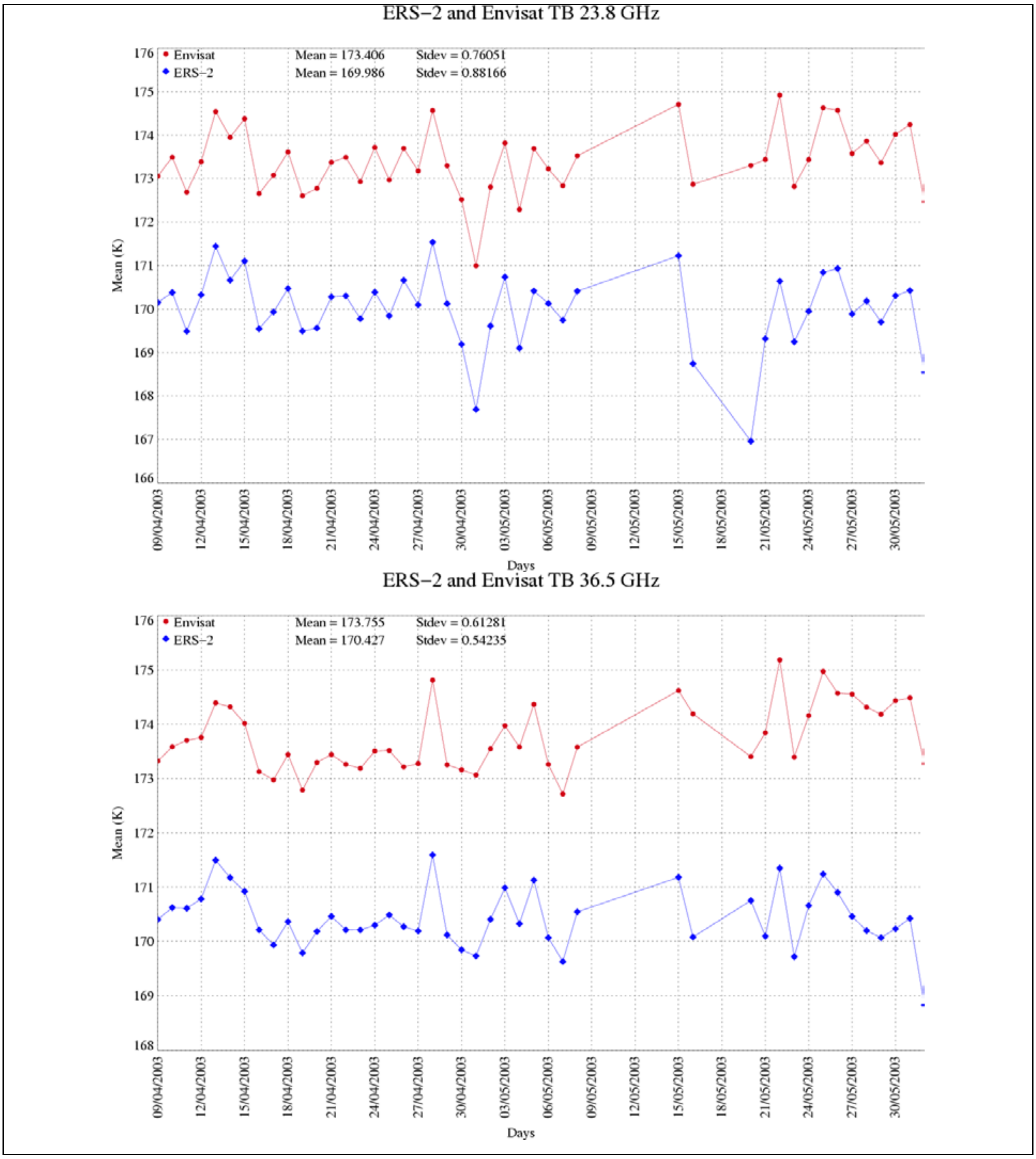

Figure 102 : Mean of ERS-2 and Envisat TB 23.8 GHz (top) and 36.5 GHz (bottom) for each day of cycles 15 and 16 Envisat

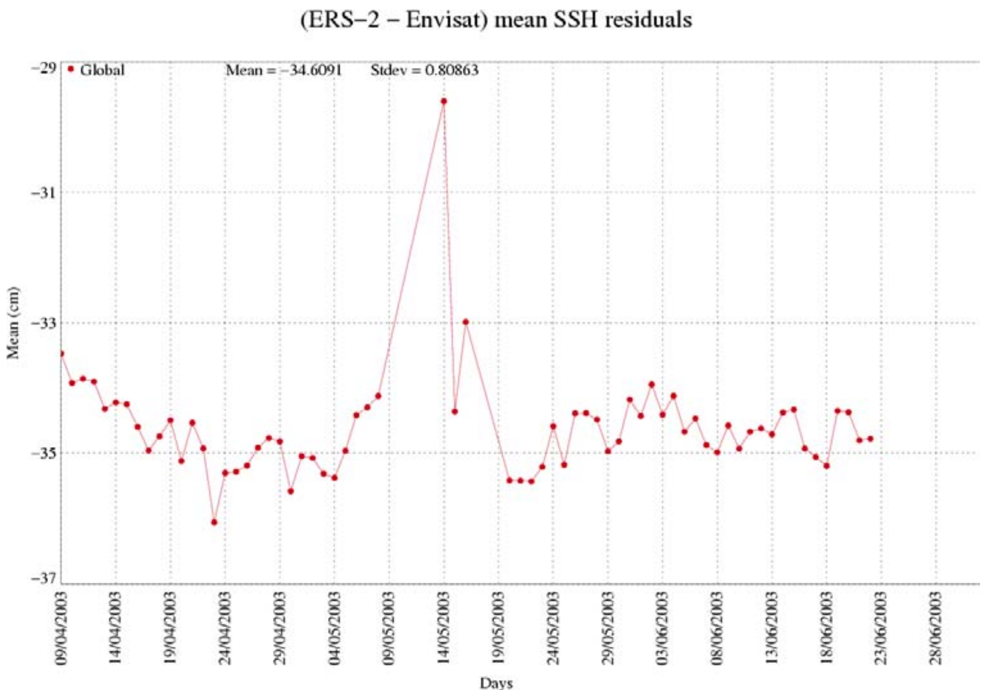

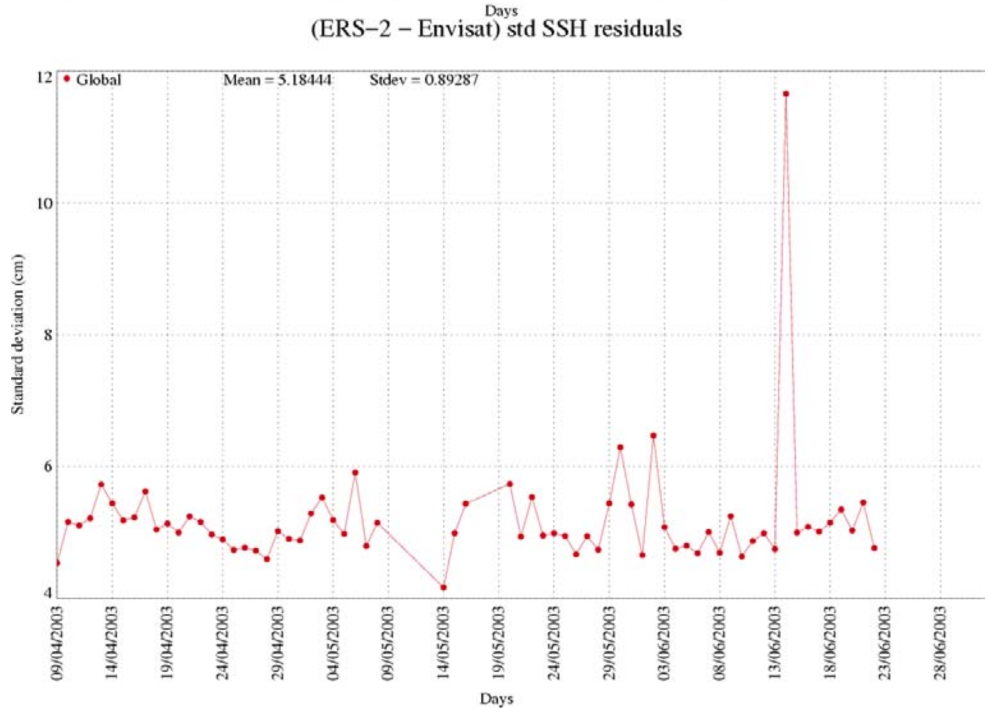

Figure 103 : Mean and standard deviation of (ERS-2 – Envisat) SSH along track residuals for each day from cycle 15 to 17.

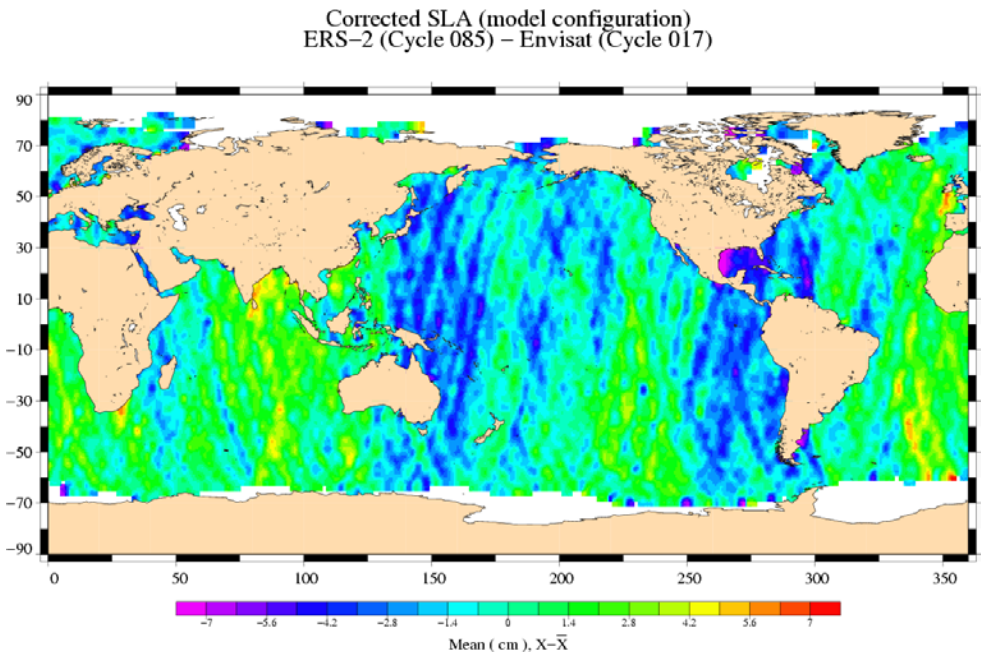

Figure 104 : (ERS-2 – Envisat) SSH differences for cycle 17.